Boron and Phosphorus Removal from Si-Fe Solvent Using SiO_2-CaO-Al_2O_3 Slag

by

Ali Hosseinpour

B.Sc., University of Tehran, 2015

A THESIS SUBMITTED IN PARTIAL FULFILLMENT OF THE REQUIREMENTS FOR THE DEGREE OF

MASTER OF APPLIED SCIENCE

in

THE FACULTY OF GRADUATE AND POSTDOCTORAL STUDIES
(Materials Engineering)

The University of British Columbia
(Vancouver)

May 2018

The following individuals certify that they have read, and recommend to the Faculty of Graduate and Postdoctoral Studies for acceptance, a thesis/dissertation entitled:

Boron and Phosphorus Removal from Si-Fe Solvent Using SiO_2-CaO-Al_2O_3 Slag

submitted by Ali Hosseinpour in partial fulfillment of the requirements for

the degree of Master of Applied Science

in Materials Engineering

Examining Committee:

Leili Tafaghodi Khajavi, Materials Engieering
Supervisor

Steve Cockcroft, Materials Engieering
Supervisory Committee Member

Edouard Asselin, Materials Engineering
Supervisory Committee Member

Abstract

This study investigates the efficiency of B and P removal from ferrosilicon alloy via slag refining. Silicon was alloyed with iron and the alloy was subjected to different compositions of $CaO\text{-}SiO_2\text{-}Al_2O_3$ ternary slag at 1600 °C. Distributions of B and P between alloy and slag phases were investigated by ICP-OES analysis. Results indicate that oxygen potential and basicity of slag can enhance removal of these impurities from the alloy. However, the partition ratio values decrease when the oxygen potential surpasses a critical value ($P_{O2,\ critical}$). $P_{O2,\ critical}$ for B and P was calculated as 9.01×10^{-18} and 6.29×10^{-18}, respectively. In addition, the highest partition ratios of B and P achieved in this study were 11.25 and 0.11, respectively. The effect of basicity on partition ratio values was also isolated through two parameters called borate (phosphate) capacity and normalized distribution of B (P). Results show that these parameters directly relate to optical basicity of slag.

Lay Summary

Among the current renewable energy sources, solar power is generally regarded as one of the most appropriate for satisfying the thriving demand. High-purity silicon, which is the key raw material in solar cells, is currently produced through an energy-intensive route, called Siemens process. The major challenge in producing high-purity silicon that operates efficiently is the need to meet the purity requirement (99.99999%) through an energy efficient route. This is primarily because of the lack of a dedicated process for the production of silicon suitable for solar applications at acceptable cost and high production rate. This study investigates silicon refining via metallurgical processes and evaluates the impurity removal efficiency. To benefit from the advantages of metallurgical processing methods such as high productivity and low cost, a combination of two techniques, i.e. slag treatment and solvent refining has been employed.

Preface

This dissertation is the original work I have done to investigate the removal of boron and phosphorus from ferrosilicon alloy by slag treatment. Following steps were taken to fulfill the aforementioned objective:

- Designed a setup for high-temperature experiments and the quenching process of the samples.
- Conducted the high-temperature experiments, leaching of the quenched samples and digestion of the alloy and slag.
- Analysis of the data presented in chapter 4.

A modified version of the literature review presented in sections 2-2-4-4 and 2-2-4-6 was published in the Journal of Mineral Processing and Extractive Metallurgy Review (A. Hosseinpour and L. Tafaghodi Khajavi, Slag refining of silicon and silicon alloys: a review, https://doi.org/10.1080/08827508.2018.1459616). Also, the results presented in chapter 4 are submitted for publication (A. Hosseinpour and L. Tafaghodi Khajavi, A Cleaner Route for Removal of Boron from Ferrosilicon Alloy via Slag Treatment).

I am the primary author of both publications mentioned above. Also, the second author of these publications is my supervisor, Dr. Leili Tafaghodi Khajavi who provided a continuing support and guidance in every step of this research work.

Table of content

List of Tables

List of Figures

List of Symbols

A	Activity
Γ	Activity coefficient
$C_{BO_3^{3-}}$	Borate capacity
G^{excess}	Excess Gibbs free energy of mixing
G	Gibbs free energy
γ°	Henrian activity coefficient
R	Ideal gas constant
X	Molar concentration
MW	Molecular weight
D_B	Normalized distribution of boron
D_P	Normalized distribution of phosphorus
Λ	Optical basicity
P_{O2}	Partial pressure of oxygen
L_B	Partition ratio of boron
L_P	Partition ratio of phosphorus
$C_{PO_4^{3-}}$	Phosphate capacity
T	Temperature

Acknowledgments

I would like to offer my special thanks to my supervisor Dr. Leili Tafaghodi for her patience, motivation, and useful constructive suggestions during the course of my research. Thank you for giving your valuable time so generously whenever I encountered problems in my research. I would also like to thank Dr. Ainul Akhtar for providing me with his precious technical recommendations.

My special thanks are extended to all of my friends, specially my officemates at FF 201C, for their frequent help and support. I also wish to acknowledge the technical help provided by dear Dr. Farzaneh Farhang Mehr during some of my experiments.

Finally, I wish to express my deepest gratitude to my family without whom none of my accomplishments would have been possible. Thank you for your unconditional love and encouragement.

1-Introduction

Solar energy is currently in great demand mainly because it is much cleaner than traditional sources of energy, namely fossil fuels. Silicon is the most important base-material of commercial solar cells [1]. Thus, developing an energy efficient, low cost process for production of silicon for solar applications can be of great help for advancing the photovoltaic industry.

Considering the purity level of silicon, there are three grades for this semiconductor material: Metallurgical grade silicon (MG-Si) with purity of 98-99.5%, which is commercially produced by carbothermal reduction of high-purity silica. Semiconductor grade silicon (SeG-Si) with purity of 11N is the purest grade of silicon and it is commercially produced via Siemens process. This process involves conversion of MG-Si to a volatile compound (e.g. Silicon tetrachloride or trichlorosilane) [2, 3]. Solar grade silicon (SoG-Si), which has the purity requirement of 7N, is mostly produced with Siemens process as well, while processes specific to SoG-Si production constitute a very small part of this industry. Because of the difference in purity specifications of SoG-Si and SeG-Si, developing processes with improved cost/energy efficiency which are dedicated to SoG-Si production has been of great interest to researchers.

Among the alternative methods for silicon refining, metallurgical routes, such as slag treatment and solvent refining, have attracted wide research interest. In the case of solvent refining, silicon is first alloyed with another metal. Under controlled solidification, silicon crystals can grow from the alloy melt while the impurities are rejected to the solidification front [4]. In slag treatment, elements that have higher affinity for oxygen than for silicon are first oxidized and then dissolved in the slag phase. Therefore, when slag is separated from silicon after solidification, impurities that have been transferred to the slag phase are removed [5]. Slag treatment has also

been applied on alloys of Si-Cu [6] and Si-Sn [7]. These studies have confirmed that the removal efficiency of impurities can be enhanced when slag treatment and solvent refining are combined. In other words, applying a combination of these two methods, fewer repetitions of slag treatment are required to reach acceptable levels of impurities for solar applications.

The current study is focused on developing a metallurgical route for removal of two detrimental elements, B and P, through combination of slag treatment and solvent refining. A silicon-iron alloy is employed and $CaO\text{-}SiO_2\text{-}Al_2O_3$ ternary system is used as the slag. The removal efficiency of this process is measured through chemical analysis of slag and alloy phase. The effects of oxygen potential and basicity of the slag on the removal of B and P are investigated. The critical partial pressures of oxygen for B and P removal are calculated separately. At last, the effect of basicity on partition ratios of B and P is isolated via thermodynamic analysis of the results.

2-Literature Review

2-1- Grades of Silicon

Silicon constitutes about 26% of the earth's crust. Silica and silicates are the main sources of silicon in nature [8]. Silicon can be categorized into three different grades based on its application or purity: metallurgical grade silicon (MG-Si) with purity of 98-99.5%, solar grade silicon (SoG-Si) with purity of 7N and semiconductor grade silicon (SeG) which has the purity of 11N [9].

2-1-1- Metallurgical grade silicon (MG-Si)

MG-Si is produced via carbothermic reduction of quartz, mostly in countries that benefit from inexpensive coal, electricity and quartz deposits. USA, South Africa, Brazil, and Australia are among the major producers of MG-Si. This grade of silicon is mostly used for steel deoxidation, production of electronic grade silicon, and production of silicone. Quality, purity and particle size are the main factors that determine the price of MG-Si [10]. Table 2.1 shows the typical impurities in MG-Si.

2-1-2- Semiconductor grade silicon (SeG-Si)

High purity silicon is the most basic material used for producing semiconductor devices such as solar cells and computer chips. Purifying MG-Si to semiconductor silicon is carried out through an energy intensive and complicated process (Siemens process). This process involves the reaction between silicon and HCl which leads to production of silicon tetrachloride ($SiCl_4$) or trichlorosilane (TCS, HCl_3Si). Next, TCS and H_2 gas react and as a result, pure silicon is deposited on silicon seeds [3, 11].

Table 2. 1. Impurities of metallurgical-grade silicon [3].

	Impurity content, ppm	
Impurity	**98-99%**	**99.5%**
Al	1000–4000	50–600
Fe	1500–6000	100–1200
Ca	250–2200	100–300
Mg	100–400	50–70
Mn	100–400	50–100
Cr	30–300	20–50
Ti	30–300	10–50
V	50–250	<10
Zr	20–40	<10
Cu	20–40	<10
B	10–50	10–15
P	20–40	10–20
C	1000–3000	50–100

2-1-3- Solar grade silicon (SoG-Si)

The acceptable impurities concentration is SoG-Si is presented in Table 2.2 [3]. The impurity content of the silicon used in the photovoltaic industry, i.e. solar grade silicon can be

considerably higher than that of semiconductor grade silicon. However, at present, most SoG-Si is produced through the Siemens or Siemens-like processes and a very small part of the production is via the processes dedicated to SoG-Si production. The difference in silicon specifications required in microelectronics and photovoltaic applications, and the cost and energy associated with the Siemens process have led to various investigations directed towards developing specific technologies for production of low cost SoG-Si [12-15].

Table 2. 2. Permissible levels of impurities in solar grade silicon [3]

Impurity	**Impurity content, ppm**
Al	< 0.1
Fe	< 0.1
Ca	< 1
Mg	< 1
Mn	<< 1
Cr	<< 1
Ti	<< 1
V	<< 1
Cu	< 1
B	0.1-1.5
P	0.1-1
C	0.5-5

Figure 2.1 shows the effect of various impurity elements on the conversion efficiency of p-type solar cells. Efficiencies are all normalized to 100 mW cm^{-2}. As it is obvious, the solar cell conversion efficiency is degraded as the concentrations of impurities are increased in SoG-Si [8].

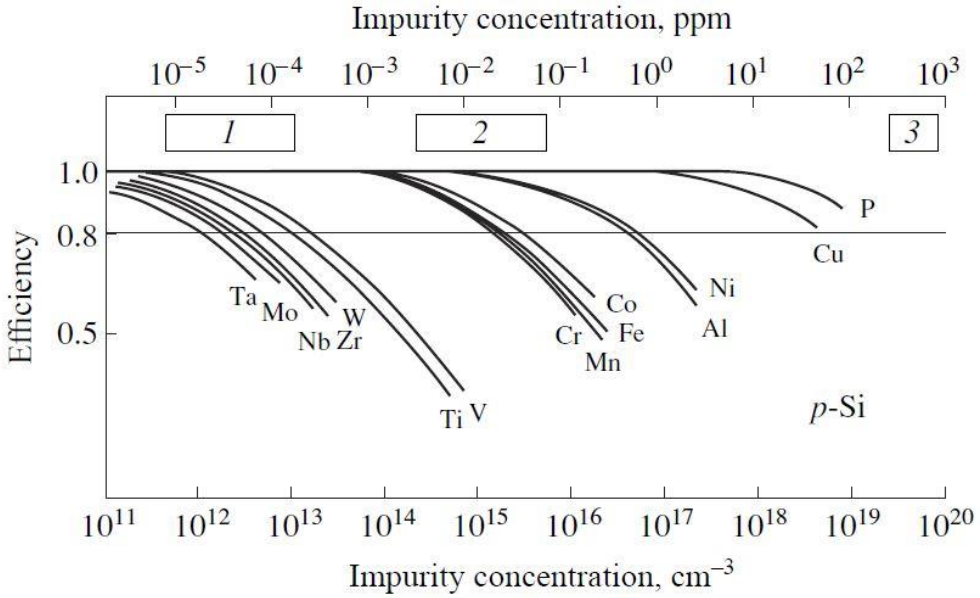

Figure 2. 1. P-type solar cell normalized conversion efficiency versus impurity concentration (atom / cm^{-3}): (1) semiconductor-grade, (2) solar-grade and (3) metallurgical-grade silicon [8].

2-2- Refining Processes

Since 1975, production of low cost SeG-Si and SoG-Si have drawn researchers' attention [10, 16-18]. The process for obtaining high purity silicon can be divided into two steps. First, reduction of silica to obtain MG-Si. Second, purification of MG-Si to SeG-Si and SoG-Si. In other words, MG-Si is the primary material for production of higher grades of silicon. MG-Si is commercially produced via reducing silicon oxide (quartz) with carbon (Eq.2.1) in submerged arc furnaces.

SiO_2 (s) + 2C (s) ⟶ Si (l) + 2CO (g) Eq. 2. 1

Figure 2.2 shows the schematic of quartz reduction in an electric arc furnace. The product of the process, molten silicon, is collected from the bottom of the furnace [19].

MG-Si produced through the aforementioned method cannot be used in solar or electronic applications since the concentrations of impurities in the final product are much higher than the tolerable levels for these applications. In the following sections, various routes for producing high purity silicon are described.

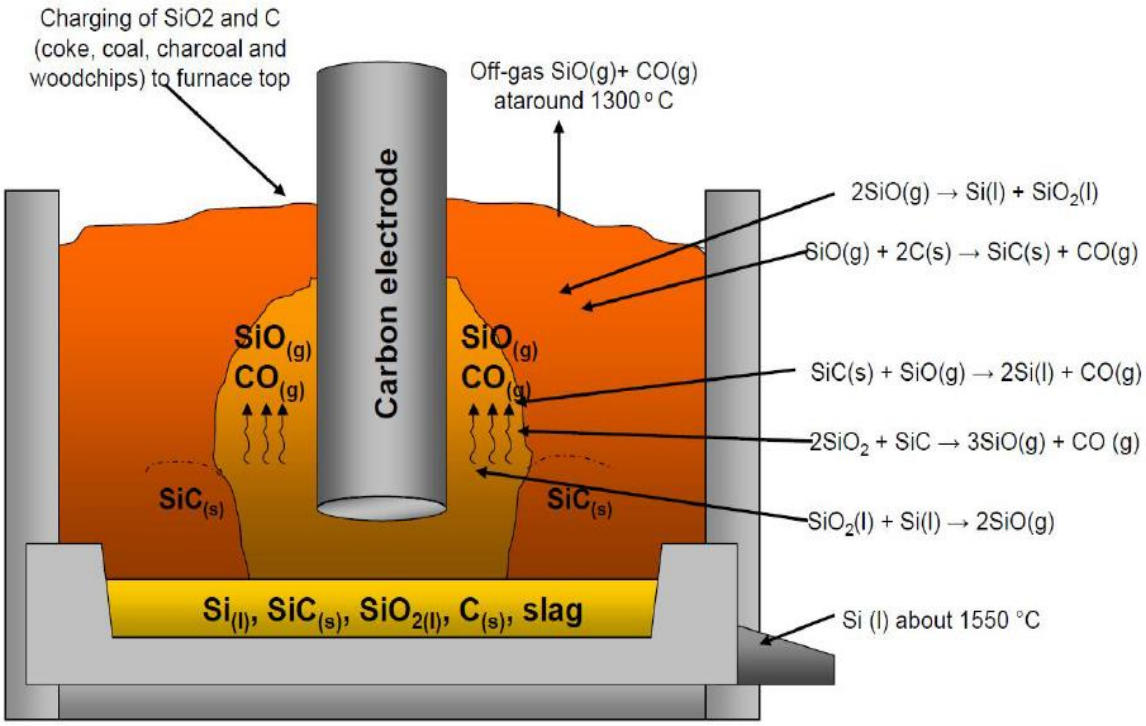

Figure 2. 2. Electric arc furnace used for reduction of quartz with carbon [19].

2-2-1- Reduction or pyrolysis of volatile silicon compounds (Siemens process)

Traditionally, the Siemens process, developed in the 1950s, has been used to produce high purity silicon. In this method, trichlorosilan ($SiHCl_3$), known as TCS, is produced via the reaction between MG-Si and hydrogen chloride gas, HCl (Eq. 2.2). The reaction typically takes place at 500 °C and 30 MPa.

$$Si\,(s) + 3HCl\,(g) \rightarrow SiHCl_3\,(g) + H_2\,(g) \qquad \text{Eq. 2. 2}$$

Subsequently, $SiHCl_3$ which is a volatile compound with the boiling point of 31.8 °C, is distilled in the presence of hydrogen (H_2) according to Eq. 2.3. This reaction is carried out on silicon seeds which are electrically heated to 1000-1100 °C. In other words, while impurities are removed from TCS based on their different boiling points, pure silicon is deposited on the seeds.

$$SiHCl_3\,(g) + H_2\,(g) \rightarrow Si\,(s) + 3HCl(g) \qquad \text{Eq. 2. 3}$$

The final product of this reaction is high purity silicon. Also, the gaseous byproduct of the distillation reaction (HCl) is reused in the first reaction (Eq. 2.2) [19, 20].

The two main drawbacks of the Siemens process are:

- Production of toxic and corrosive compounds such as chlorosilanes as the intermediate product
- High energy consumption as the distillation reaction occurs in the vapor phase[20, 21]

Although great efforts have been made to propose alternatives for the Siemens method, it remains the dominant silicon refining process with a market share of almost 90% of high purity silicon [22].

2-2-2- Reduction of silicon halides by alkali metals

SoG-Si can be produced through reduction of SiO_2, SiF_4, $SiCl_4$ and SiB_4 using several metals or compounds such as NH_3 and CH_4. However, the only method that can bring about large-scale commercial production of SoG-Si is reduction of silicon halides by alkali metals such as Na and K. Gaseous Na or K reacts with vaporized silicon halides such as $SiCl_4$, $SiHCl_3$ or SiF_4 according to the following reactions:

$$SiC1_4\ (g) + 4K\ (4Na)\ (g) \rightarrow Si\ (l) + 4KC1\ (4NaC1)\ (g) \quad \text{Eq. 2. 4}$$

$$SiHCl_3\ (g) + 3K\ (3Na)\ (g) \rightarrow Si\ (l) + 3KC1\ (3NaC1)\ (g) + \tfrac{1}{2}\ H_2\ (g) \quad \text{Eq. 2. 5}$$

$$SiF_4\ (g) + 4K\ (4Na)\ (g) \rightarrow Si\ (l) + 4KF\ (4NaF)\ (g) \quad \text{Eq. 2. 6}$$

Figure 2.3 demonstrates the thick walled graphite reactor and the collector for the reaction of Na and $SiCl_4$ (Eq. 2.4) [8].

Another similar silicon production process involves reducing SiF_4 gas with Na chips. In this method fluosilic acid (H_2SiF_6), which is a byproduct of the phosphate fertilizer industry, reacts with NaF and produces Na_2SiF_6 (sodium fluosilicate) with purity of ~99% through the following reaction.

$$H_2SiF_6\ (aq) + NaF\ (s) \rightarrow 2HF\ (aq) + Na_2SiF_6\ (s) \quad \text{Eq. 2. 7}$$

Subsequently, dry Na_2SiF_6 is thermally decomposed at ~700 °C according to Eq. 2.8:

$$Na_2SiF_6\ (s) \rightarrow 2NaF\ (s) + SiF_4\ (g) \quad \text{Eq. 2. 8}$$

Finally, a reactor which is preheated to 400 °C is filled with SiF_4 gas produced through Eq. 2.8. Reduction of SiF_4 starts when Na chips are fed to the reactor (Eq. 2.9).

$$SiF_4\ (g) + 4Na\ (s) \rightarrow Si\ (s) + 4NaF\ (s) \quad \text{Eq. 2. 9}$$

Liquid Na with temperature of 130 °C can also be used instead of solid Na. The products (Si + NaF) are removed from the bottom of reactor. When they are heated to some temperature above 1420 °C, molten silicon gets separated from the NaF (gaseous) and it is easily collected at the bottom of the crucible [8].

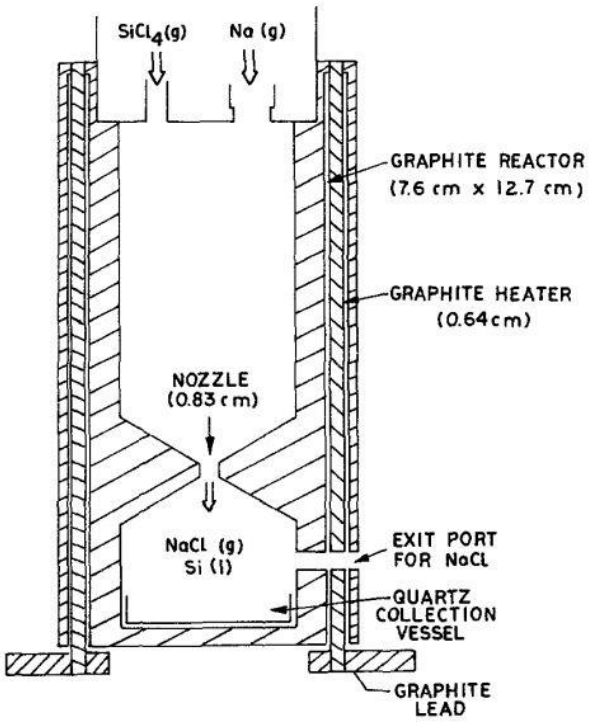

Figure 2. 3. Schematic of reactor and collector for the reaction of Na and $SiCl_4$ [23].

2-2-3- Carbothermal reduction of high purity silica

As mentioned before, MG-Si can be commercially produced by carbothermal reduction of silica according to Eq. 2.1. The commercial quartz sand used for this process contains a high level of impurities e.g. phosphorus (P) and boron (B). However, if this method is to be used for production of SoG-Si, pure quartz with lower impurity concentration should be employed [24]. Crushing, sieving, and washing are the conventional processes that can be utilized to improve the

purity of quartz through removing the soluble compounds [3]. The total impurity content of quartz after these processes approches ~100 ppm. However, silicon with less than 1 ppm of impurities can be achieved by purifying the quartz via using glass-forming materials such as boron oxide and alkali-metal carbonates or oxides. In this method, the aforementioned glass-forming materials are mixed with the quartz sand and then melt to form a glass. Annealing the glass results in two separate phases, namely a SiO_2-rich phase and an impurity-rich phase. Finally, strong acids like nitric acid helps extracting the impurity-rich phase [25].

The impurity level of reductant and their reactivity with quartz play a vital role in the purity of final silicon. Various reductants such as oil coke, charcoal, graphite, and carbon black (with different combinations and grades) can be used to extract Si. The best results are achieved using carbon black (produced by cracking of methane or propane) because of its good reducing ability and high purity. In other words, the highest purity of silicon is obtained when gas black and high purity quartz are chosen as the reactants in carbothermal reduction of quartz. Silica powder and carbon black are granulated with the help of binders before the reduction process [3].

2-2-4- Refining of MG-Si

MG-Si produced via carbothermal reduction contains high levels of detrimental impurities. Comparison of the impurity content of MG-Si (table 2.1) with permissible levels of impurities in solar grade silicon (table 2.2) suggests that it is almost impossible to use the silicon obtained from carbothermal reduction in photovoltaic applications. For instance, carbon is one the impurities that is mostly in the form of SiC inclusions and the rest of it is dissolved in the melt [3, 26].

Non-metallic impurities like B and P can easily be avoided by opting suitable raw materials with the minimum amount of impurities for the production of silicon. However, high-purity raw materials are very costly. Thus, from an economical point of view, it is more desirable to use a simple and inexpensive purification process instead of utilizing high-purity raw materials in order to reduce the amount of impurities in the silicon metal [27]. Some of the techniques that have been used to purify MG-Si to SoG-Si are delineated in what follows.

2-2-4-1- Directional solidification

Directional solidification is one of the methods for reducing the level of impurities in MG-Si in order to make it suitable for solar applications. During slow cooling of molten silicon, pure silicon precipitates from the melt while the impurities are rejected to the solidification front. The segregation coefficient, k, which is defined as the ratio of concentration of an element in solid silicon (C_s) to its concentration in liquid silicon (C_l) (Eq. 2.10), is a crucial factor in this process.

$$k = \frac{C_s}{C_l} \qquad \text{Eq. 2. 10}$$

The segregation coefficient of several impurities in silicon are given in table 2.3. Since most of impurity elements except B, P and As have small segregation coefficients, directional solidification can be effective in reducing their concentrations to an acceptable level for solar applications [8, 28]. However, research findings show that the conversion efficiency of solar cells fabricated by the purified Si produced via two steps of directional solidification cannot exceed 14.1% as B and P concentrations are not decreased sufficiently [29]. As a result, it can be concluded that directional solidification needs to be repeated or combined with other refining processes in order to reach purity levels suitable for photovoltaic applications

2-2-4-2- Plasma melting

Plasma melting is one of the methods that can be applied for removing impurities such as B. Impurities in silicon react with reactive gases like Cl_2, O_2, $SiCl_4$, CO_2 and wet hydrogen or their combinations and form volatile compounds. In other words, adding reactive gases to plasma results in the volatilization of impurities on the surface of molten silicon [8, 30]. For example, Trassy et al. [30] showed that the concentration of B decreases from 15 ppmw to 2 ppmw after plasma treatment. In this experiment, B was volatilized in the form of BOH when hydrogen and oxygen were simultaneously utilized as the reactive gas. The schematic of this process is presented in Figure 2.4.

Table 2. 3. Segregation coefficients for various impurities in silicon [8, 31]

Impurity	Segregation Coefficient	Impurity	Segregation Coefficient
Aluminum	2.0×10^{-3}	Manganese	1.3×10^{-5}
Antimony	2.3×10^{-2}	Molybdenum	4.5×10^{-8}
Arsenic	3.0×10^{-1}	Nickel	1.0×10^{-4}
Bismuth	7.0×10^{-4}	Niobium	4.4×10^{-7}
Boron	8.0×10^{-1}	Palladium	5.0×10^{-5}
Carbon	5.0×10^{-2}	Phosphorus	3.5×10^{-1}
Chromium	1.1×10^{-5}	Silver	1.7×10^{-5}
Cobalt	2.0×10^{-5}	Tantalum	2.1×10^{-8}
Copper	4.0×10^{-4}	Tin	1.6×10^{-2}
Gallium	8.0×10^{-3}	Titanium	2.0×10^{-6}
Indium	4.0×10^{-4}	Tungsten	1.7×10^{-8}
Iron	8.0×10^{-6}	Vanadium	4.0×10^{-6}
Lithium	1.0×10^{-2}	Zinc	1.0×10^{-5}
Magnesium	3.2×10^{-6}	Zirconium	1.6×10^{-8}

Kato et al. [32] proposed a deboronization mechanism based on steam-added plasma melting (Figure 2.5). According to their observation, a SiO_2 film is formed on the surface of molten Si when the steam content is increased. Thus, not only does it cause loss of silicon but also reduces the deboronization rate. On the contrary, increasing the hydrogen content resulted in an increase in the rate of B removal as hydrogen ruins the SiO_2 film (Eq. 2.11).

$$SiO_2\,(s) + H_2\,(g) \rightarrow SiO\,(S) \qquad \text{Eq. 2. 11}$$

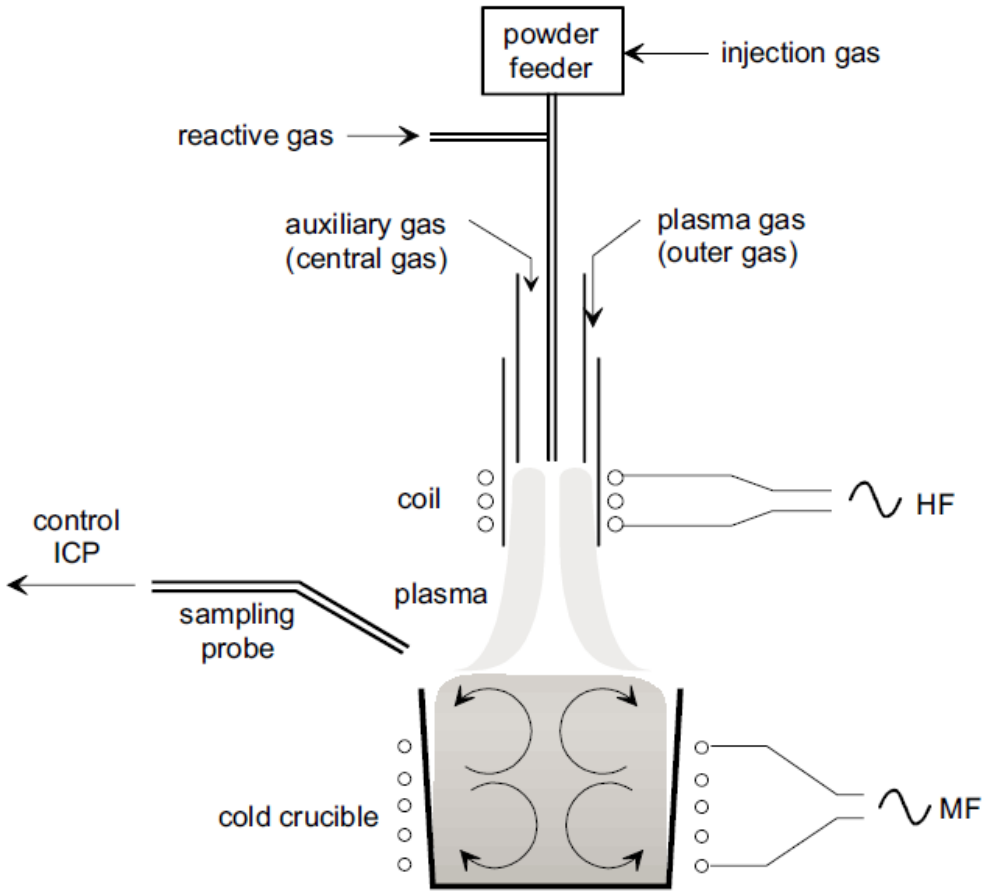

Figure 2. 4. Schematic of plasma melting process [30].

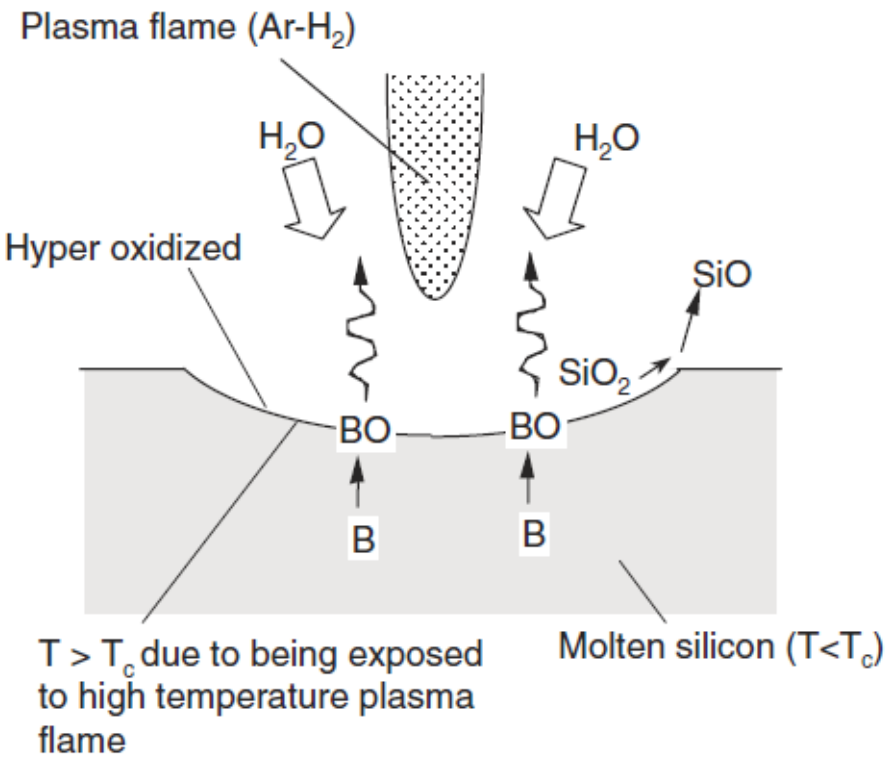

Figure 2. 5. Mechanism of deboronization [32].

2-2-4-3- Electron beam melting (EBM)

Electron beam melting (EBM) is another technique used for purification of MG-Si. The process involves melting Si in a high vacuum electron beam furnace to remove volatile impurities through evaporation [33]. Dong et al. [34] investigated the removal mechanism of aluminum from MG-Si via electron beam melting. They showed that diffusion of Al from molten silicon to the molten/vacuum interface controls its removal rate from MG-Si. Al content of MG-Si decreased from 80.5 ppmw to 0.5 ppmw using 21 kW power and process duration of 1920 seconds. However, evaporation weight loss of silicon was ~ 40 g after 1920 seconds (initial amount of silicon was 300 g).

Ikeda and Maeda [18] studied the behavior of numerous impurities, including C, P, B, Ca, Al, Fe and Ti in MG-Si during EBM purification. According to their findings, 90 percent of C, 93 percent of P, 89 percent of Ca and 75 percent of Al were removed from the MG-Si under 10^{-2} Pa in 30 minutes.

2-2-4-4- Slag refining

One of the techniques employed for lowering the concentration of various impurities in silicon or silicon alloys is slag treatment [35, 36]. Slag refining is one of the metal purification methods based on a liquid-liquid extraction. This method is comprised of two steps; oxidation of impurities followed by dissolution of oxides in the slag phase. Thus, when the slag is finally separated from the metal, concentrations of impurities dissolved in slag phase are decreased in the target metal. Numerous studies have been carried out for purification of MG-Si through slag treatment. Slag mixtures used for silicon purification should meet the following requirements:

- Slag should be immiscible with the molten metal phase
- The melting point of slag should be almost equal to the melting point of silicon
- Slag should not contaminate the molten silicon (dissolution of slag components in metals phase changes the resistivity of silicon crystal)
- There should be a greater chemical affinity between impurities and slag rather than silicon and slag [5]

According to the Ellingham diagram for oxides (Figure 2.6), elements like Al, Mg, Ba and Ca are more likely to be oxidized than silicon. Hence, these impurities can be preferentially removed from silicon by slag refining. On the other hand, removing impurities such as B and P is

challenging because of their lower affinity for oxygen compared with silicon. Thus, slag composition should be carefully adjusted in order to achieve effective B and P removal via slag treatment. Previous studies on B and P removal from silicon via slag refining, have been mainly focused on optimizing slag chemistry (slag basicity and oxygen potential which is shown as p_{O_2}) in order to maximize the removal process of these deleterious elements [37-41].

As mentioned before, slag treatment consists of two reactions: oxidation and dissolution. These two reactions for the extraction of B from silicon are shown in Eq. 2.12 and Eq. 2.13, respectively. The square brackets show the solute, i.e. B, in the solvent, i.e. Si while the round brackets show the solute in the slag.

$$[B] + 3/4\ O_2 \rightarrow 1/2\ (B_2O_3) \qquad \text{Eq. 2. 12}$$

$$1/2\ (B_2O_3) + 3/2\ O^{2-} \rightarrow (BO_3^{3-}) \qquad \text{Eq. 2. 13}$$

Eq. 2.14 represents the overall reaction of B removal:

$$[B] + 3/2\ O^{2-} + 3/4\ O_2 \rightarrow (BO_3^{3-}) \qquad \text{Eq. 2. 14}$$

Depending on partial pressure of oxygen (p_{O_2}), P can be dissolved in slag in two different forms. When p_{O_2} surpasses some critical value, phosphate is formed and dissolved in the slag (Eq. 2.15). Otherwise, P can also be removed in the form of phosphide (Eq. 2.16).

$$[P] + 3/2\ O^{2-} + 5/4\ O_2 \rightarrow (PO_4^{3-}) \qquad \text{Eq. 2. 15}$$

$$[P] + 3/2\ O^{2-} \rightarrow (P^{3-}) + 3/4\ O_2 \qquad \text{Eq. 2. 16}$$

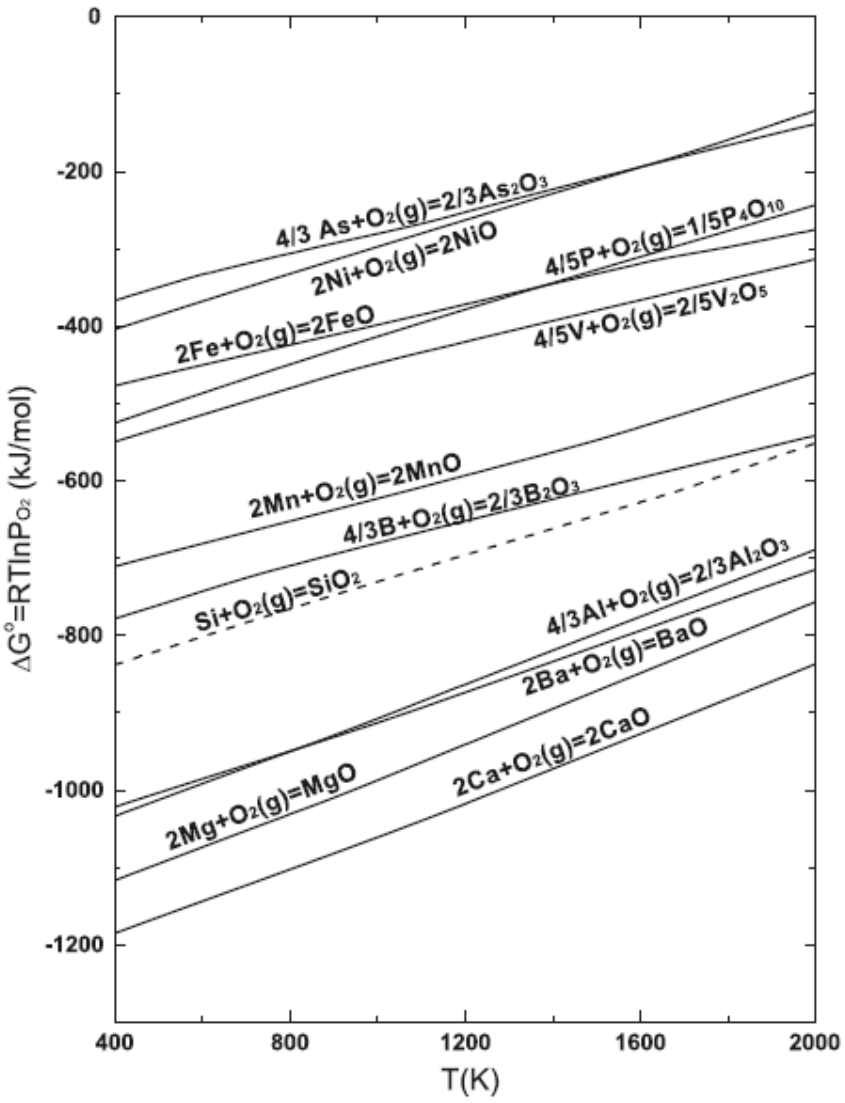

Figure 2. 6. Ellingham diagram for various oxides [42].

Slag basicity is a factor that plays a vital role in removal of impurities. It is defined as the concentration of free oxygen ions obtained from dissociation reaction of basic oxides (Eq. 2. 17). This reaction provides the free oxygen ions required in B and P removal reactions. Considering the acidic nature of B and P oxides, basic slags are needed to promote their removal from silicon. In order to increase the basicity of slag, alkali and alkali earth oxides can be used as suitable

components of slag [43]. Oxygen potential, which is defined as the oxygen that is produced in Si-SiO_2 equilibrium (Eq. 2. 18), is another parameter that affects the removal of impurities [9, 44-46]. Eq. 2.18 provides the required oxygen (O_2) in B and P removal reactions. To remove the impurities effectively, SiO_2 content of the slag should be carefully controlled.

$$(CaO) \rightarrow Ca^{2+} + O^{2-} \quad \text{Eq. 2. 17}$$

$$(SiO_2) \rightarrow Si + O_2 \quad \text{Eq. 2. 18}$$

Partition ratio, L_I, also known as distribution coefficient of impurity I (Eq. 2.19), is often used for evaluating the removal efficiency of the slag for each impurity after reaching equilibrium. Depending on the partition ratios of various impurities and the purity requirement of the high-purity silicon, slag treatment should be repeated to reach the target purity level.

$$L_I = \frac{\text{Mass fraction of impurity in slag}}{\text{Mass fraction of impurity in silicon}} \quad \text{Eq. 2. 19}$$

Excessive amount of basic oxides results in lower oxygen potential because there is a great affinity between basic oxides and SiO_2. The above behavior may lead to a decline in removal efficiency of impurities [47]. In other words, while higher slag basicity is expected to improve impurity removal, it causes a decrease in activity of SiO_2 which in turn affects the oxygen potential and may interfere with the removal of impurities.

In the following section, the slag mixtures previously employed for silicon refining are categorized as binary, ternary and quaternary systems. Detailed information on the composition of the slag and the partition ratios are also provided.

Binary systems

Teixeira and Morita [48] used the CaO–SiO_2 binary system at 1823 K in order to investigate the efficiency of slag refining for B removal. Figure 2.7 shows the partition ratio of B (L_B) vs. basicity (CaO/SiO_2). While increasing basicity up to 0.8 results in a decrease in L_B, further

increase in the basicity leads to an opposite effect. They have also investigated the effects of CaF_2 and Na_2O addition. Their results associated with the addition of CaF_2 and Na_2O are presented in the next section (Ternary systems).

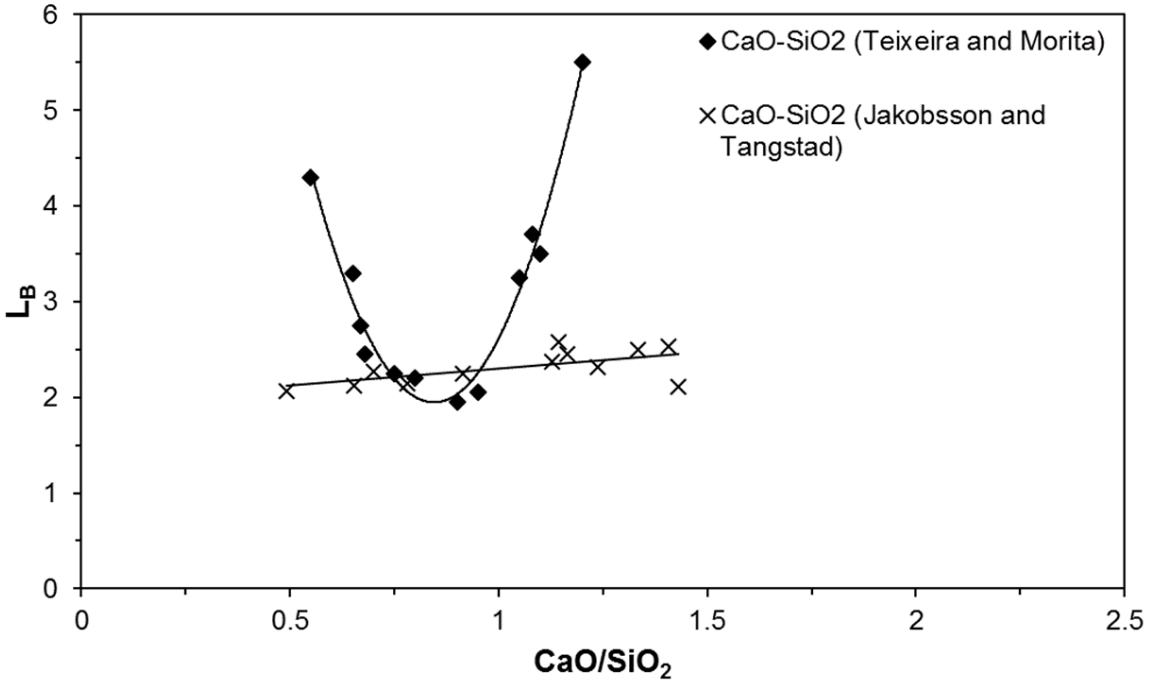

Figure 2. 7. Partition ratio of B as a function of basicity of $CaO\text{-}SiO_2$ slag [48, 49].

Jakobsson and Tangstad [49] studied the partition ratio of B in $CaO\text{-}SiO_2$ and $MgO\text{-}SiO_2$ binary slags at 1873 K. Figures 2.7 and 2.8 represent the results of $CaO\text{-}SiO_2$ and $MgO\text{-}SiO_2$, respectively. The difference in the results of the aforementioned studies presented in Figure 2.7 might be associated with different experimental conditions such as refining process duration and slag/metal ratio. Higher slag/metal mass ratio (2.2:1 vs. 1:1) and longer holding time (18 h vs. 6 h) are the potential reasons for higher partition ratio values in Teixeria's results.

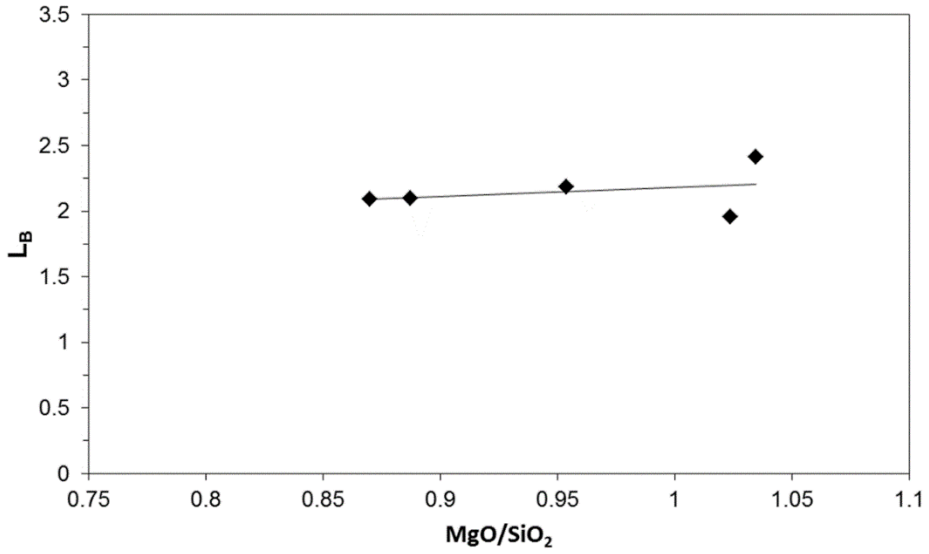

Figure 2. 8. B partition ratio in MgO-SiO2 slag as a function of slag composition[49].

B removal from MG-Si using Li_2O-SiO_2 slag at 1973 K was investigated by Lai et al. [50]. According to their findings, higher amount of basic oxide, i.e. Li_2O, can lead to lower B content in silicon. However, B content levels off at Li_2O/SiO_2 values above 1.5. Thus, they concluded the Li_2O/SiO_2 ratio of 1.5 is the optimum point for obtaining maximum B removal efficiency in this binary. B concentration of MG-Si was successfully reduced to 0.4 ppmw (from 8.6 ppmw) after 30 minutes of holding time when slag with composition of 60 wt.% Li_2O-40 wt.% SiO_2 and slag/metal ratio of 3 were applied. B removal is hindered with further increase in Li_2O/SiO_2 ratio since it causes a decrease in oxygen potential. It is worth mentioning that Li_2O is an expensive oxide therefore its application in slag refining is not favorable from economical point of view.

Ternary systems

Following the initial CaO-SiO_2 binary system, CaO-SiO_2-CaF_2 and CaO-SiO_2-Na_2O ternary slags have been utilized for the purpose of broadening the basicity range [51]. 25 and 40 wt%

CaF_2 were added to the $CaO\text{-}SiO_2$ binary system in order to assess the effect of basicity on silicon refining. As depicted in Figure 2.9, CaF_2 addition does not have a significant effect on B removal, comparing with $CaO\text{-}SiO_2$ binary system. The slag/silicon ratio was equal in both the binary and ternary experiments. As a result, the effective amounts of silica and lime were lower in the ternary systems compared to the $CaO–SiO_2$ binary. This might be responsible for not obtaining an improvement in L_B despite the addition of CaF_2. Na_2O addition to the CaO-SiO2 binary (CaO/SiO_2=1.21) led to higher partition ratio and lower melting temperature. However, since Na_2O becomes volatile at high temperatures, it is necessary to reduce the duration of experiments containing Na_2O. Three slags containing 0%, 7% and 10% Na_2O were examined and the results are indicative of a direct relation between L_B and the Na_2O content of slag.

The addition of Li_2O to $CaO\text{-}SiO_2$ binary [14] has also been examined with the aim of improving B removal. It was found that the final concenteration of B in Si, while the slag/metal ratio was 1:1, is not significantly affected when the LiO_2 content of slag increases up to 20%. However, by increasing slag/metal ratio to 4:1, B concentration in the refined Si decreased to 1.3 ppmw from 18 ppmw.

Wang et al. [52] employed $CaO\text{-}SiO_2\text{-}CaCl_2$ ternary as the slag at 1723 K. The process involves B oxidation (Eq. 2. 12) in presence of an oxidizing slag followed by transferring boron oxide to the slag phase and its chlorination with $CaCl_2$ (Eq. 2.20). Finally, B leaves the molten slag in form of BOCl gas.

$$BO_{1.5}\ (l \text{ in slag}) + 1/2\ CaCl_2\ (l) \rightarrow BOCl\ (g) + 1/2\ CaO\ (s) \qquad \text{Eq. 2. 20}$$

Eq. 2.21 is the overall reaction of oxidized chlorination and evaporation for B removal from Si.

$$B\ (l \text{ in slag}) + 3/4\ O_2\ (g) + 1/2\ CaCl_2\ (l) \rightarrow BOCl\ (g) + 1/2\ CaO\ (s) \qquad \text{Eq. 2. 21}$$

Figure 2.10 shows the mechanism of this process.

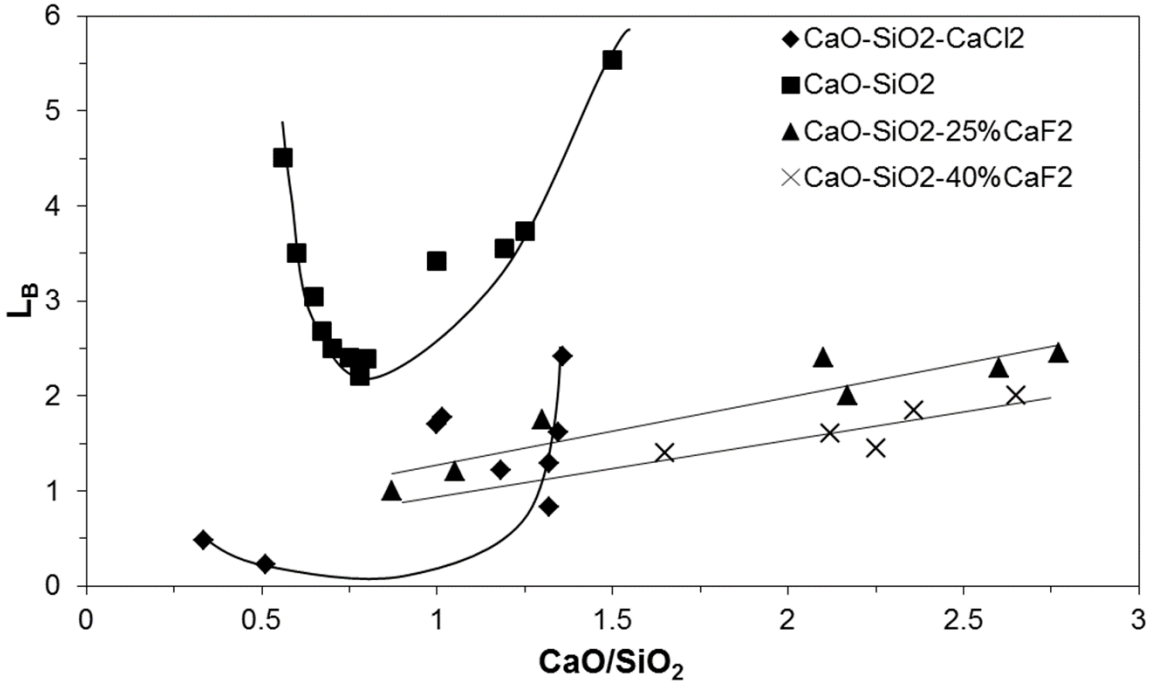

Figure 2. 9. Partition ratio of B as a function of basicity of slags for $CaO\text{-}SiO_2$, $CaO\text{-}SiO_2\text{-}CaCl_2$, $CaO\text{-}SiO_2\text{-}25\%CaF_2$ and $CaO\text{-}SiO_2\text{-}40\%CaF_2$ systems [48, 51, 52].

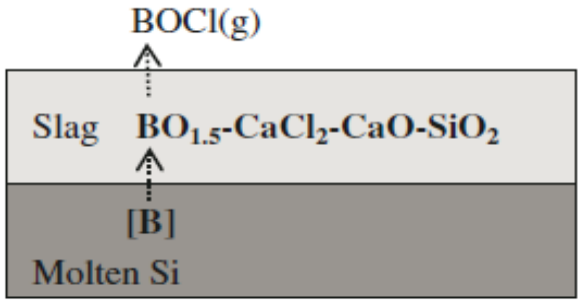

Figure 2. 10. Mechanism of B-removal through oxidized chlorination and evaporation process [52].

Figure 2.9 also demonstrates a comparison between the L_B results of oxidized chlorination process and those of the binary and ternary slags used by Teixeira and Morita [51]. The L_B values in this study are less than that of $CaO\text{-}SiO_2$ binary system since the activity of oxygen in

the ternary system is lower than the binary. However, the variation of L_B versus basicity follows the same pattern in both systems, i.e. L_B reaches a minimum at the basicity (CaO/SiO_2) of around 0.8. If the mass of silicon is assumed constant after the refining process, the removal efficiency of B is calculated as $1\text{-}C_{B\ final\ in\ Si}$ (ppmw)/$C_{B\ initial}$ (ppmw) where C_B is the concentration of B. Three binary systems of 33 mol% CaO-67 mol% SiO_2, 15 mol% CaO-85 mol% $CaCl_2$, and 50 mol% SiO_2-50 mol% $CaCl_2$ were examined in this work. An improved B removal efficiency in the ternary systems, compared with the three binary systems mentioned above was reported. It is worth mentioning that the data point with the lowest basicity on $CaO\text{-}SiO_2\text{-}CaCl_2$ line in figure 2.9 is indicative of the $CaO\text{-}SiO_2$ binary in this study. It is clear that L_B for this point (0.47) is well less than L_B obtained in Teixeira and Morita's work (4.51) [48].

Using $CaCl_2$ as one of the slag components, B concentration decreased to 30 ppmw from 150 ppmw while 47 mol% CaO-23 mol% SiO_2-30 mol% $CaCl_2$ was utilized. Although both $CaO\text{-}SiO_2\text{-}CaCl_2$ and $CaO\text{-}SiO_2\text{-}CaF_2$ ternaries led to similar L_B values, the $CaCl_2$ slag is more favorable because B can also be removed in the form of BOCl. In another method based on chlorination of borate, Cl_2 gas was utilized as a part of the furnace atmosphere while $CaO\text{-}SiO_2$ binary was utilized as slag [53]. Cl_2 gas treatment decreases B content of the slag by 21%. It should be noted that a considerable amount of Si is lost by chlorination in this method.

CaF_2 addition to the binary of $Li_2O\text{-}SiO_2$ was examined to lower the melting point and viscosity of the slag, which is followed by an improvement in B removal [50]. However, CaF_2 was unable to improve the removal efficiency. It was proposed that the activity of SiO_2 is probably reduced as the CaF_2 is added. In other words, F^- ion, which is derived from CaF_2, breaks the silica network and the bridging oxygen is transformed into free oxygen so that CaO is formed. This resulted in lowering the activity of SiO_2 which had a negative effect of removal efficiency of B.

The effect of basicity of 20%Al_2O_3–BaO–SiO_2 ternary on removal of B and P was investigated by Johnston and Barati [54]. Their results are indicative of a direct relationship between L_B and BaO/SiO_2 ratio until BaO/SiO_2 ratio equals 0.8. L_P remains constant with no significant change by variations in slag basicity. Since the L_B and L_P values reported for this system are all less than unity, the 20%Al_2O_3–BaO–SiO_2 ternary looks inefficient for B and P removal.

B removal from Si by ternary slags of CaO-MgO-SiO_2 and CaO-Al_2O_3-SiO_2 was investigated by Jakobsson and Tangstad [49]. Changing the amount of CaO or MgO in the ternary of CaO-MgO-SiO_2 did not have a major effect on partition ratio of B and most of the values were between 2 to 2.5. Moreover, varying SiO_2 content of the slag had a negligible effect on L_B. In the case of the CaO-Al_2O_3-SiO_2 system, L_B drops from ~2.4 to ~1.3 by increasing Al_2O_3 content while CaO is constant. Also, the CaO content of slag was not an effective factor for B removal. Fujiwara et al. [55] used the same ternary system (CaO-Al_2O_3-SiO_2) for removal of P from Si. According to their results, the presence of certain amount of calcium in Si melt results in P precipitation in grain boundaries in the form of phosphide. Based on their findings, dephosphorization occurs via phosphide formation (Eq. 2.16) which is attributed to the presence of Ca in Si melt. When CaO content of slag increases from 20 wt% to 31 wt%, L_P increases from ~0.01 to ~3. Higher CaO content results in higher basicity and lower oxygen potential, both of which promote the dephosphorization via phosphide formation.

Quaternary systems

Aiming at improving the partition ratio of P and B, distribution of impurities in slag treatment of metallurgical grade silicon using Al_2O_3–CaO–MgO–SiO_2 quaternary system at 1773 K has been studied [47]. The effect of basicity (CaO/SiO_2 ratio) and oxygen potential (SiO_2 /Al_2O_3 ratio) of

the slag on the partition ratios of B and P between slag and silicon have been investigated. Based on the findings of this study presented in figure 2.11, L_P slightly increases because of an increase in the basicity of slag. L_B initially increases until it reaches a maximum and then drops with further basicity increase. L_B decreases because of the decrease in oxygen potential which is due to lower activity of silica. In other words, partition ratio of B is controlled by two counterbalancing factors, namely oxygen potential and basicity of slag.

Figure 2.12 depicts the partition ratios of B and P versus oxygen potential of the slag. Both L_B and L_P have direct relation with SiO_2/Al_2O_3 ratio. A significant increase in L_P was observed when SiO_2/Al_2O_3 ratio was above 2. The highest L_B and L_P values were achieved when the slag with the highest SiO_2/Al_2O_3 ratio was utilized. Based on the above behavior, oxygen potential is a more operative factor compared with the slag basicity for optimization of B and P removal.

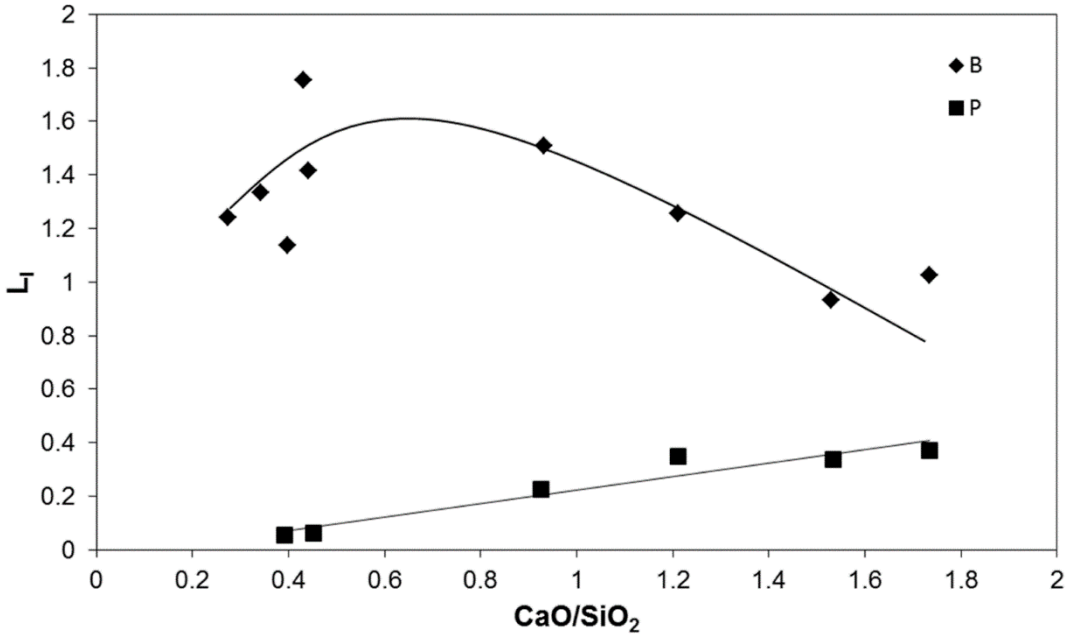

Figure 2. 11. Partition ratios of P and B vs. the basicity of 35 wt% Al_2O_3–CaO–3wt% MgO–SiO_2 slag at 1773 K [47].

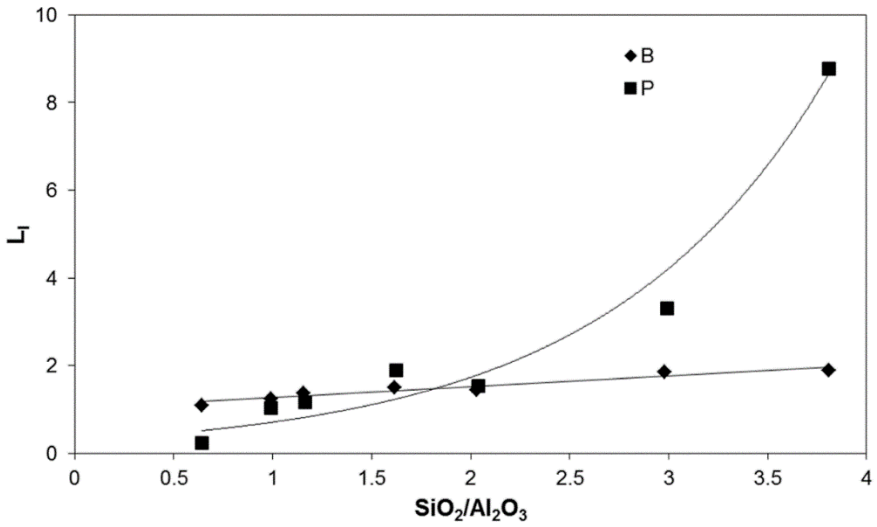

Figure 2.12. Partition ratios of P and B vs. oxygen potential of Al_2O_3–42wt% CaO–10wt% MgO–SiO_2 slag at 1773 K [47].

Results of the above study indicate that acceptable levels of B and P for SoG-Si cannot be achieved through a single-step slag refining of MG-Si. Strictly speaking, a multi-step route is required to achieve SoG-Si because the difference between the partition ratios of various impurities as well as their dissimilar response to the variations of the slag composition lead to the insufficiency of a one-step slag refining process [47].

2-2-4-5- Solvent refining

Solvent refining is a metallurgical refining technique based on solidification of silicon from a molten alloy. Basically, silicon is melted in the presence of a solvent metal to form an alloy. Metals that are chosen as solvent should fulfill the following requirements:

- Solvent metal should be immiscible with silicon below the melting point
- It should be miscible with silicon above the melting point

- The solvent should have higher affinity for P and B
- It should allow the separation of the alloy phase from purified silicon

When the temperature of the molten alloy is reduced, pure silicon is precipitated from the melt and the vast majority of impurity elements with low solubility in solid silicon are left in the molten phase. This happens because of the higher solubility of impurities in liquid compared with solid as well as the higher affinity of impurity elements for getter metal than silicon. After solidification, several routes can be employed in order to separate the purified silicon from the solvent metal or solvent-Si alloy. These routes include electrochemical dissolution, pyrometallurgical processes such as high temperature distillation, electromagnetic stirring [56, 57] and heavy media separation.

Added to the requirements mentioned above, the following factors should be considered before choosing a metal as the solvent.

- Availability of the pure metal in large quantities
- Evaporation loss of metal at working temperature
- Toxicity
- Cost [4, 58]

The metals that have been employed as the solvent in metallurgical refining of Si along with their advantages and disadvantages are presented below.

Aluminum

Metallic elements like titanium and iron have small segregation coefficient between solid and molten silicon, therefore they can be easily removed through solidification of silicon. However,

elements with relatively large segregation coefficient such as B and P (k_B=0.8, k_P=0.35 [31]) are not responsive to this process. Yoshikawa and Morita [56] investigated solidification of silicon from Si-Al melt. Figure 2.13 shows the binary phase diagram of Si-Al. They experimentally determined the segregation coefficient of impurities between solid silicon and molten Si-Al alloy. They found that these values were much smaller than segregation coefficients between solid and molten silicon. For instance, Figure 2.14 demonstrates the reduction of segregation coefficient of B and P after alloying silicon with 55.3 mol% aluminum. It also shows that reducing the temperature brings about segregation coefficient reduction. Therefore, they concluded that solvent refining of Si-Al melt is an effective purification method for removing B and P. Considering the small density difference between Al and Si, physical separation of Al from silicon dendrites might be problematic. However, applying electromagnetic stirring on the solidifying bath has shown to be successful for obviating this issue [56, 59].

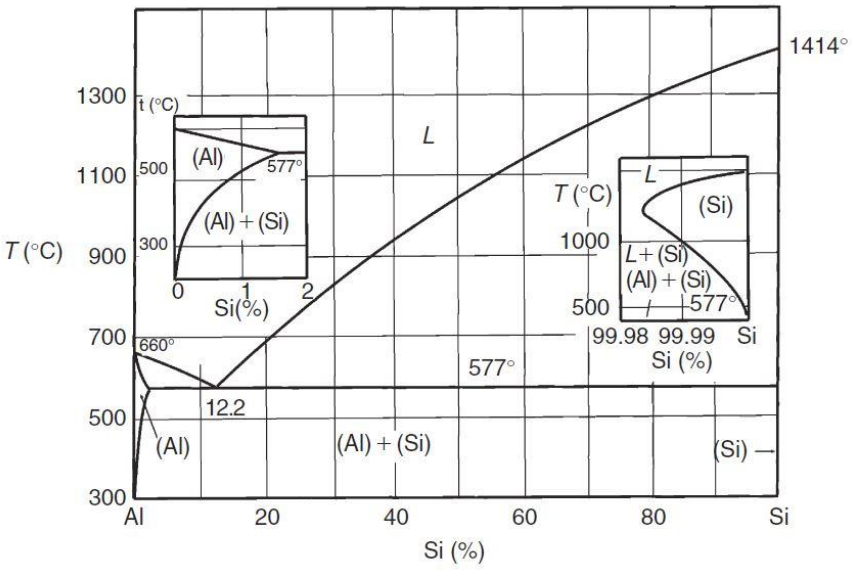

Figure 2. 13. Binary phase diagram of Fe-Si [60].

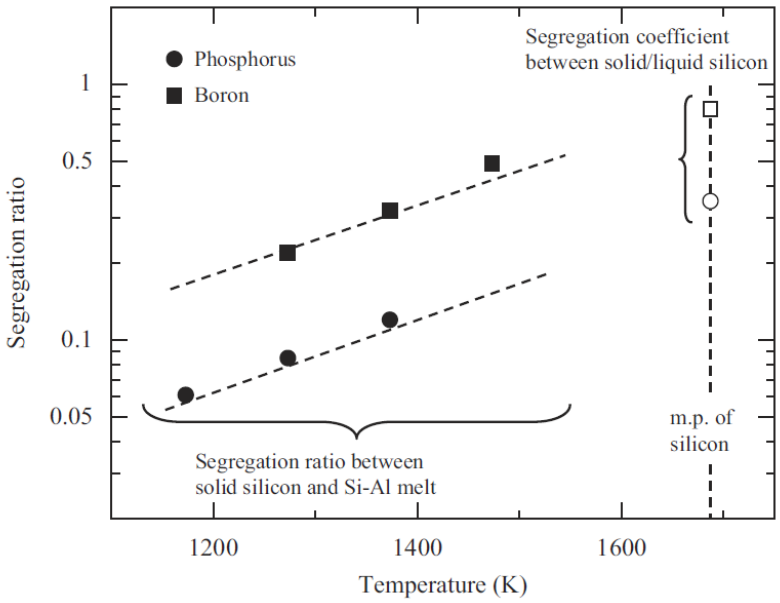

Figure 2. 14. Segregation coefficient of B and P as a function of temperature [56].

Copper

In order to address the challenges associated with physical separation, copper has been utilized as a solvent metal for silicon refining. Copper is considered as a potential solvent metal because of the following reasons:

- Lower solid solubility of copper in silicon compared with other solvents such as Al, Sn, Sb and As.
- Copper is the fastest diffusing element in solid state silicon (surface precipitation even at room temperature)
- Simple recovery of copper through aqueous electrolysis (for its reuse in the refining process) [61, 62]

Mitrašinović and Utigard [62, 63] performed solvent refining using Si-Cu followed by gravity separation to recover silicon from Si-Cu alloy. The biggest drawback of using copper as a

solvent metal is the separation of pure silicon and copper-silicon intermetallic after solidification process. In gravity separation method, the separation container is filled with the heavy liquid media and crushed particles of alloy. A minimum of 2 hours is considered as the sedimentation time. Three separate layers are formed: the light layer (upper layer) consists of pure silicon particles, the middle layer is the heavy liquid media and the heavy layer (bottom layer) consists of Cu-Si intermetallic particles. Heavy liquid media can be collected and re-used in next experiments. 86 percent of silicon was recovered through the above separation process. The parameter of separation ratio is defined as the ratio of concentration of impurities in Cu-Si intermetallic to that in Si particles. Results indicate that this technique is mostly effective for removal of Ag, Fe, Zr, and V with separation ratio of 11, 11.5, 12, 12.5, respectively. Figure 2.15 shows the Cu-Si binary phase diagram.

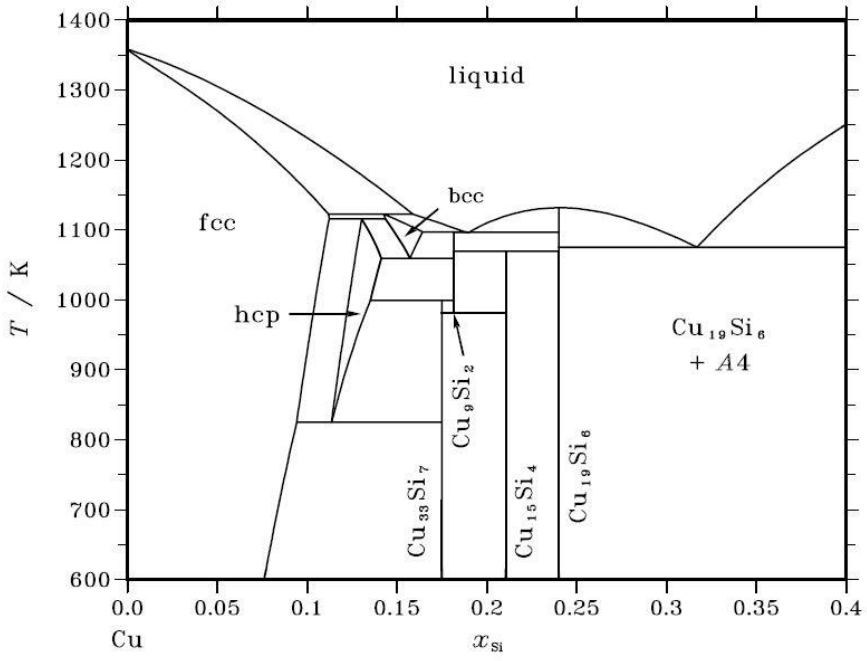

Figure 2. 15. Binary phase diagram of Cu-Si [64].

Tin

Tin has been successfully employed for removing impurities from silicon [65]. More than 98%of metallic impurities such as aluminum, iron, calcium, and titanium, over 60% of B and over 70% of P can be removed from silicon through solidification of Sn-Si alloys. Since tin is an electrically inactive element in silicon, small amounts of retained tin (10 ppmw) in SoG-Si is acceptable. In this process, Sn-Si alloys with initial compositions of 50, 70 and 95.8 mol% Si were prepared. Figure 2.16 shows the Si-Sn binary phase diagram. The bulk of purified silicon was mechanically separated and crushed into small particles. In order to remove any retained Sn-Si alloy, Si particles were leached with hydrochloric acid. Table 2.4 presents the concentration of the impurities in initial materials and refined Si.

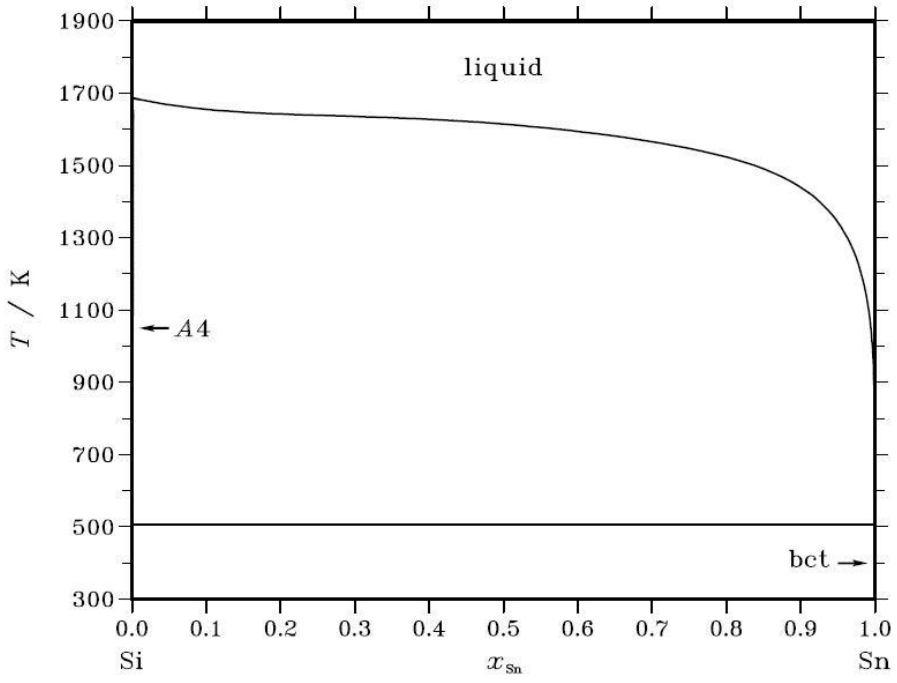

Figure 2. 16. Binary phase diagram of Si-Sn [64].

Table 2. 4. Impurity contents of initial Si, Sn and purified Si(ppmw) after solidification of Sn-Si alloy [65]

	Initial Materials		Purified Silicon		
Impurities	Sn	MG-Si	Sn-Si (50 mol% Si) (1605-1555K)	Sn-Si (70 mol% Si) (1633-1603K)	Sn-Si (95.8mol% Si) (1666-1636K)
Fe	39.8	2880	49.5	35.8	57.8
Al	11.7	1170	11.0	15.8	15.9
Ca	5.1	405	5.6	4.3	6.5
Ti	6.3	158	1.5	0.7	1.1
B	2.2	37.0	14.1	11.2	9.2
P	-	36.2	9.1	10.2	9.6
Sn	Major	122	5670	5680	3310

Iron

Esfahani and Barati [66] investigated the effectiveness of iron as an alloying metal for purification of MG-Si via solvent refining. They used alloys of Si-17wt% Fe for their experiments. Two different cooling conditions were studied. In the first condition, the alloy is cooled to 200 °C below the eutectic temperature, namely 1007 °C with rates between 0.5-3 °C/min. Next, the solidified alloy was quenched in water. In the second set of experiments, the alloy was cooled to 15 °C above the eutectic temperature, namely 1222 °C with the rate of 0.5 °C/min. The sample containing purified Si crystals and near-eutectic molten alloy is quenched in water. Figure 2.17 shows Fe-Si binary phase diagram.

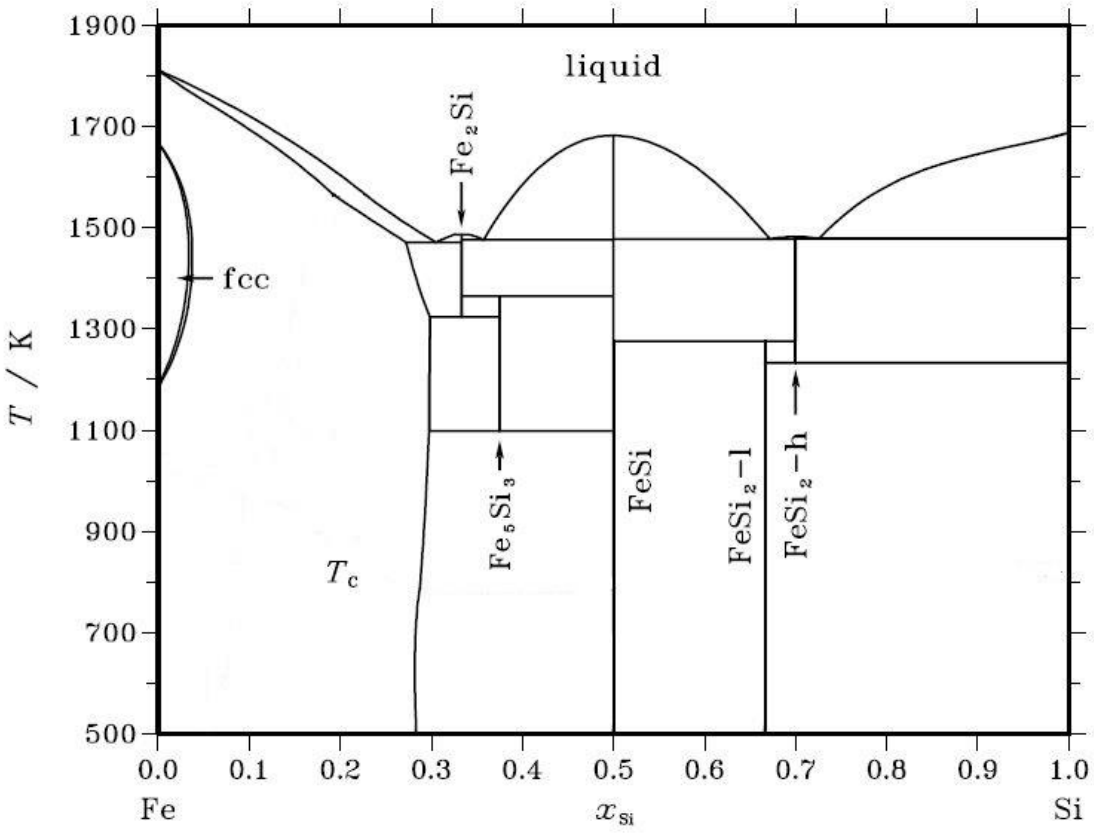

Figure 2. 17.Binary phase diagram of Fe-Si [64].

Based on their findings, when the alloy is cooled to below the eutectic temperature with a slow rate, concentration of impurities in the purified Si increases because of impurities diffusion from the alloy to Si. However, in the second condition, when the alloy is quenched from a temperature above the eutectic temperature, this issue is obviated. In other words, quenching from above the eutectic leads to a purer silicon. Concentration of some of the impurities in purified Si quenched from above eutectic temperature are as follows: Al: 10 ppmw, B: 2 ppmw, Mn: 3 ppmw, Ni: 3 ppmw, Cr: 1 ppmw, Fe: 1 ppmw, P: 29 ppmw. Also, concentration of V, Ba, Li, Be and Mg were all bellow 0.5 ppmw.

2-2-4-6- Combination of solvent refining and slag refining

The highest partition ratio of B reported for slag refining of silicon was about 5.5 when the SiO_2-CaO binary slag was utilized. An acceptable impurity level in SoG-Si can only be achieved if several times of slag treatment is applied, which in turn will result in employing large amount of slag. In order to improve the partition ratio, slag composition (namely basicity or oxygen potential of the slag) should be optimized. As previously discussed, these two slag properties are counterbalancing factors which means they cannot increase simultaneously. Thus, it is challenging to improve the partition ratio of impurities between slag and liquid Si only by slag treatment.

Slag refining of a Si-metal alloy is equivalent with simultaneous slag and solvent refining of Si. Simultaneous application of slag and solvent treatment is more efficient compared with using one of those processes. Additionally performing two high temperature processes at the same time is favorable in terms of the process energy efficiency. A few researchers have attempted slag refining of Si alloys with the aim of improving the impurity removal from silicon. A summary of their findings is presented in the following section:

Ma et al. [7, 67] examined B removal via slag refining of Si-Sn alloy at 1673 K. A mixture of CaO-SiO_2-24 mol% CaF_2 was utilized as the slag in their experiments. The slag composition and alloy composition effects on B removal were separately investigated. For studying the effect of slag composition, Si-30.5 mol% Sn was chosen as the alloy while CaO/SiO_2 ratio was varied. Partition ratios obtained in their study (between molten alloy and slag) and previous studies (between slag and molten Si [50]) are depicted in figure 2.18. It is obvious that B partition ratio in both cases (Si/slag and Sn-Si/slag) is directly related to CaO/SiO_2 ratio. The partition ratios

associated with Sn addition, are almost five times higher than that of Si/slag system which indicates the major effect of Sn addition. It is worthwhile mentioning that the slag used in Si/Slag case originally contained 25 and 40 wt% CaF_2. However, in figure 2.18 these compositions are converted to mol% to be comparable with the results of Sn-Si/slag case.

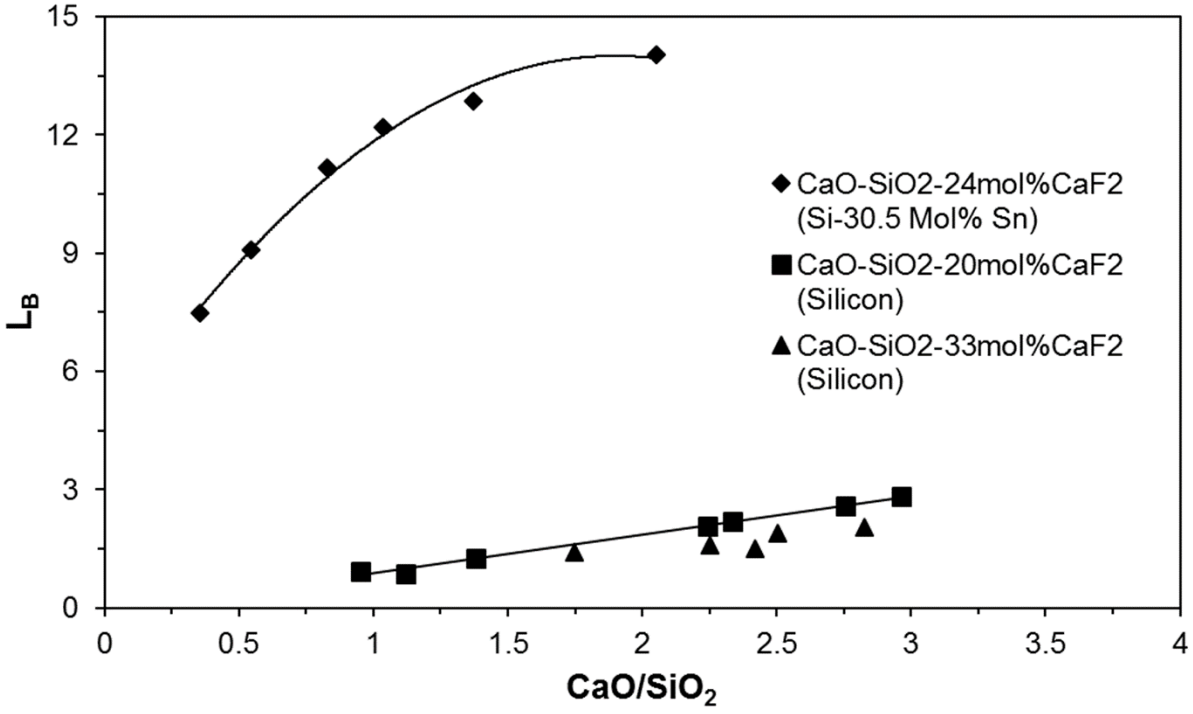

Figure 2. 18. Relationship between partition ratio of B and CaO/SiO2 ratio at 1673 K [7, 51].

Ma et al. [7] also studied the effect of alloy composition. Slag composition was fixed at 40.5% CaO-35.5% SiO_2-24 mol% CaF_2 while the Sn content of the alloy varied between 5-82 mol%. Figure 2.19 shows the partition ratio of B as a function of Sn content of the alloy. Partition ratio of B has dramatically increased with increasing Sn content of the alloy. Partition ratio of 200 was achieved employing Si-82.4 mol% Sn. The downside with higher Sn content is the decrease in silicon yield per unit mass of the alloy.

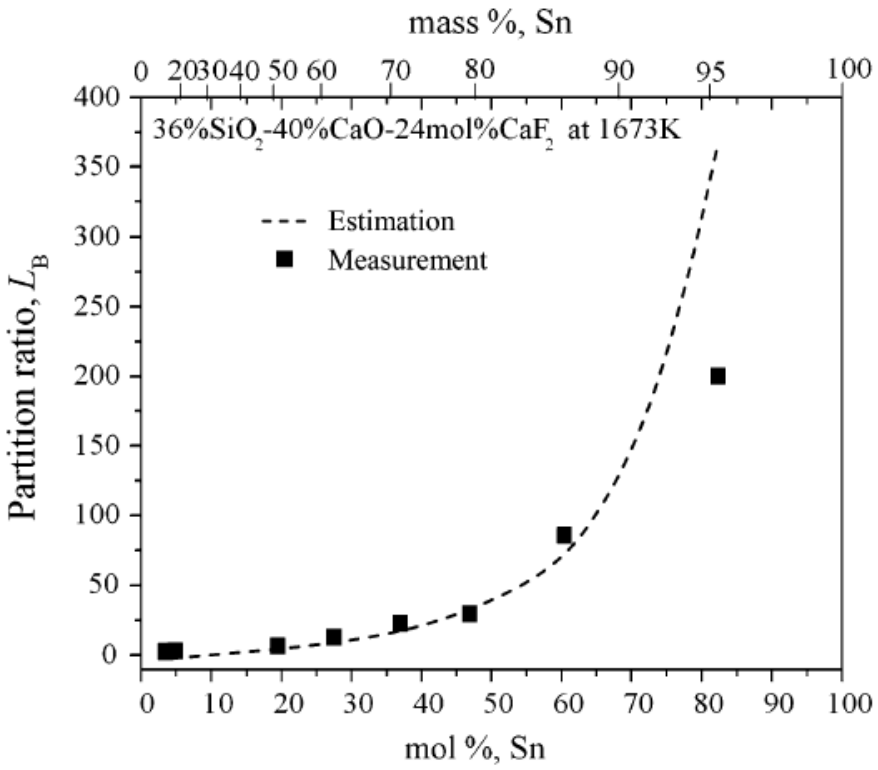

Figure 2. 19. Dependence of B partition ratio on Sn content of Si-Sn alloy [7].

Combination of solvent refining with Mn and slag treatment with $CaO-CaF_2$ at 1823 K has also been examined [68]. The dephosphorization efficiency was defined as $1-C_{P\ final\ in\ Si}$ (ppmw)/$C_{P\ initial}$ (ppmw) in this study. According to the results, the dephosphorization efficiency is in direct relation with the CaO content of slag up to 20 mass%. However, the dephosphorization efficiency levels off with further CaO increase. Dephosphorization of Si can be enhanced by high vapor pressure of P. This implies the contribution of two distinct removal mechanisms, i.e. slag treatment and evaporation.

B and P removal from Si-Cu alloy, at 1823 K, while $CaO-SiO_2-CaCl_2$ ternary was used as slag was investigated by Huang et al. [69]. Three various alloys of Si–Cu (Cu = 30, 50, and 70 wt%) were examined in order to investigate the effect of alloy composition. $CaCl_2$ was intentionally

added to decrease the melting point and viscosity of slag. Four various amounts of $CaCl_2$ in the range of 5-30 wt% were utilized. As results indicate, B and P concentrations of the refined alloy decrease when Cu content of alloy increases. In addition, B and P concentration of the alloy decreases with increasing $CaCl_2$ content of slag to 5 and 10 wt%, respectively. However, further increase in $CaCl_2$ negatively affects the B and P removal. 50 wt% Cu and 10 wt% $CaCl_2$ were chosen as the optimum condition considering the yield of silicon and the extent of impurity removal. When alloy of Si-50 wt% Cu and slag of 45 wt% CaO–45 wt% SiO_2–10 wt% $CaCl_2$ with 30 minutes slag treatment are employed, the final concentration of B and P in Si decreases from 3.12 to 0.35 ppmw and from17.14 to 7.27 ppmw, respectively. Partition ratios of B and P (between Si and slag) can be calculated as 5.26 and 0.53 form the data presented in this study. In addition, partition ratios of B and P (between Cu-Si and slag) are calculated as 2.75 and 0.39, respectively.

B and P removal from a Si-Cu alloy was also studied by Li et al. [6]. They applied various compositions of CaO-SiO_2-Na_2O-Al_2O_3 quaternary slag for refining an alloy of Cu and MG-Si at 1773 K (1500 °C). Results show that L_B and L_P values increase when Na_2O is added to the slag system but they decline after reaching maximums of 44.6 and 1.1 at 17 and 13 wt% Na_2O, respectively. Figure 2.20 depicts the effects of basicity (CaO/SiO_2) and oxygen potential (SiO_2/Al_2O_3) on B and P partition ratios while the concentration of Na_2O was constant at 20 wt%. It is clear that these two factors can significantly affect the partition ratios of B and P.

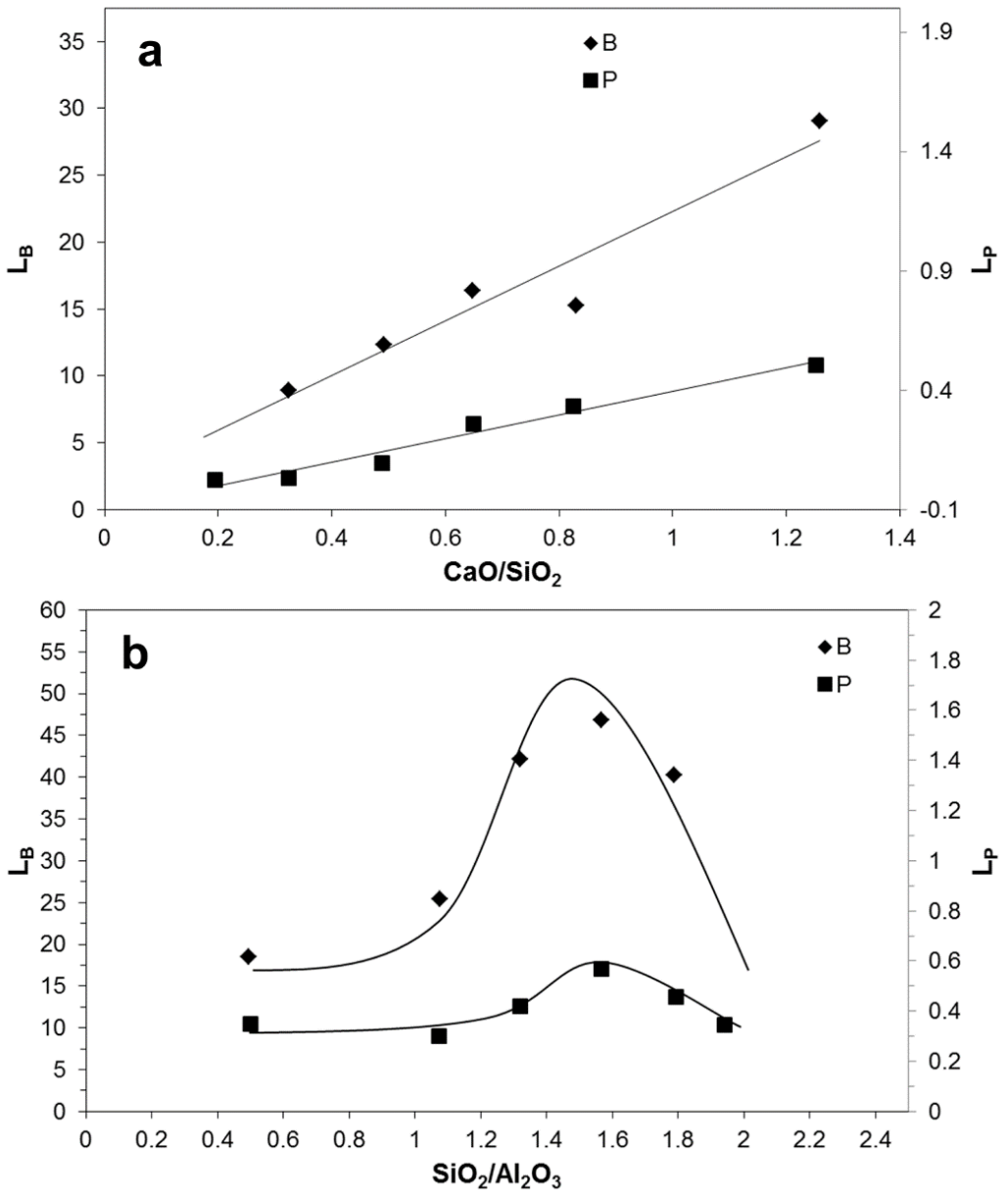

Figure 2. 20. Partition ratios of B and P as a function of a) CaO/SiO_2 and b) SiO_2/Al_2O_3 at 1773 K in two slags of $CaO\text{-}SiO_2$-20wt% Na_2O-24wt% Al_2O_3 and 36wt% $CaO\text{-}SiO_2$-20wt% $Na_2O\text{-}Al_2O_3$, respectively [6].

2-3- Scope and Objective

The current project investigates silicon purification via metallurgical refining processes with the ultimate goal of replacing the Siemens process with alternative less energy intensive routes. The objective of this research is to improve the removal efficiency of B and P from Si through combining two metallurgical processes, namely slag refining and solvent refining. Fe was chosen as the solvent metal in this study due to the following reasons: 1) it has low solid solubility in Si which leads to lower residual Fe in purified Si, 2) from an economical point of view, Fe is more favorable than other solvent metals such as Sn and Cu because of its lower price and 3) the byproduct of this process, ferrosilicon, can be used in other metallurgical processes. A ternary system of CaO-SiO_2-Al_2O_3 was also used as the slag. The effects of oxygen potential and basicity of slag on removal of B and P were investigated through changing the SiO_2/Al_2O_3 and CaO/SiO_2 ratios of slag, respectively. Also, normalized distribution and borate (phosphate) capacity for each slag composition was calculated. The objective of these calculations was to remove the effect of oxygen potential from the partition ratio values.

3-Materials and Methods

In this chapter, the specification of materials used in this study is presented together with the detailed description of the methods applied for slag refining of Si-Fe alloy. First, a master alloy of Si-Fe was prepared. The required time for the alloy and the slag to reach equilibrium was determined by some preliminary tests. Then, each slag was melted together with the same amount of alloy. After quenching each sample, the alloy phase was separated from the slag phase and each phase was separately digested in an acid solution for chemical analysis. Different steps of the experimental work are presented in figure 3.1.

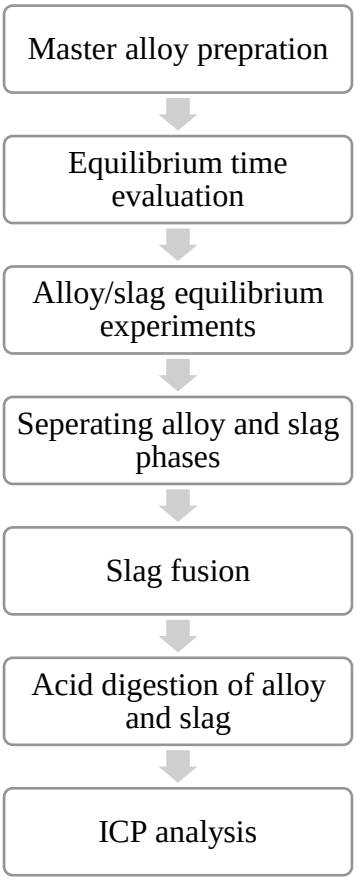

Figure 3. 1. Flowchart of the experimental procedure.

3-1- Materials

Si and Fe powders were used as the main components for preparing the ferrosilicon alloy in this study. This alloy may be referred to as the master alloy hereafter. Elemental B and P powders were also used as impurities in the master alloy. CaO, Al_2O_3 and SiO_2 powders were used as the slag making compounds. Table 3.1 shows a brief description of the materials and their suppliers. Chemical analyses of silicon and iron powders (main components of alloy phase) are shown in table 3.2 and table 3.3, respectively.

Table 3. 1. Characteristics of materials used for making alloy and slag.

Material	Description	Supplier
Silicon powder	Crystalline, -140 mesh, purity of min 98.5% (metals basis)	Alfa Aesar CA
Iron powder	Purity of min 99%	Sigma-Aldrich
Boron powder	Purity of 99.9%, 1 micron average	CERAC
Phosphorus powder	Purity of min 97%, containing less than 2000 ppm Fe	Sigma-Aldrich
Calcium oxide	CaO, 0.015% Fluoride max	Fisher Scientific
Aluminum oxide	Al_2O_3, purity 99.5 % (metals basis), containing less than 260 ppm Si and 90 ppm Fe	Alfa Aesar CA
Silicon (IV) oxide	SiO_2, purity of 99.5 % (metals basis), ~325 fused amorphous powder	Alfa Aesar CA
Sodium hydroxide	NaOH, , purity of min 97%, containing 10 ppm Fe max	Anachemia

Also, three different acids namely, nitric acid, sulfuric acid and hydrofluoric acid were used for digestion of alloy and slag phases (for ICP-OES analysis). Table 3.4 provides the purity and suppliers of these acids. It is worthwhile noting that B and P contents of the above acids are negligible.

Table 3. 2. Chemical analysis of silicon powder (provided by the supplier).

Impurity	Content
Si	98.5% min
Fe	0.5% max
Al	0.4% max
Ca	0.4% max
Ti	0.1% max

Table 3. 3. Chemical analysis of iron powder (provided by the supplier).

Impurity	Content (ppm)	Impurity	Content (ppm)
As	5	Pb	20
Cu	100	Zn	50
Mn	1000	Cl	20
Ni	500	S	100

Table 3. 4. Characteristics of acids used for digestion of alloy and slag samples.

Acid	Description	Supplier
Nitric acid	HNO_3, purity of 70%	Anachemia
Sulfuric acid	H_2SO_4, purity of 95%-98%	Fisher Scientific
Hydrofluoric acid	HF, purity of 48%	Sigma Aldrich

3-2- High Temperature Experiments

Before running any high-temperature experiment, the furnace was calibrated through the following procedure. The temperature of the furnace (shown on the furnace controller) was set at 1000 °C and was maintained there for one hour. Also, argon was purged into the furnace during the experiment. When it reached the desired temperature, another thermocouple was inserted through the upper cap of the furnace and placed in the uniform heating zone. The temperature shown on the thermocouple was recorded every two minutes for an hour. Figure 3.2 shows the difference between the temperature shown on the controller of the furnace and the one shown on the thermocouple. Since the additional thermocouple was directly exposed to the heating zone of the furnace while the furnace controller thermocouple was located outside of alumina tube, the temperature of the additional thermocouple is closer to the sample temperature. The difference of these two temperatures, which is about 14 °C is indicative of measurement error of the furnace thermocouple. Therefore, this correction was applied for all of the following experimental temperatures.

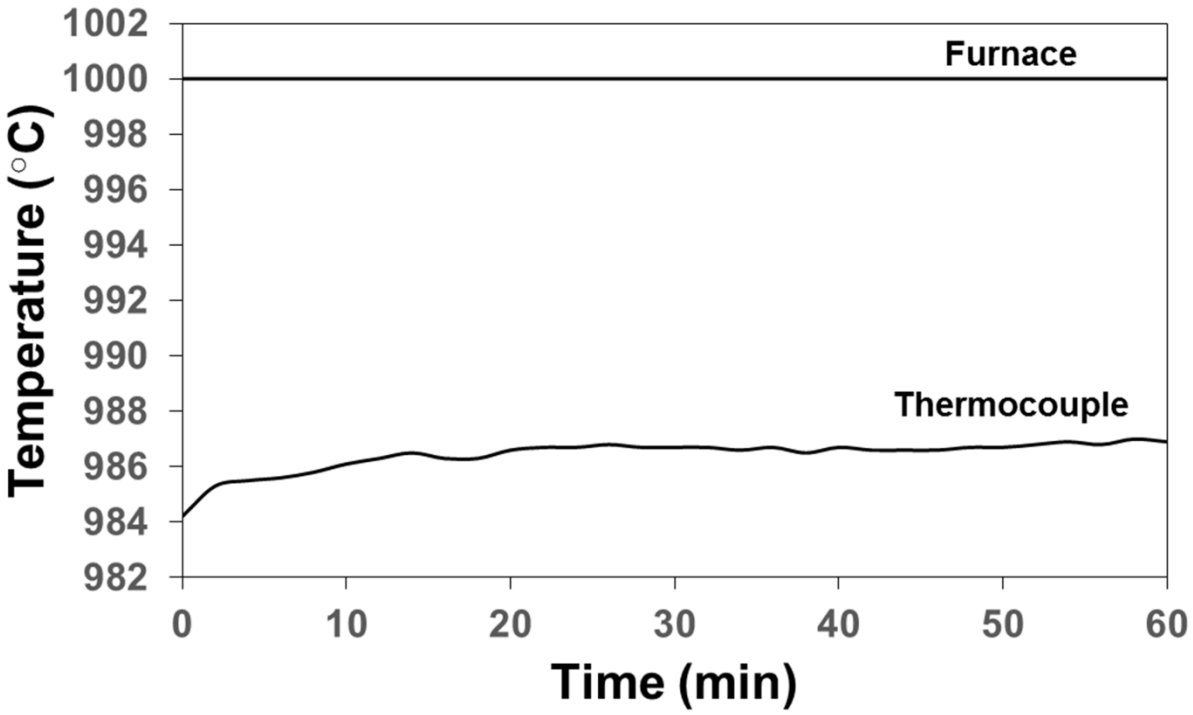

Figure 3. 2. The temperature difference between the furnace thermocouple and the external thermocouple at 1000 °C.

3-2-1- Fe-Si Master alloy

240 gram of silicon powder was thoroughly mixed with 60 gram of iron powder (Si-20 wt% Fe). B and P were also added as initial impurities. The mixture was charged into an alumina crucible with the diameter and height of 84 mm and 160 mm respectively (figure 3.3). The crucible was placed in a vertical tube furnace. Figure 3.4 and figure 3.5 show the schematic of the setup and the temperature profile that was used for melting the master alloy, respectively. As it is clear in the temperature profile, the sample was held at 1600 °C for 10 hours. Then it was slowly cooled down to room temperature. During the experiment, argon gas was purged with flow rate of ~8 lit/h from the upper cap to avoid sample oxidation. The prepared master alloy (Figure 3.3) was then crushed and ground for the subsequent refining experiments.

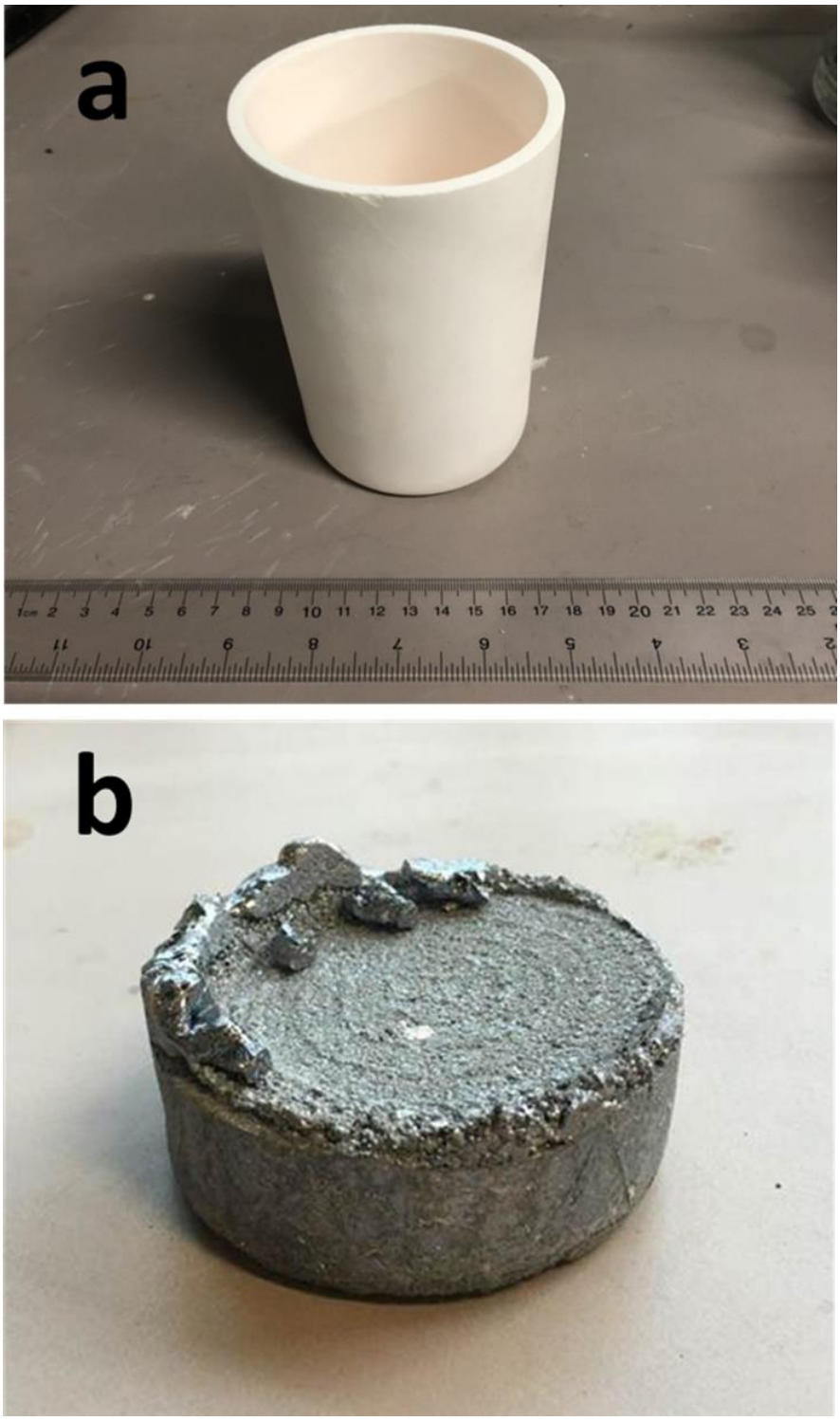

Figure 3. 3. a) Alumina crucible used for making master alloy b) Master alloy after melting.

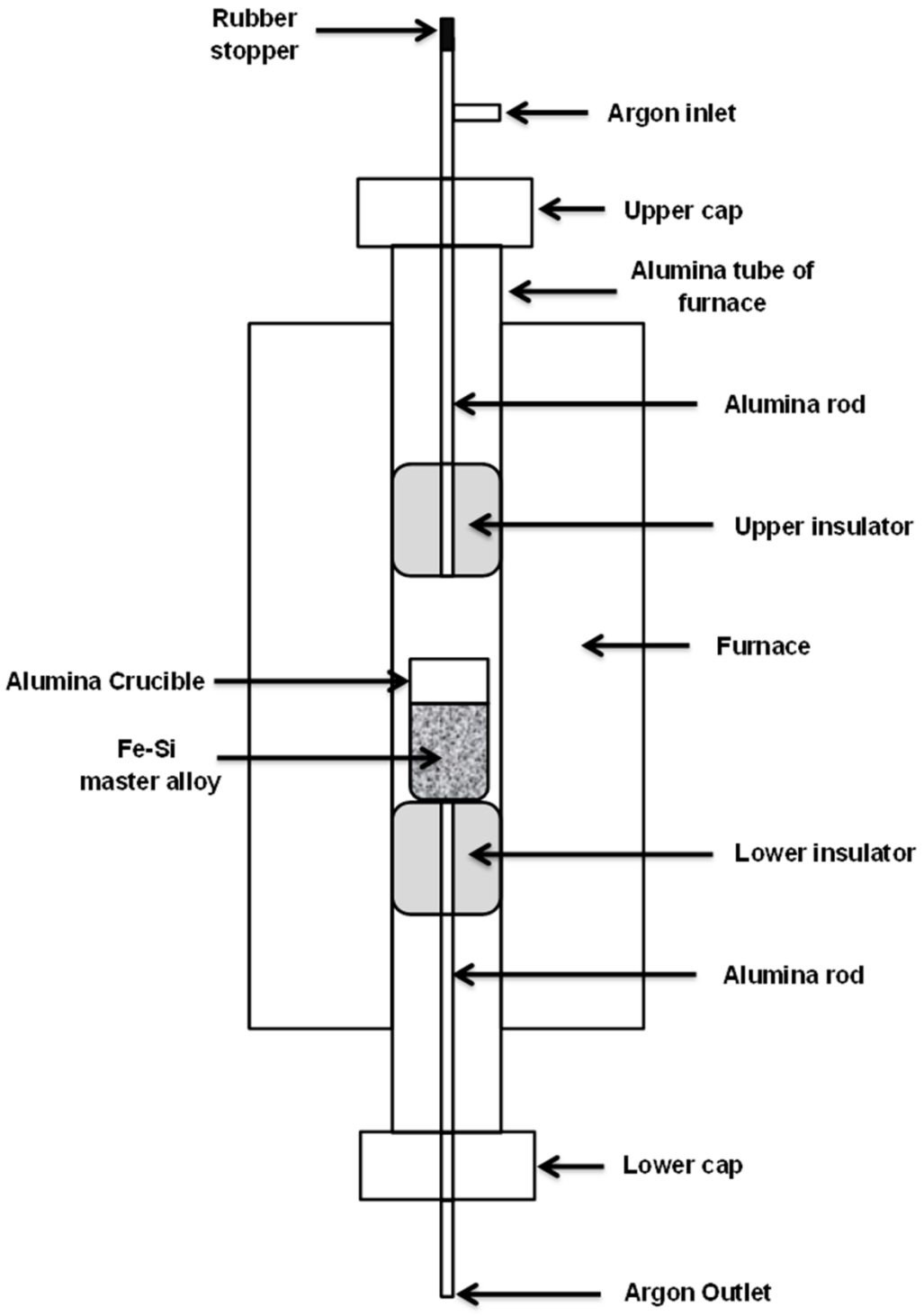

Figure 3. 4. Schematic of furnace setup used for making master alloy.

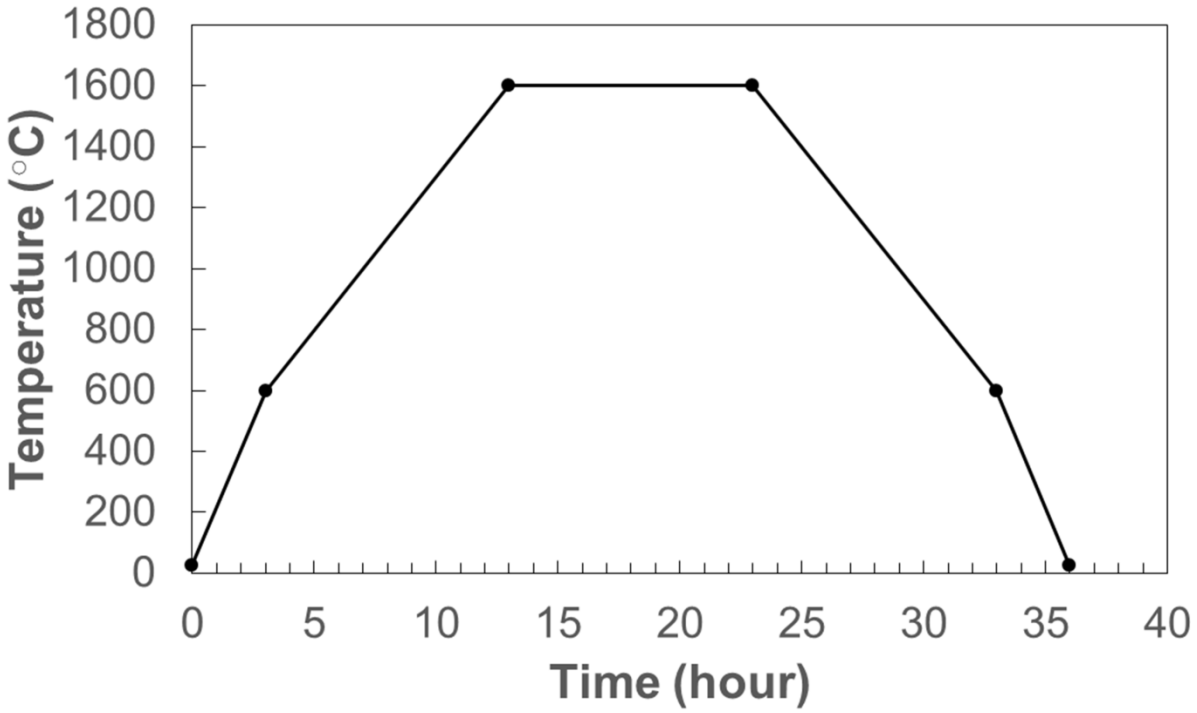

Figure 3. 5. Temperature profile for making master alloy.

According to the Fe-Si binary phase diagram (Figure 3.6), when a composition of 80 wt% Si-20 wt% Fe is cooled down, $FeSi_2$ will be stable in form of ζ_α and ζ_β phases at high and low temperatures, respectively. In other words, the $FeSi_2$ compound changes from a metallic phase with a tetragonal structure to a semiconducting phase with an orthorhombic structure at 982 °C (ζ_α to ζ_β) [70]. Scanning electron microscope (SEM) images and X-Ray diffraction (XRD) analysis results of the master alloy powder are shown in Figure 3.7 and 3.8, respectively. Energy-dispersive X-ray spectroscopy (EDX) results show that the dark phase in figure 3.7 are silicon while the bright phase is composed of $FeSi_2$. Sharp peaks of Si and $FeSi_2$ in XRD results also confirm that the master alloy was successfully prepared.

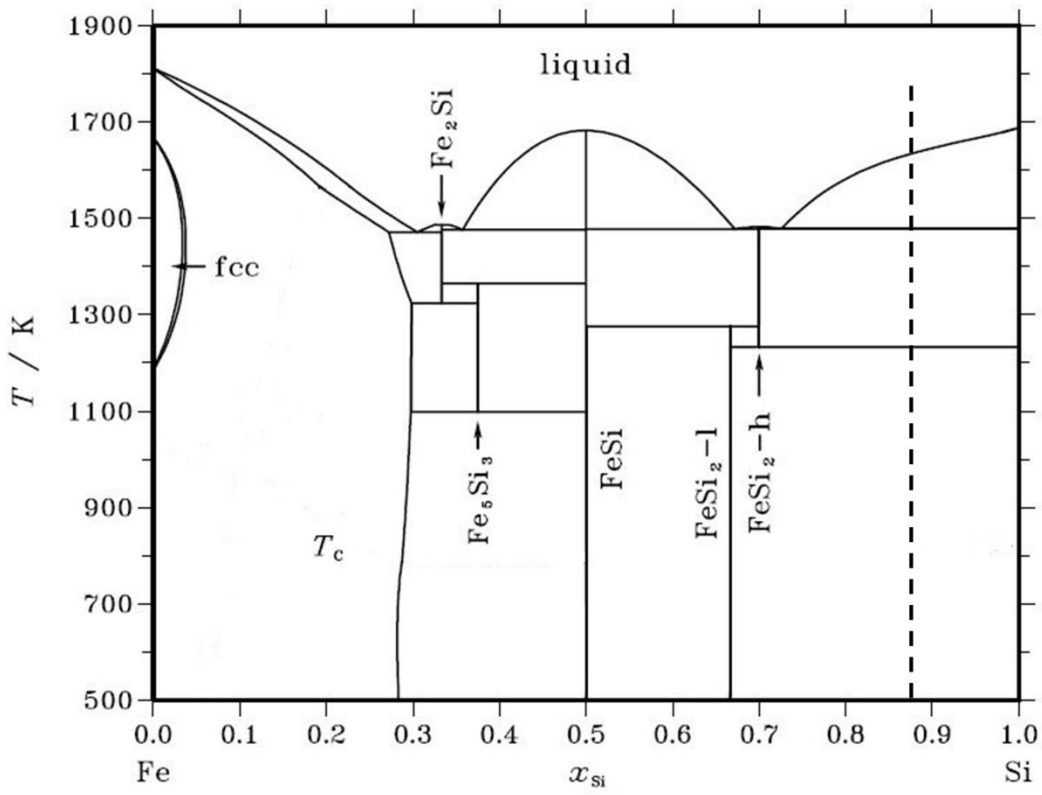

Figure 3. 6. Fe-Si binary phase diagram [64].

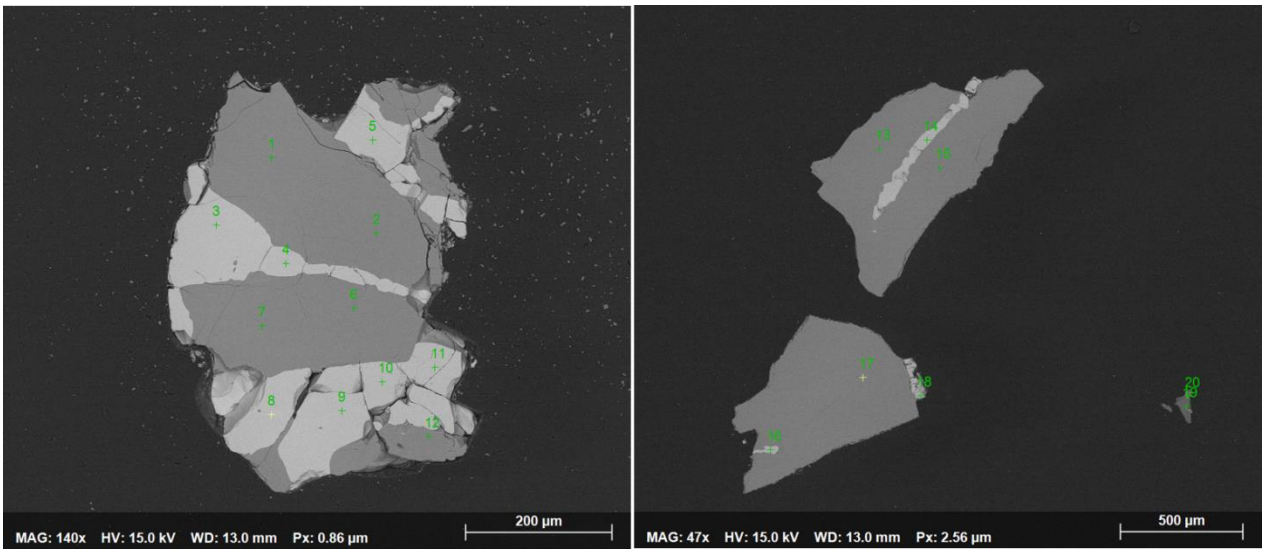

Figure 3. 7. SEM image of Fe-Si master alloy.

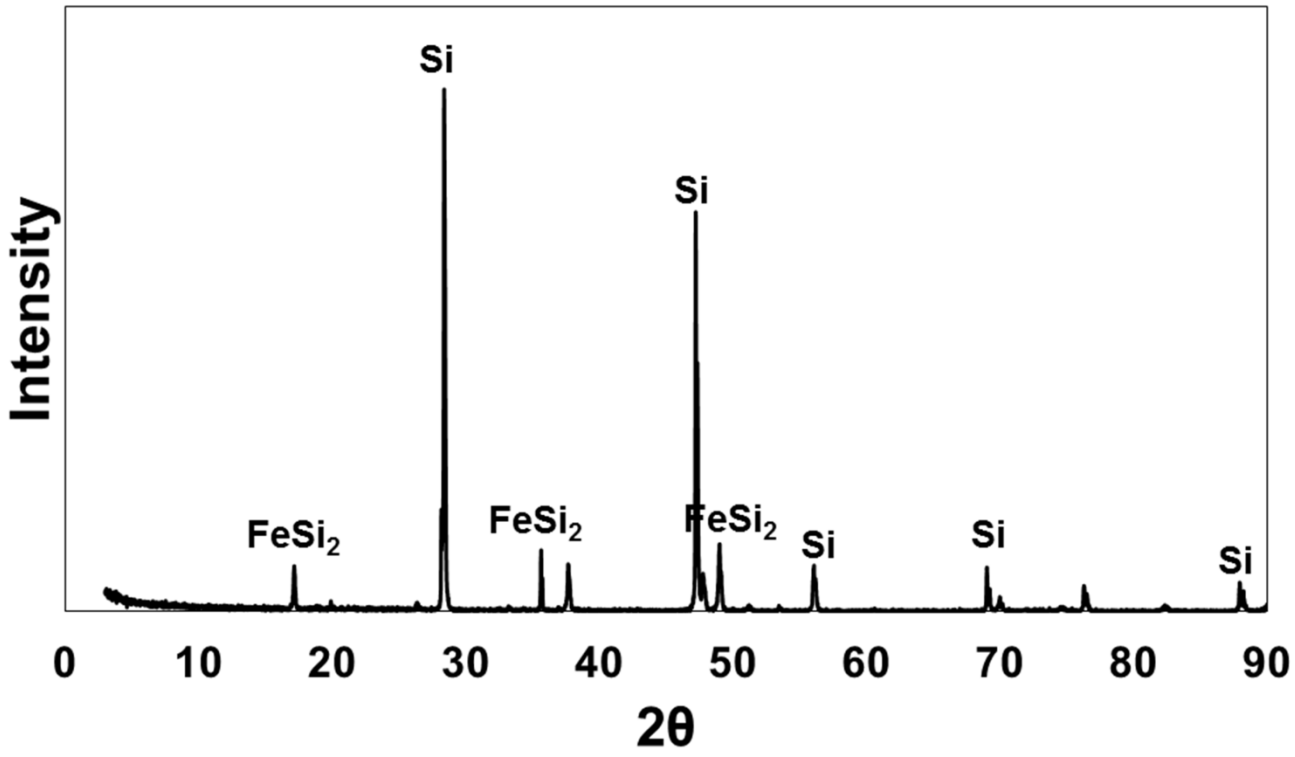

Figure 3. 8. XRD spectrum of the Fe-Si master alloy.

3-2-2- Alloy/Slag samples

CaO-Al_2O_3-SiO_2 ternary system with various compositions was used as the slag in the refining experiments. Table 3.5 shows these slag compositions. Each slag system was first pre-melted in a vertical tube furnace (figure 3.9). For this purpose, 5 g of each slag (e.g. slag #1: 2g of CaO + 0.25g of Al_2O_3 + 2.75g of SiO_2) was charged in a small alumina crucible and placed in the hot zone of the furnace. It was heated to 1600 °C followed by 10 hours of holding at the same temperature. Next, it was slowly cooled down to room temperature. 5 g of ground master alloy was added on top of the pre-melted slag. The alumina crucible was sealed with an alumina cap and a high-temperature ceramic adhesive. It was then placed in a larger graphite crucible and

they were suspended from the rubber stopper on the upper cap of the furnace. Figure 3.10 shows the schematic of the furnace set up for alloy/slag equilibrium experiments.

Table 3. 5. Initial slag compositions.

Samples	CaO (wt%)	Al_2O_3 (wt%)	SiO_2 (wt%)
1	40	5	55
2	40	7	53
3	40	10	50
4	40	15	45
5	40	20	40
6	40	30	30
7	40	35	25
8	20	15	65
9	25	15	60
10	30	15	55
11	35	15	50
12	45	15	40

Figure 3. 9. Vertical tube furnace used in the experiments and the top view of alumina crucible placed in a graphite crucible.

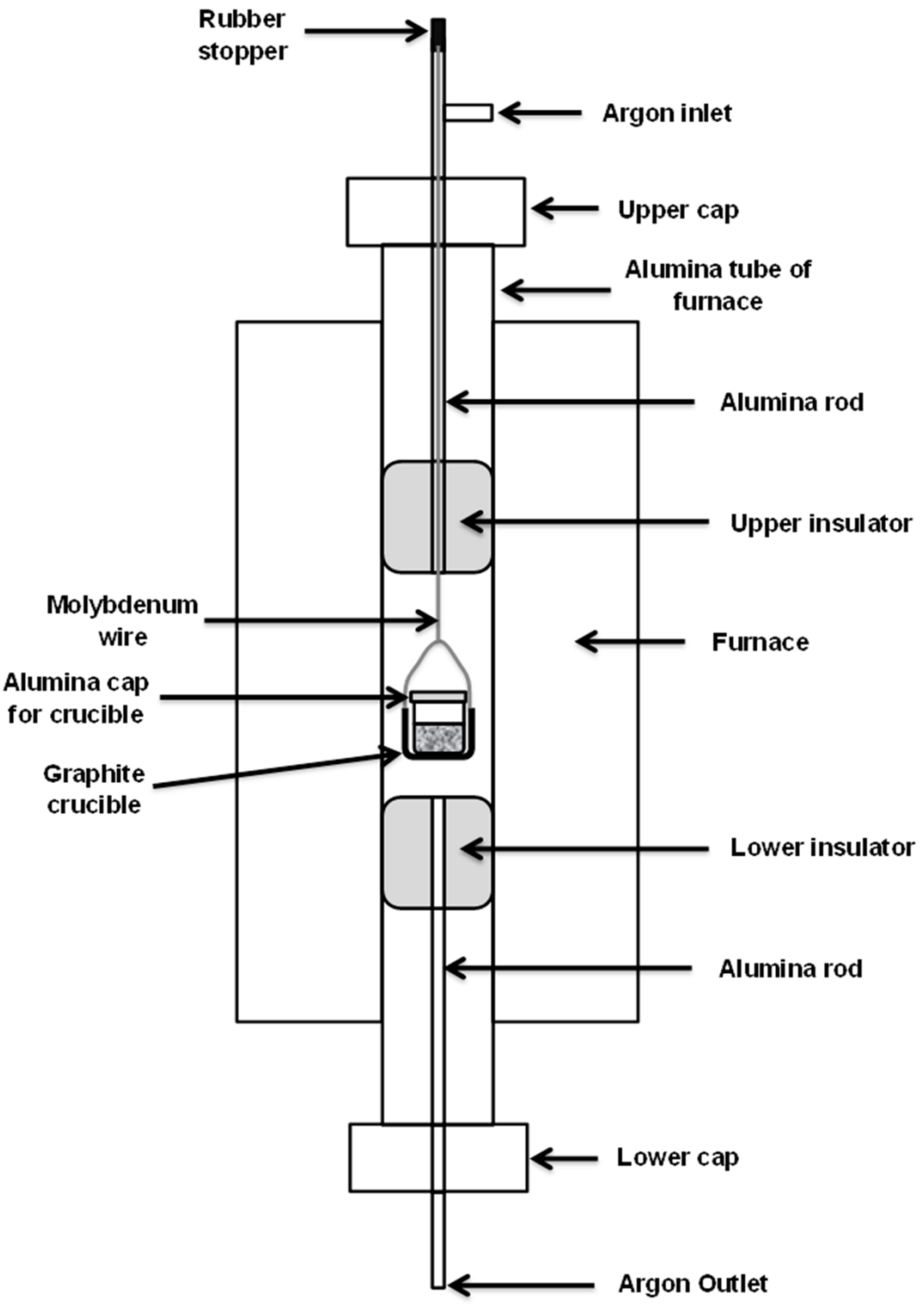

Figure 3. 10. Schematic of furnace setup used for hanging the alloy/slag samples.

Figure 3.11 shows the temperature profile used for alloy/slag equilibrium experiments. According to this profile, each sample was held at 1600 °C for 8 hour (equilibrium time). At this stage, the lower cap was opened and a bucket of water was placed under the lower part of the alumina tube. Next, the rubber stopper was pulled out of the upper cap and the Mo wire was cut so that the whole sample dropped down and quenched in the bucket of water. During all of these experiments, high purity argon was injected from the upper cap of furnace with flow of ~4 lit/h to avoid oxidation of the samples.

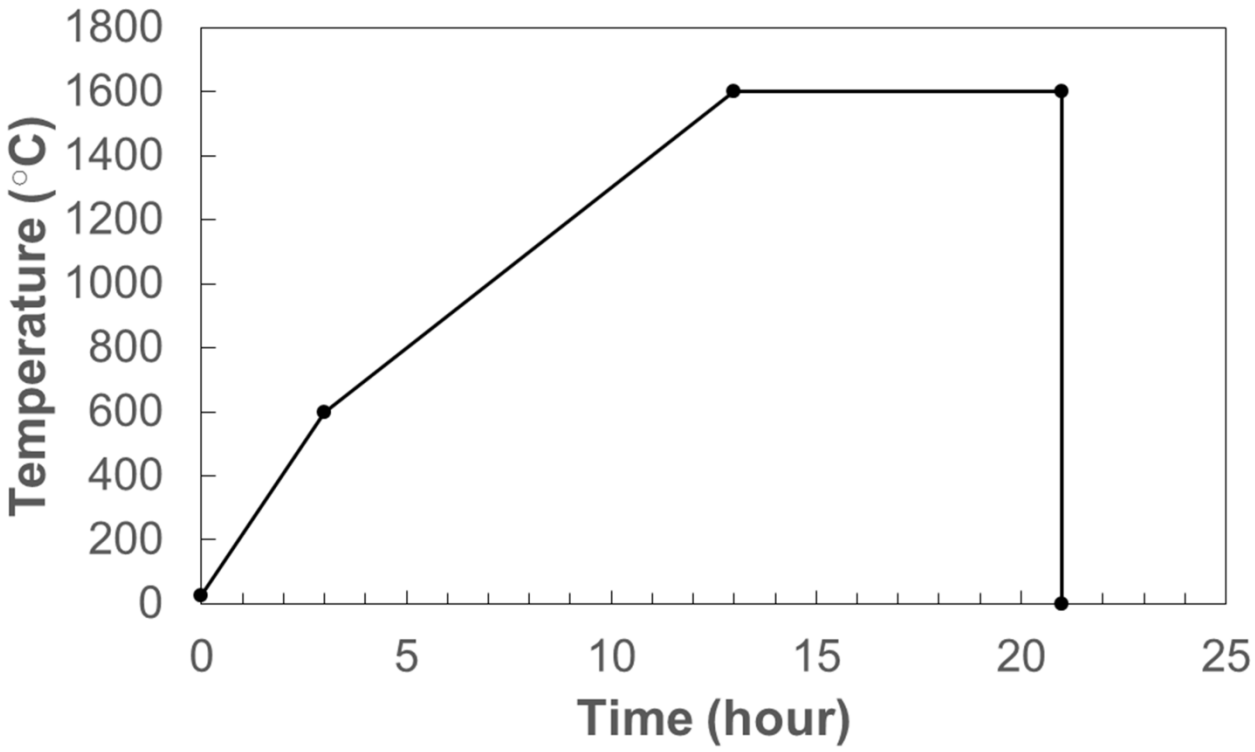

Figure 3. 11. Temperature profile for alloy/slag samples.

3-2-3- Slag fusion

After quenching, the slag phase was manually separated from the alloy phase. Each phase was separately crushed and ground in a tungsten carbide ball mill grinder (shown in figure 3.12). Since the slag composition used in this study is not acid-soluble, the slag phase was first fused with an alkali salt to make it soluble in acid. For this purpose, 0.3 g of ground slag of each sample was mixed with 4.5 g of NaOH pellets. The mixture was charged in a zirconium crucible (highly resistant to corrosion) and placed in the furnace. It was heated to 450 ºC and maintained at this temperature for 2 hours. Then, it was slowly cooled to room temperature and the fused slag was ground into a fine powder.

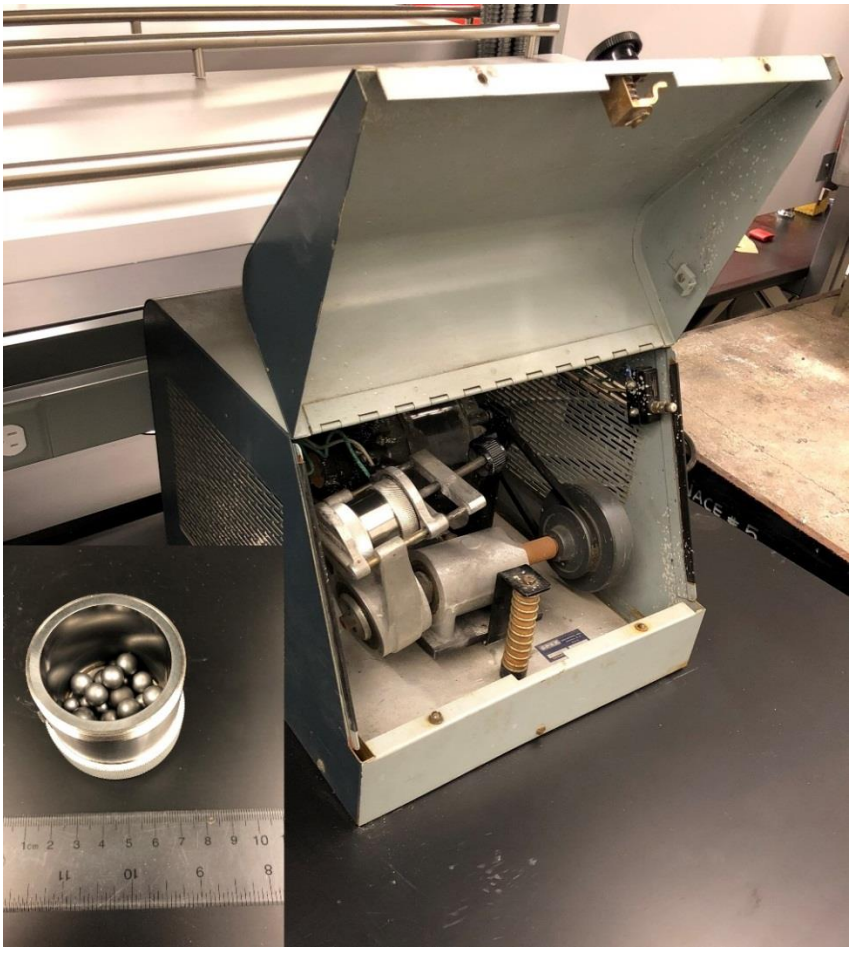

Figure 3. 12. Ball mill grinder and its tungsten carbide-lined vial set.

3-3- Leaching

Inductively Coupled Plasma-atomic Emission Spectrometry (ICP −AES) was used to analyze the impurity content of slag and alloy. Since the samples for this method should be in solution form, both phases were separately leached in an acid solution. The details of the leaching process for both alloy and slag are presented in the following section:

3-3-1- Alloy leaching

0.1 g of ground ferrosilicon alloy was charged in a Teflon beaker containing 2 ml of sulfuric acid (H_2SO_4) and 5 ml of nitric acid (HNO_3). Hydrofluoric acid was added to the solution drop by drop to avoid the sudden increase of the solution temperature. The beaker was also kept in a water/ice bath during the leaching process in order to maintain the low temperature of the solution. Figure 3.13 shows the Teflon beaker containing the solution placed in a water/ice bath during the leaching process. After complete leaching, the solution was diluted to 20 ml with distilled water.

3-3-2- Slag leaching

As mentioned in section 3.1, the initial concentration of HNO_3 used in the experiments was 70%. For slag leaching process, 2 ml of HNO_3 was mixed with 3 ml of distilled water to dilute the concentration of the acid to 28%. Then, 0.1 g of the ground fused slag (slag + NaOH) was charged in a beaker containing 5 ml of diluted HNO_3.

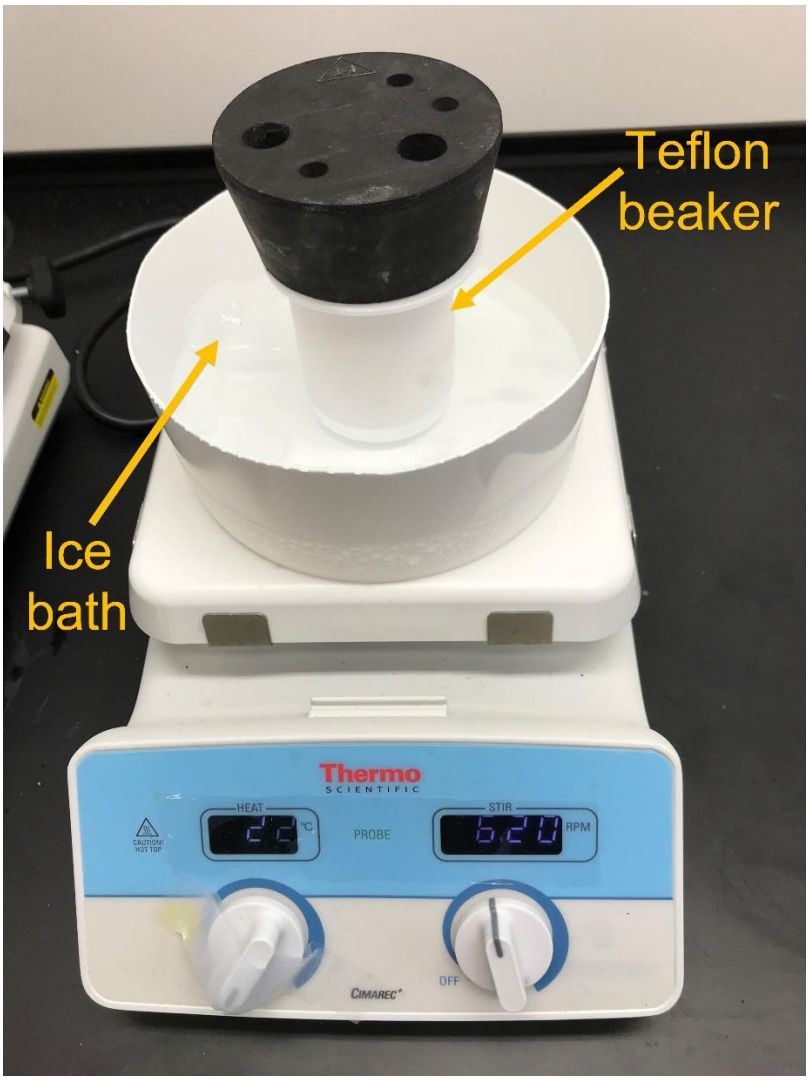

Figure 3. 13. Teflon beaker containing alloy solution in an ice bath.

3-4- Characterization

3-4-1- Scanning Electron Microscopy (SEM) and Electron Diffraction X-Ray (EDX)

Scanning electron microscope (SEM) is a technique in which images are produced through a focused beam of electrons. In other words, the images are the result of interaction of the beam and atoms of the sample in different depth. Signals produced in SEM are categorized in the

following groups: secondary electrons (SE), reflected or back-scattered electrons (BSE), characteristic X-rays. Energy-dispersive X-ray spectroscopy (EDX) is also a method for elemental analysis of samples. It is based on interaction of an electron beam excitation (which is used in SEM) and a sample. The electron beam penetrates the sample on an atomic level and results in displacements of electrons. Each displacement brings about the emission of electrons or X-rays. Since each element has a unique atomic structure, a unique peak on the final spectrum is observed for each element.

The FEI, Quanta 650 scanning electron microscope was used for observing the phase distribution in solidified master alloy. The powder sample was mounted with an epoxy and coated with carbon to cover the non-conductive areas. The SEM was operated at 15 kV with a 13-mm working distance.

3-4-2- X-Ray Diffraction (XRD)

X-Ray Diffraction (XRD) is an analytical technique used for atomic and molecular analysis of a crystal. In this method, the atoms of crystal cause a diffraction of the incident X-Ray beam into many specific directions. Angles and intensities of the diffracted beams are used for determining the positions of atoms in crystal, and their chemical bond.

X-ray diffraction (MultiFlex XRD, Rigaku) was utilized to confirm the formation of $FeSi_2$ and Si phases in the master alloy. For this purpose, the sample holder was charged with the powdered sample and it was analyzed using a CuKα radiation (λ= 1.54056Å).

3-4-3- Inductively Coupled Plasma Atomic Emission Spectroscopy (ICP-AES)

Inductively Coupled Plasma-atomic Emission Spectrometry (ICP–AES) is the most common technique for measuring the concentration of impurities in silicon refining processes. It is a flame technique with the flame temperature ranging from 6000 to 10000 K. The argon gas flowing through the torch is ionized at this temperature. When aqueous sample is introduced into the plasma flame, it collides with the charged ions and is itself broken down into charged ions. Each molecule's break up emits radiation at a characteristic wavelength. The detectors measure the intensity of each wavelength and based on this intensity, the concentration of element in sample is analyzed.

Varian 725-ES ICP spectrometer was used for analyzing the impurity content of slags and alloys. Conversion of concentrations of impurities in solution to their concentrations in the solid sample was done through Eq. 3.1 and Eq. 3.2. C, V, and W stand for concentration, volume, and weight, respectively. It should be noted that, in Eq. 3.2, fused slag refers to the mixture of slag and NaOH after fusion. Eq. 3.2 is multiplied by 16 since slag powder was diluted 16 times with NaOH in fusion process.

$$C_{\text{solid alloy}}\ (\text{ppm}) = \frac{C_{solution}(\text{mg/L}) \times V_{solution}\ (\text{ml})}{W_{digested\ alloy}\ (\text{g})} \qquad \text{Eq. 3. 1}$$

$$C_{\text{solid slag}}\ (\text{ppm}) = 16 \times \left(\frac{C_{solution}(\text{mg/L}) \times V_{solution}\ (\text{ml})}{W_{digested\ fused\ slag}\ (\text{g})}\right) \qquad \text{Eq. 3. 2}$$

4-Results and Discussion

This chapter presents the finding of the current study on B and P removal using various compositions of CaO-Al_2O_3-SiO_2 ternary system. First, the effect of holding time on partition ratios of B and P is investigated in order to find the time required for the equilibrium experiments. Then, the effect of basicity and oxygen potential on B and P partition ratios is described. Two parameters, namely borate (or phosphate) capacity and normalized distribution of B (or P), are defined in the last section of this chapter. The objective of calculating these parameters for each slag composition is to isolate the effect of basicity.

4-1- Determining holding time

Viscosity of the slag is defined as the ability of slag to resist movement of one layer of molecules over another under a stress [71]. Mass transfer in the slag is directly proportional to the diffusivity of slag. Increasing viscosity results in slower mass transfer [49] due to higher resistance against the movement of molecules. Increasing silica content promotes slag polymerization, which in turn increases the viscosity of the slag. In other words, viscosity is inversely proportional to mass transfer [49]. Therefore, slags with higher viscosity take longer time to reach equilibrium. Figure 4.1 shows viscosity of CaO-SiO_2-Al_2O_3 ternary at 1500 °C. It can be seen that the slags with the same CaO content have almost equal viscosity values; however increasing CaO content in this ternary results in lower viscosity of slag.

Based on the above discussion for the viscosity of CaO-SiO_2-Al_2O_3 ternary, the slag with the lowest CaO content (20 wt% CaO-65 wt% SiO_2-15 wt% Al_2O_3) was chosen for determining the equilibrium time. 5 g of this slag was charged in an alumina crucible and pre-melted at 1600 °C for 10 h. Next, 5 g of alloy was added to the pre-melted slag and the slag/alloy sample was

heated and quenched according to the temperature profile in figure 3.11. This experiment was repeated four times with different holding times of 2, 4, 6 and 8 hours. Figure 4.2 and 4.3 show the partition ratio of B and P for the four holding times applied, respectively. As it is clear in both of the aforementioned figures, partition ratio values for B and P increase with holding time. However, they both level off at about 8 hours, which indicates that the equilibrium between the slag and the alloy has been reached. Thus, the holding time of 8 hours was chosen for the rest of experiments.

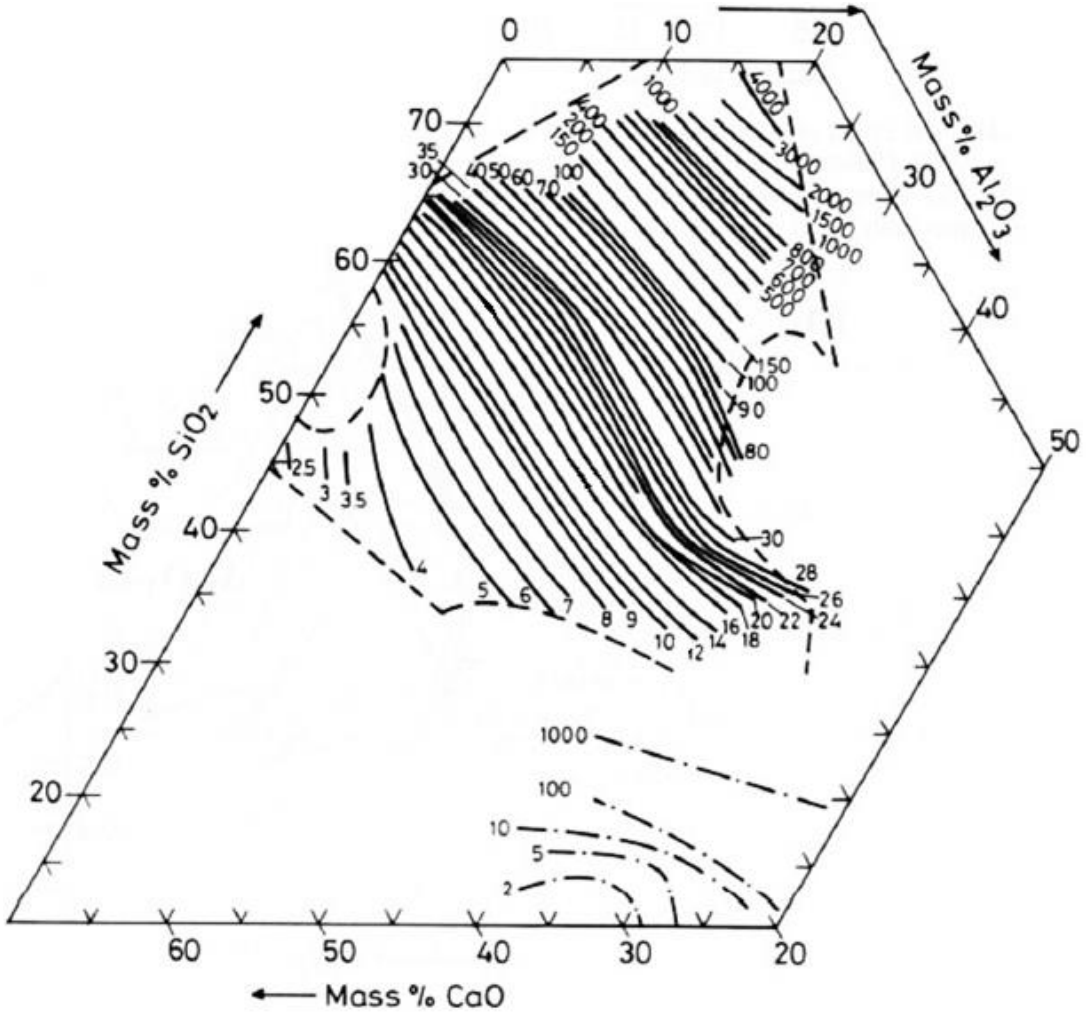

Figure 4. 1. Viscosity (poise = 10^{-1} Pa.s) of CaO-Al_2O_3-SiO_2 ternary at 1500 °C [72].

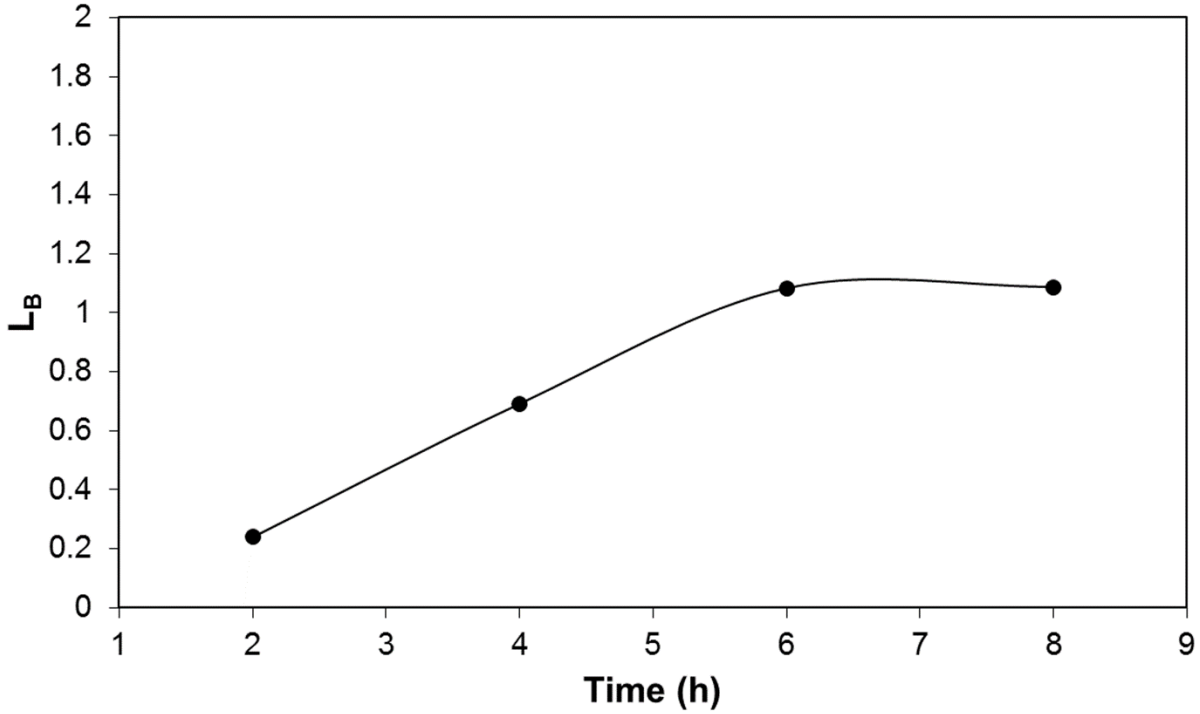

Figure 4. 2. Partition ratio of B (L_B) as a function of holding time.

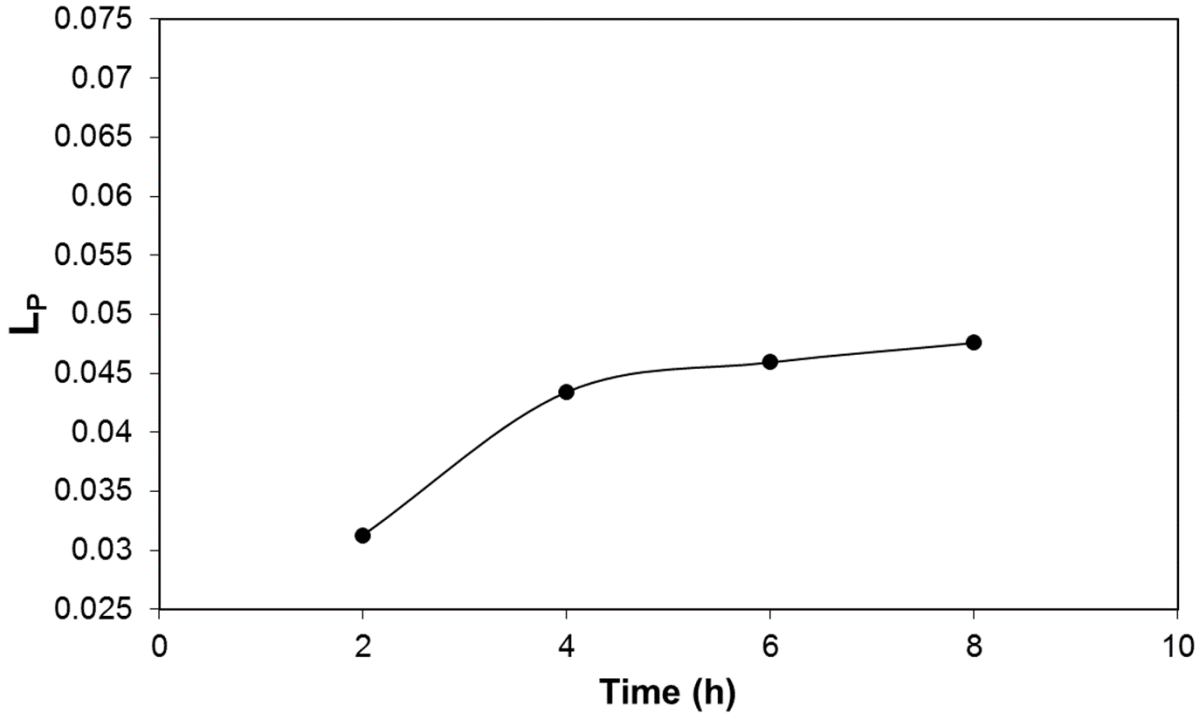

Figure 4. 3. Partition ratio of P (L_P) as a function of holding time.

4-2- Chemical analysis of alloys and slags

The concentrations of B and P in both alloy and slag phases are presented in table 4.1. Using the concentrations of B and P in solution, measured by ICP-OES analysis, final concentrations of B and P in alloy and slag can be calculated. For instance, the concentrations of B in alloy and slag solutions for sample 1 were measured as 1.266 and 0.2895 ppm, respectively. Following calculations were applied to obtain the concentrations of B in alloy and slag, based on Eq. 3.1 and 3.2.

$$\text{C (alloy) in ppmw} = 1.266\ (\text{ppm}) \times 20\ (\text{ml}) / 0.1\ (\text{g}) = 253.2\ \text{ppmw} \qquad \text{Eq. 4. 1}$$

$$\text{C (slag) in ppmw} = 16 \times [0.2895\ (\text{ppm}) \times 5\ (\text{ml}) / 0.1\ (\text{g})] = 231.6\ \text{ppmw} \qquad \text{Eq. 4. 2}$$

4-3- Effect of oxygen potential

As described in section 2-2-4-4, the oxygen potential plays a vital role in removal of impurities from silicon. In order to investigate the effect of oxygen potential on B and P removal from the Fe-Si alloy, the SiO_2/Al_2O_3 ratio of slag was changed while the CaO content was kept constant at 40 wt%. The first seven compositions of the Al_2O_3-SiO_2-CaO ternary presented in table 3.5 were chosen for this purpose. Table 4.2 includes L_B and L_P values achieved at these slag compositions. Also, figures 4.4 and 4.5 show the effect of SiO_2/Al_2O_3 ratio on B and P partition ratios respectively.

Table 4. 1. Chemical analysis of samples in ppmw.

Samples	$C_{B\ in\ solid\ alloy}$	$C_{B\ in\ solid\ slag}$	$C_{P\ in\ solid\ alloy}$	$C_{P\ in\ solid\ slag}$
1	253.2	231.6	1289.2	21.7
2	218.1	213.8	1659.5	39.4
3	320.2	1024.0	1170.1	39.0
4	248.1	1317.1	988.6	51.2
5	213.2	982.8	1126.7	119.1
6	207.8	360.8	1198.6	80.5
7	226.8	335.0	1231.4	67.6
8	144.1	156.5	1664.0	79.2
9	289.6	237.4	1105.2	47.2
10	207.7	280.9	1363.1	63.8
11	213.6	324.1	1277.2	102.2
12	182.9	2088.8	1104.7	115.4

Considering the B removal reaction, i.e. [B] + 3/2 O^{2-} + 3/4 O_2 $\rightarrow$(BO_3^{3-}), partial pressure of oxygen and basicity of slag are the two factors that enhance the removal process. However, these two factors are in conflict which means they cannot increase simultaneously. Based on the

findings of this series of experiment presented in figure 4.4, increasing the oxygen potential of slag (SiO_2/Al_2O_3 ratio) initially leads to an increase in L_B; however, its value decreases by further increase in SiO_2/Al_2O_3 ratio. Increasing the SiO_2/Al_2O_3 ratio results in higher activity of SiO_2 followed by an increase in P_{O_2}. On the other hand, comparing the basicity of SiO_2 (0.48) and Al_2O_3 (0.6) [73], slags with higher amount of SiO_2 are more acidic (lower amount of free oxygen ions). Therefore, these two competing effects bring about a maximum value in figure 4.4.

The oxygen potential at the maximum point is called the critical oxygen potential ($P_{O_2,\ critical}$). In other words, $P_{O_2,\ critical}$ is the oxygen potential at which the highest impurity removal can be achieved. In other words, the balance between P_{O_2} and $a_{O^{2-}}$ results in the highest partition ratio at this point. $P_{O_2,\ critical}$ for B removal is calculated as 9.01×10^{-18} atm in this study (detailed calculations are presented in section 4-5).

Table 4. 2. L_B and L_P results for Al_2O_3-SiO_2-CaO ternary at different oxygen potentials.

CaO (wt%)	**Al_2O_3 (wt%)**	**SiO_2 (wt%)**	**SiO_2/Al_2O_3**	**L_B**	**L_P**
40	5	55	11	0.91	0.017
40	7	53	7.5	0.98	0.024
40	10	50	5	3.20	0.033
40	15	45	3	5.31	0.052
40	20	40	2	4.61	0.11
40	30	30	1	1.74	0.067
40	35	25	0.71	1.48	0.055

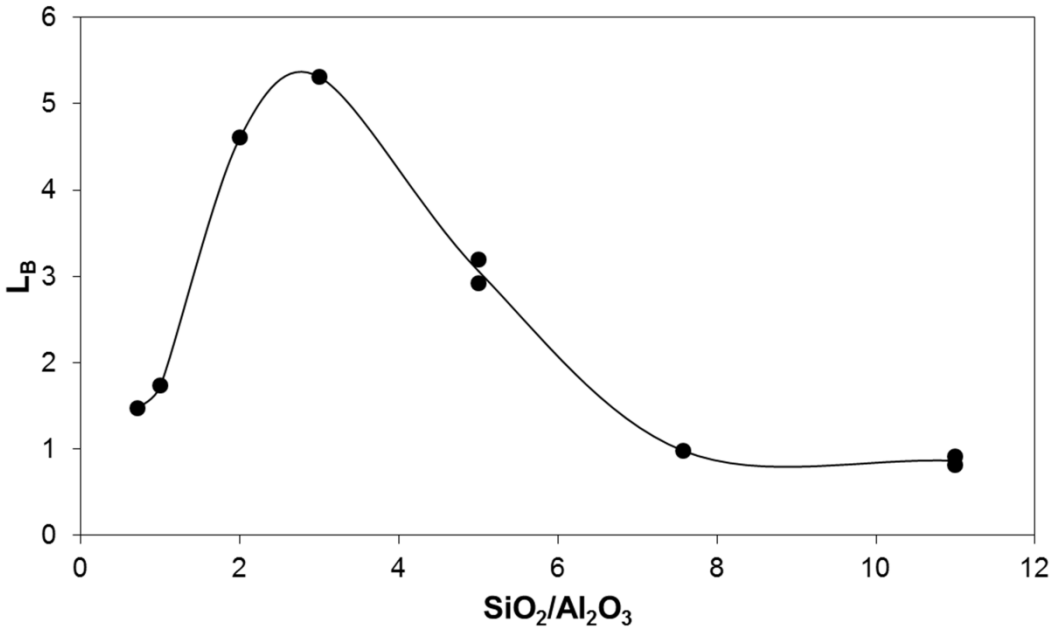

Figure 4. 4. Partition ratio of B (L_B) as a function of SiO_2/Al_2O_3 ratio.

Since the presence of SiO_2 in slag leads to higher P_{O_2} values, phosphate becomes the predominant P species in the slag. In other words, P is mostly removed through Eq. 2.15 ([P] + 3/2 O^{2-} + 5/4 $O_2 \rightarrow PO_4^{3-}$) [43, 74]. Similar to the argument presented for the observed trend of L_B in figure 4.4, due to the two counterbalancing factors (P_{O_2} and $a_{O^{2-}}$), L_P initially increases with SiO_2/Al_2O_3 ratio; however is starts decreasing after a certain SiO_2/Al_2O_3 ratio (figure 4.5). The highest L_P recorded in present work, by changing the oxygen potential of slag, is 0.11 at SiO_2/Al_2O_3 of 2. $P_{O_2,\ critical}$ for P removal process is found to be 6.29×10^{-18} atm (detailed calculations are presented in section 4-5).

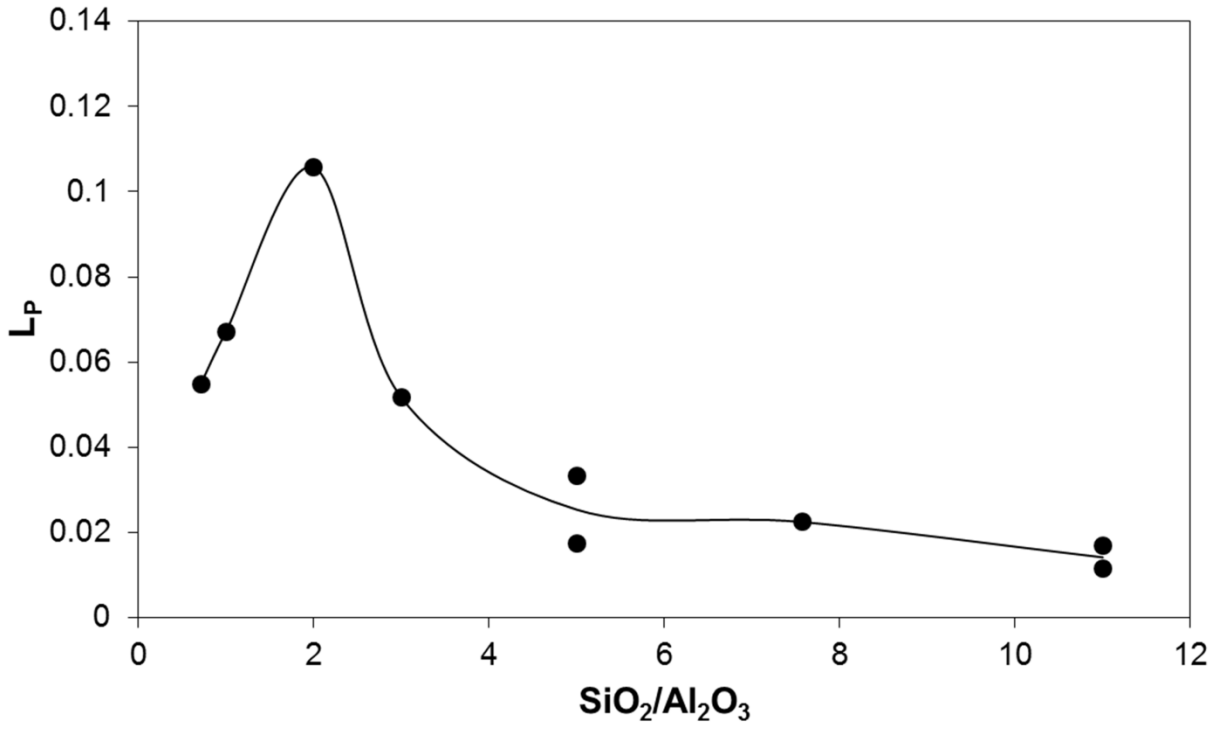

Figure 4. 5. Partition ratio of P (L_P) as a function of SiO_2/Al_2O_3 ratio.

It should be noted that all the L_P values are less than 0.12 which means most of the initial P is still present in the alloy phase and a very small amount of it has been transferred to the slag phase. Therefore, these slag compositions do not seem very effective in P removal from Fe-Si alloy. Low P removal from Si by CaO-SiO_2-Al_2O_3 ternary have also been reported by Fujiwara et al. [55].

4-4- Effect of basicity

Basicity of slag, which is directly related to free oxygen ions, is another crucial factor that is used for improving impurity removal from silicon. The effect of the concentration of free oxygen ions on partition ratio of B and P was investigated through changing the CaO/SiO_2 ratio in Al_2O_3-SiO_2-CaO ternary, with Al_2O_3 content fixed at 15 wt%. Slags 8 to 12 and slag 4 in table

3.5 were chosen for this purpose. Partition ratio results are shown in table 4.3, figure 4.6 and figure 4.7.

Because of the aforementioned conflictive relationship between basicity and oxygen potential of slag, it is expected to observe a negative parabola when L_B and L_P values are plotted against CaO/SiO_2 ratio. However, as shown in Figure 4.6, B partition ratio increases exponentially when the CaO/SiO_2 ratio of slag changes in the range of 0.31 to 1.125. This implies that the effect of lower oxygen potential does not overcome the effect of free oxygen ions (basicity) in the range examined in this study. The highest value of L_B achieved in the present work is 11.42 when the CaO/SiO_2 ratio is equal to 1.125. This means the slag with the highest basicity is the most successful one in removal of B. As mentioned in section 2-2-4-4, Jakobsson and Tangstad [49] applied the $CaO\text{-}SiO_2\text{-}Al_2O_3$ ternary slag for B removal from silicon metal at 1600 °C. However, the L_B values achieved in their work were all less than 2.1. Comparing L_B results of the mentioned study with those of the current study, the higher L_B values in current study can be attributed to the presence of Fe as a solvent metal.

The slag with the highest CaO/SiO_2 ratio has the lowest value of oxygen potential (1.40×10^{-17} atm). However, P_{O_2} calculations for different slag compositions (section 4-5) show that even the P_{O_2} of slag with the highest CaO/SiO_2 ratio is still higher than $P_{O_2,\ critical}$ for B ($1.40 \times 10^{-17} > 9.01 \times 10^{-18}$ atm). This means the expected maximum value of L_B cannot be observed in the range of CaO/SiO_2 ratio examined in this study. In other words, further increase in basicity is required to reach $P_{O_2,\ critical}$ where maximum B removal occurs.

Table 4. 3. L_B and L_P results for Al_2O_3-SiO_2-CaO ternary at different basicity.

CaO (wt%)	Al_2O_3 (wt%)	SiO_2 (wt%)	CaO/SiO_2	L_B	L_P
20	15	65	0.31	1.09	0.048
25	15	60	0.42	0.82	0.043
30	15	55	0.55	1.35	0.047
35	15	50	0.70	1.52	0.080
40	15	45	0.89	5.31	0.052
45	15	40	1.12	11.42	0.104

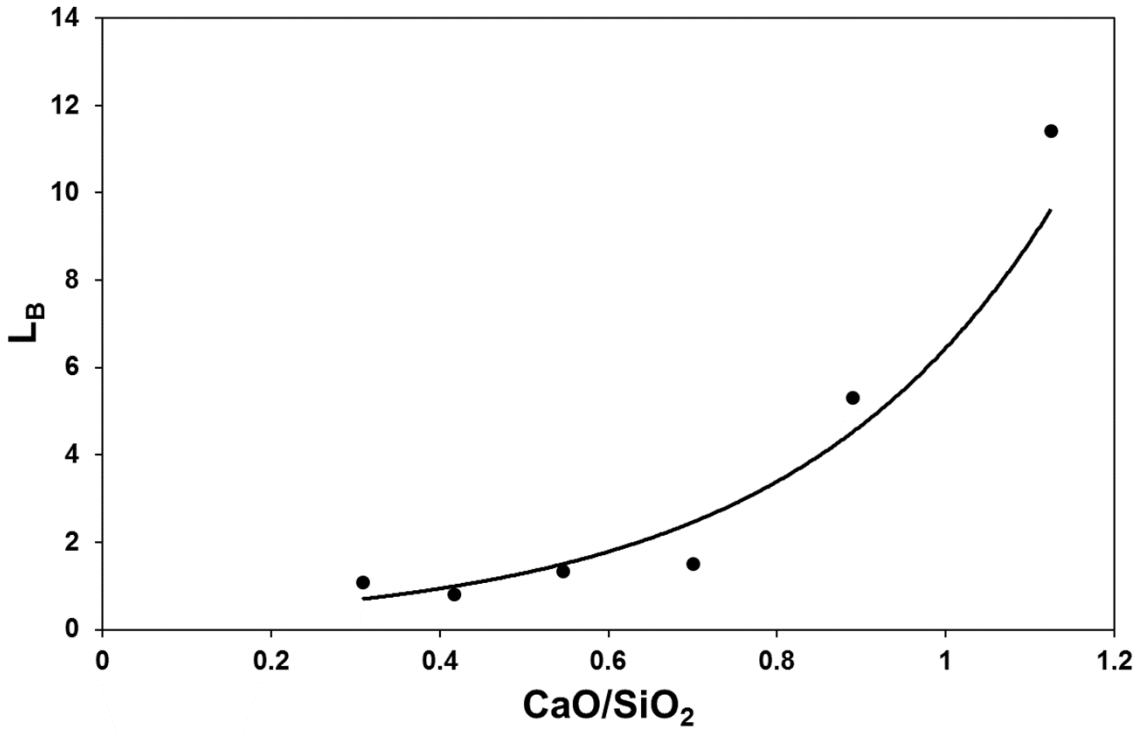

Figure 4. 6. Partition ratio of B (L_B) as a function of CaO/SiO_2 ratio.

According to the results presented in figure 4.7, L_P increases when the CaO/SiO_2 ratio increases from 0.31 to 0.125. Similar to the case of B, this is due to the fact that P_{O_2} at the highest CaO/SiO_2 ratio is still higher $P_{O_2,\ critical}$ for P ($1.40 \times 10^{-17} > 6.29 \times 10^{-18}$ atm). Thus, the anticipated maximum value for L_P is not observed in this plot.

Moreover, varying the basicity of slag does not show a significant change in L_P. In other words, small values of the P partition ratio indicate the retention of most of the initial P in the alloy phase.

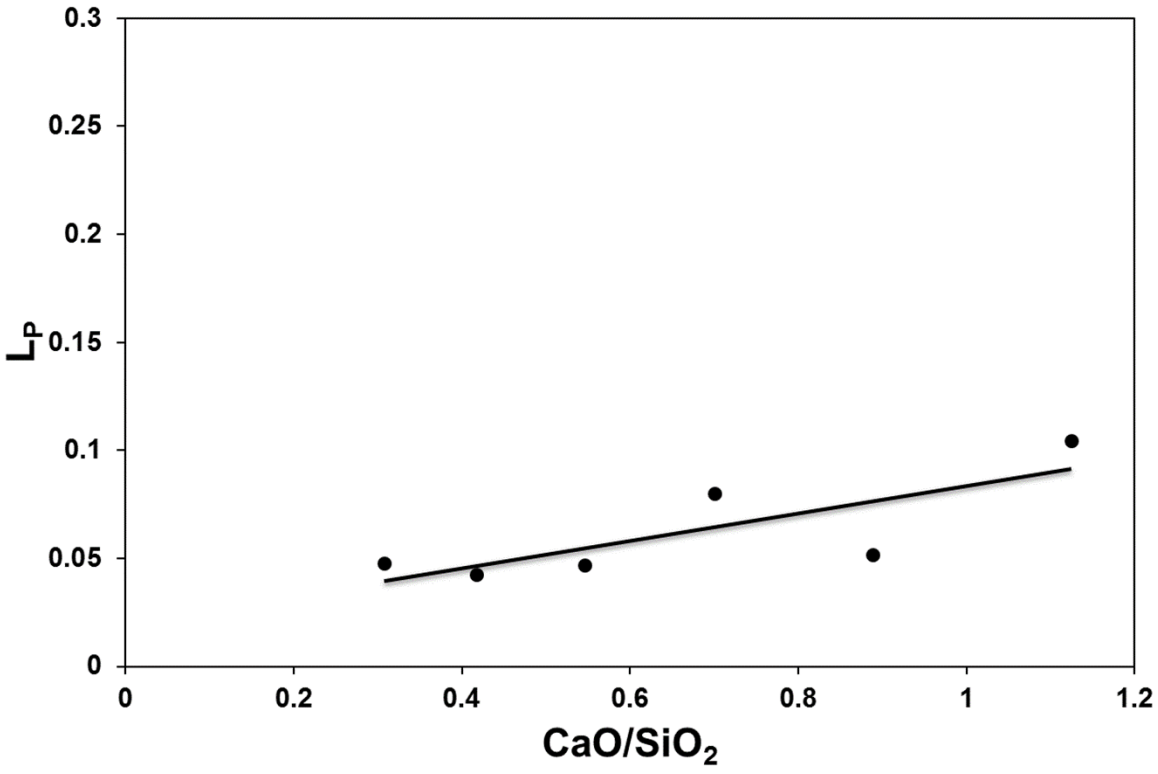

Figure 4. 7. Partition ratio of P (L_P) as a function of CaO/SiO_2 ratio.

4-5- Normalized distribution

As it was stated before, B and P enter the slag phase according to Eq. 2.14 and 2.15. Eq. 4.3 and 4.4 express the equilibrium constant of removal reactions of B and P, respectively:

$$K_1 = \frac{a_{BO_3^{3-}}}{a_B\, a_{O_2}^{3/4}\, a_{O^{2-}}^{3/2}} = \frac{C_1(B)\gamma_{BO_3^{3-}}}{[B]\,\gamma_B\, P_{O_2}^{3/4}\, a_{O^{2-}}^{3/2}} \qquad \text{Eq. 4. 3}$$

$$K_2 = \frac{a_{PO_4^{3-}}}{a_P a_{O_2}^{5/4}\, a_{O^{2-}}^{3/2}} = \frac{C_2(P)\gamma_{PO_4^{3-}}}{[P]\,\gamma_P\, P_{O_2}^{5/4}\, a_{O^{2-}}^{3/2}} \qquad \text{Eq. 4. 4}$$

where γ_B and γ_P are activity coefficients of B and P in liquid alloy and $\gamma_{BO_3^{3-}}$ and $\gamma_{PO_4^{3-}}$ are activity coefficient of BO_3^{3-} and PO_4^{3-} in slag phase. C_1 and C_2 are the conversion factors of mass percent of BO_3^{3-} and PO_4^{3-} to mass percent of B and P in the slag phase. Also, (B) and [B] are representative of concentrations of B in slag and alloy, respectively.

Eq. 4.3 and 4.4 are rearranged as Eq. 4.5 and 4.6 to clarify the effect of free oxygen ions and oxygen potential on the partition ratio of B and P. In these equations, K_6 is the equilibrium constant $\left(\frac{a_{Si}.P_{O2}}{a_{SiO_2}}\right)$ for Si/SiO_2 equilibrium (Eq. 2.18).

$$L_B = \frac{(B)}{[B]} = \frac{K1}{C_1}\ \frac{\gamma_B\, P_{O_2}^{3/4}\, a_{O^{2-}}^{3/2}}{\gamma_{BO_3^{3-}}} = \frac{K1}{C_1}\ \frac{\gamma_B\ a_{O^{2-}}^{3/2}}{\gamma_{BO_3^{3-}}} \left(\frac{K_6\, a_{SiO2}}{a_{Si}}\right)^{3/4} \qquad \text{Eq. 4. 5}$$

$$L_P = \frac{(P)}{[P]} = \frac{K1}{C_1}\ \frac{\gamma_P\, P_{O_2}^{5/4}\, a_{O^{2-}}^{3/2}}{\gamma_{PO_4^{3-}}} = \frac{K1}{C_1}\ \frac{\gamma_P\ a_{O^{2-}}^{3/2}}{\gamma_{PO_4^{3-}}}\ \left(\frac{K_6\, a_{SiO2}}{a_{Si}}\right)^{5/4} \qquad \text{Eq. 4. 6}$$

According to Eq. 4.5 and 4.6, B and P partition ratios are dependent on oxygen potential and the concentration of free oxygen ions (basicity) in the slag. In order to isolate the effect of when the slag composition is changing, new parameters called borate and phosphate capacities (Eq. 4.7 and 4.8) are defined based on the oxidation reaction of B and P (Eq. 2.14 and 2.15). These parameters are only dependent on slag composition ($\gamma_{BO_3^{3-}}$) and temperature (K_1).

$$C_{BO_3^{3-}} = \frac{Mass\%BO_3^{3-}}{a_B P_{O2}^{3/4}} = \frac{K_1 a_{O^{2-}}^{3/2}}{\gamma_{BO_3^{3-}}} \quad \text{Eq. 4. 7}$$

$$C_{PO_4^{3-}} = \frac{Mass\%PO_4^{3-}}{a_P P_{O2}^{5/4}} = \frac{K_2 a_{O^{2-}}^{3/2}}{\gamma_{PO_4^{3-}}} \quad \text{Eq. 4. 8}$$

To calculate the borate and phosphate capacities in this study, mass percentages of borate and phosphate were calculated from the impurity content of slag phase measured by ICP analysis. For instance, for sample number 1 with 231.6 ppm B and 21.7 ppm P, the mass percentages of borate and phosphate are obtained as follow (MW stands for molecular weight):

$$\text{Mass\% borate} = 10^{-4} \times \frac{B\ concentration}{\frac{MW_B}{MW_B+3MW_O}} = 10^{-4} \times \frac{231.6}{\frac{10.81}{10.81+48}} = 0.126 \quad \text{Eq. 4. 9}$$

$$\text{Mass\% phosphate} = 10^{-4} \times \frac{P\ concentration}{\frac{MW_P}{MW_P+4MW_O}} = 10^{-4} \times \frac{21.7}{\frac{30.97}{30.97+64}} = 0.007 \quad \text{Eq. 4. 10}$$

By obtaining the equilibrium constant for Eq. 2.18 (from HSC 5.1 thermodynamic database), activity coefficient of silicon in molten Fe-Si (0.977) [75] and activity of silica in CaO-SiO_2-Al_2O_3 ternary [76], the P_{O2} value for each slag composition was calculated.

Si/SiO_2 equilibrium constant (K_6) at 1873 K is equal to 9.13×10^{-17}. Activity of Si in Fe-Si liquid alloy is calculated by a_{Si} (activity of silicon) = γ_{Si} (activity coefficient of silicon) × mole fraction of Si. Knowing the mole fraction of Si in the alloy, 0.89, and the activity coefficient of silicon in molten 20 wt% Fe-80 wt% Si, 0.977, the activity of Si is calculated as 0.87. K_6 and a_{Si} are constant for all the samples in this study, as the temperature and the alloy composition do not change. However, a_{SiO2} changes due to the variations in slag composition.

Activities of B and P in liquid Fe-Si were calculated using Henrian activity coefficients and mole fraction of B and P in the alloy phase, which are calculated from the ICP analysis results. The activity coefficient values were calculated from literature using Gibbs-Duhem integration method (Eq. 4.11).

$$\text{RT ln } \gamma^{\circ}_{i \text{ in } Fe-Si \text{ melt}} = X_{Si \text{ in } Fe-Si \text{ melt}} \text{ RT ln } \gamma^{\circ}_{i \text{ in molten } Si} + X_{Fe \text{ in } Fe-Si \text{ melt}} \text{ RT ln } \gamma^{\circ}_{i \text{ in molten } Fe} - G^{excess}_{Si-Fe \text{ melt}} \quad \text{Eq. 4. 11}$$

The excess Gibbs energy of mixing for Fe-Si melt was calculated from Miettinen's work (Eq. 4.12) [77], knowing that the mole fraction of Si and Fe in the alloy is constant in all samples and is equal to 0.89 and 0.11, respectively. The excess Gibbs energy of mixing for Fe-Si melt at 1600 °C equals -2579.89 J/mol. $\gamma^{\circ}_{B \text{ in molten } Si}$ [78], $\gamma^{\circ}_{B \text{ in molten } Fe}$ [79], $\gamma^{\circ}_{P \text{ in molten } Si}$ [80] and $\gamma^{\circ}_{P \text{ in molten } Fe}$ [81] were estimated form the data available in the literature. If the experimental temperature in this study (1600 °C) does not match with that of the literature, activity coefficients are estimated assuming regular solution of impurities in the alloy. Activity coefficient values are summarized in table 4.4. Borate and phosphate capacities and the required data for their calculation are provided in table 4.5.

$$G^{excess}_{Si-Fe\ melt} = X_{Si}\,X_{Fe}[\text{-164435+41.99T - 21.523T}\,(X_{Fe} - X_{Si}) + (\text{52220+5.726T})\,(X_{Fe} - X_{Si})^2 + (\text{-28955+26.275T})\,(X_{Fe} - X_{Si})^3] \quad \text{Eq. 4. 12}$$

Table 4. 4. Henrian activity coefficients of B and P in the Fe and Si melts at 1873K.

	γ_B^0	γ_P^0
Si melt	0.38 [82]	0.55 [80]
Fe melt	0.042 [79]	2.75×10^{-4} [81]

As it was stated in section 2-2-4-4, increasing the CaO/SiO_2 ratio results in decreasing the activity of SiO_2 which in turn lowers the oxygen potential. Since the two ratios defined representing oxygen potential and basicity of slag are dependent on each other, studying the individual effect of each of these parameters on impurity removal seems impossible. Thus, another parameter called optical basicity (Λ) is defined as a measure of the basicity of slag. Optical basicity is a parameter that is directly proportional to the concentration of oxygen ions [83, 84]. Optical basicity of a multi-component slag can be calculated by Eq. 4.13.

$$\Lambda = \frac{\Sigma X_i n_i \Lambda_i}{\Sigma X_i n_i} \quad \text{Eq. 4. 13}$$

In this equation, Λ_i is the optical basicity of each component of slag, n_i is the number of oxygen atoms in each slag component and X_i is the mole fraction of each component. Optical basicity of CaO, SiO_2 and Al_2O_3 was considered as 1, 0.48 and 0.6 [73]. The optical basicity values calculated for each slag composition in this study is presented in table 4.5. Figure 4.8 shows the borate and phosphate capacities obtained in this work as a function of optical basicity. The linear plots in this figure are obtained by applying the least-square minimization method.

Table 4. 5. Thermodynamic data of CaO-Al_2O_3-SiO_2 ternary system at 1600 °C.

Slag	Λ	P_{O2}	a_B	a_P	$C_{BO_3^{3-}}$	$C_{PO_4^{3-}}$	D_B	D_P
1	0.624	$1.69*10^{-17}$	$2.56*10^{-4}$	$3.60*10^{-4}$	$1.87*10^{15}$	$1.71*10^{22}$	$3.47*10^{12}$	$1.56*10^{19}$
2	0.627	$1.50*10^{-17}$	$2.21*10^{-4}$	$4.64*10^{-4}$	$2.18*10^{15}$	$2.79*10^{22}$	$4.06*10^{12}$	$2.54*10^{19}$
3	0.632	$1.25*10^{-17}$	$3.24*10^{-4}$	$3.27*10^{-4}$	$8.18*10^{15}$	$4.91*10^{22}$	$1.52*10^{13}$	$4.48*10^{19}$
4	0.640	$9.01*10^{-18}$	$2.51*10^{-4}$	$2.76*10^{-4}$	$1.74*10^{16}$	$1.15*10^{23}$	$3.23*10^{13}$	$1.05*10^{20}$
5	0.648	$6.29*10^{-18}$	$2.16*10^{-4}$	$3.15*10^{-4}$	$1.97*10^{16}$	$3.68*10^{23}$	$3.67*10^{13}$	$3.35*10^{20}$
6	0.664	$2.80*10^{-18}$	$2.10*10^{-4}$	$3.35*10^{-4}$	$1.37*10^{16}$	$6.44*10^{23}$	$2.54*10^{13}$	$5.87*10^{20}$
7	0.672	$1.77*10^{-18}$	$2.29*10^{-4}$	$3.44*10^{-4}$	$1.63*10^{16}$	$9.30*10^{23}$	$3.04*10^{13}$	$8.48*10^{20}$
8	0.560	$8.11*10^{-17}$	$1.46*10^{-4}$	$4.65*10^{-4}$	$6.84*10^{14}$	$6.78*10^{21}$	$1.27*10^{12}$	$6.19*10^{18}$
9	0.579	$6.14*10^{-17}$	$2.93*10^{-4}$	$3.09*10^{-4}$	$6.36*10^{14}$	$8.63*10^{21}$	$1.18*10^{12}$	$7.87*10^{18}$
10	0.598	$3.95*10^{-17}$	$2.10*10^{-4}$	$3.81*10^{-4}$	$1.46*10^{15}$	$1.64*10^{22}$	$2.71*10^{12}$	$1.49*10^{19}$
11	0.618	$2.11*10^{-17}$	$2.16*10^{-4}$	$3.57*10^{-4}$	$2.62*10^{15}$	$6.15*10^{22}$	$4.88*10^{12}$	$5.61*10^{19}$
12	0.663	$1.40*10^{-17}$	$1.85*10^{-4}$	$3.09*10^{-4}$	$2.68*10^{16}$	$1.34*10^{23}$	$4.99*10^{13}$	$1.22*10^{20}$

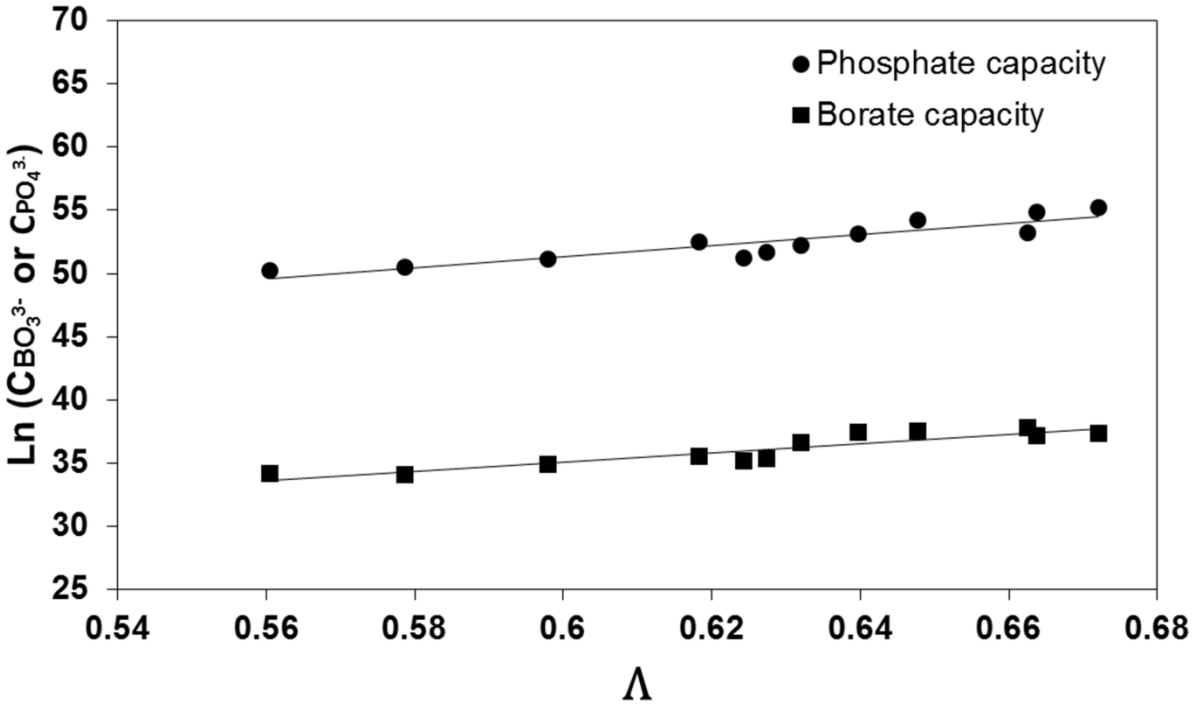

Figure 4. 8. Borate and phosphate capacities as a function optical basicity of slag.

Borate and phosphate capacities increase by increasing the optical basicity. The relation between borate or phosphate capacity and optical basicity is shown as Eq. 4.14 and 4.15, respectively.

$$\text{Ln}\,(C_{BO_3^{3-}}) = 36.51\,\Lambda + 13.19 \quad (\text{Coefficient of determination } (R^2 = 0.83)) \qquad \text{Eq. 4. 14}$$

$$\text{Ln}\,(C_{PO_4^{3-}}) = 43.50\,\Lambda + 25.23 \quad (\text{Coefficient of determination } (R^2 = 0.82)) \qquad \text{Eq. 4. 15}$$

Higher values for phosphate capacity and its stronger dependence on basicity (based on Eq. 4.14 and 4.15) are resulted from the more acidic nature of phosphorus oxide (Λ_{P2O5}=0.40 vs. Λ_{B2O3}=0.42 [85]). In other words, phosphate has a higher affinity for basic oxides compared with borate.

Another method for isolating the effect of basicity is through normalizing partition ratios by P_{O2} at each slag composition. Thus, another set of parameters called normalized distribution (D_B and

D_P) can be defined as shown in Eq. 4.16 and 4.17. According to these equations, three variable can affect the normalized distribution values: 1) K_1 which can be changed by temperature, 2) γ_B , and 3) $\gamma_{BO_3^{3-}}$ which can be altered by changing the alloy composition and the slag composition, respectively. The normalized distribution of B and P calculated for the slag compositions in this study are presented in table 4.5.

$$D_B = \frac{(B)}{[B]} \left(\frac{a_{Si}}{a_{SiO_2}\, K_6}\right)^{3/4} = \frac{K_1}{C_1} \quad \frac{\gamma_B \; a_{O^{2-}}^{3/2}}{\gamma_{BO_3^{3-}}} \qquad \text{Eq. 4. 16}$$

$$D_P = \frac{(P)}{[P]} \left(\frac{a_{Si}}{a_{SiO_2}\, K_6}\right)^{5/4} = \frac{K_1}{C_1} \quad \frac{\gamma_P \; a_{O^{2-}}^{3/2}}{\gamma_{PO_4^{3-}}} \qquad \text{Eq. 4. 17}$$

Figure 4.9 shows the relation between normalized distribution of B and P and optical basicity of the slags. It is clear that by removing the effect of oxygen potential, both B and P distribution show a direct relation with the basicity of slag. The least-square minimization method is applied to obtain the linear plots. The relation between normalized distributions of B (and P) and optical basicity of slags are presented in Eq. 4.18 and Eq. 4.19, respectively. Similar to the case of capacities, normalized distribution of P shows higher values and stronger dependence on basicity.

$\text{Log}(D_B) = 15.86\,\Lambda + 3.00$ (Coefficient of determination ($R^2 = 0.83$)) Eq. 4. 18

$\text{Log}(D_P) = 18.89\,\Lambda + 7.92$ (Coefficient of determination ($R^2 = 0.82$)) Eq. 4. 19

As it was stated in section 2-2-4-6, Ma et al. [7] used a combination of solvent refining (with Sn) and slag refining for impurity removal. In other word, they applied slag treatment on an alloy of

Si-Sn. Also, Li et al. [6] examined slag refining of an alloy of Si-Cu. Normalized distribution of B was calculated for these two studies using the thermodynamic data they reported for different slag compositions. The results of the current work and the two mentioned studies are displayed in figure 4.10 as a function of optical basicity. It is clear that, in all cases, Log (D_B) has a linear relation with optical basicity of slag. Higher temperature (1600 °C vs. 1500 °C and 1400 °C), different slag composition ($CaO\text{-}SiO_2\text{-}Al_2O_3$ vs. $CaO–SiO_2–Na_2O–Al_2O_3$ and $CaO–SiO_2–$ 24mol% CaF_2), and different activity coefficients of B (γ_B in Si-Fe vs. Si-Cu and Si-Sn) are the possible reasons for different D_B values obtained in these studies.

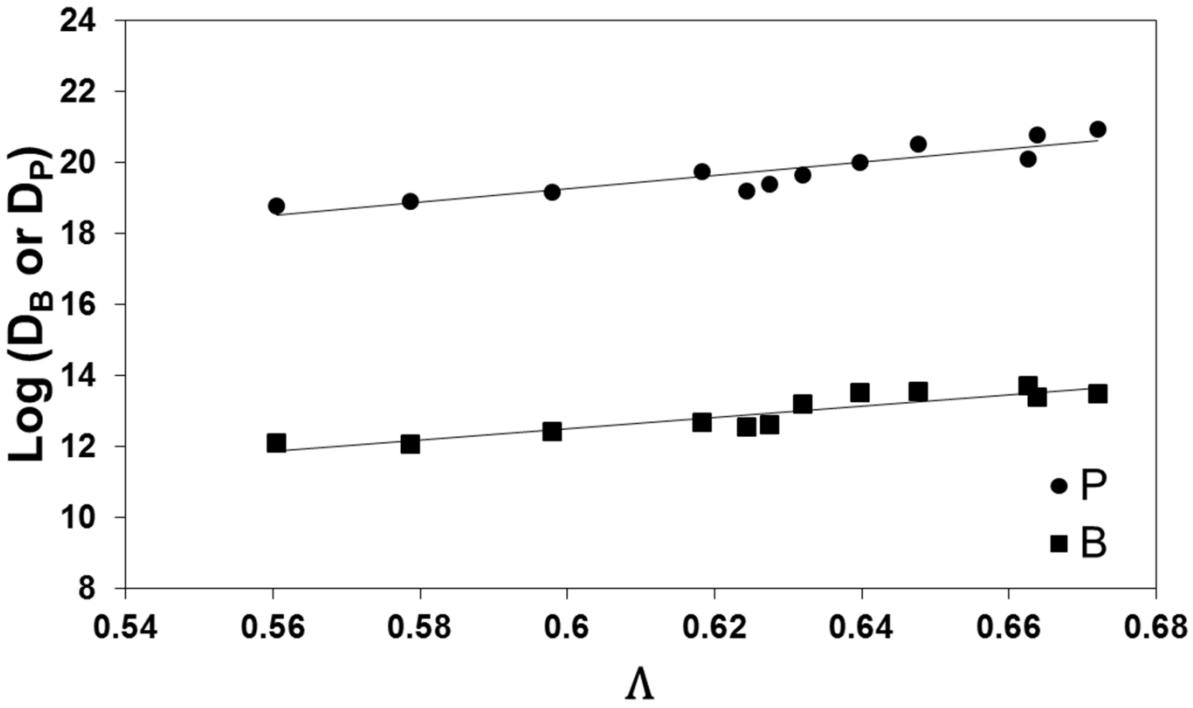

Figure 4. 9. Normalized distribution of B and P vs. optical basicity of slag.

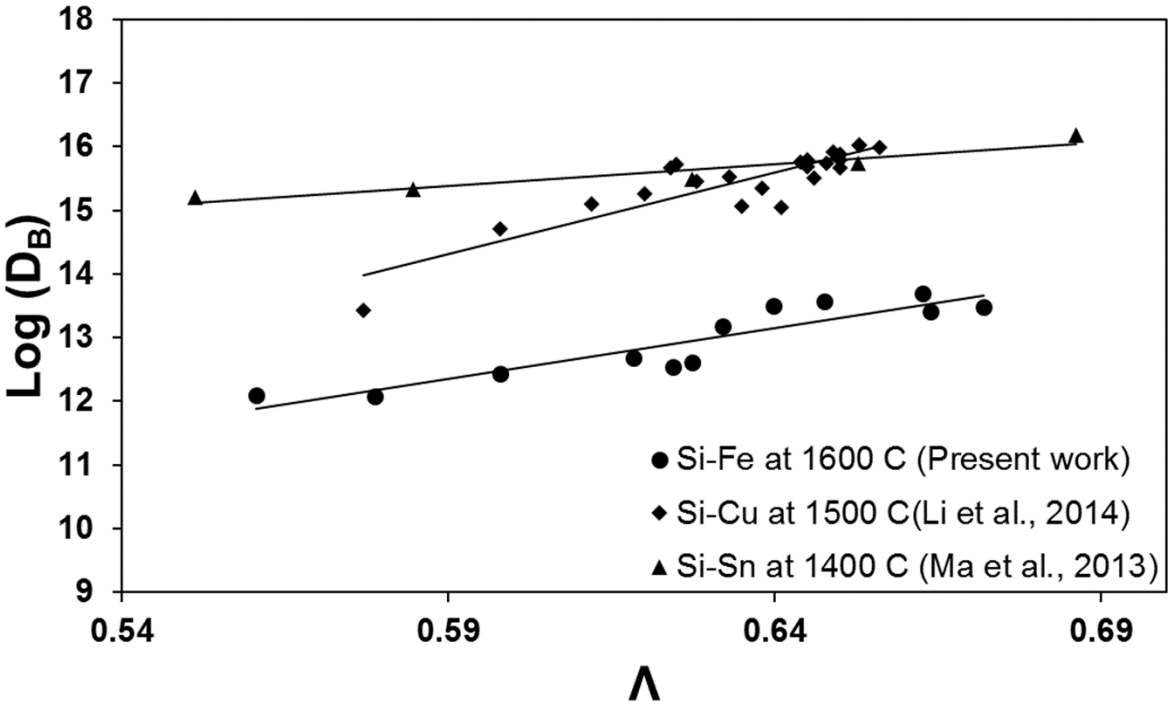

Figure 4. 10. Normalized distribution of B vs. optical basicity of slag at different temperatures.

5- Conclusions

- The holding time required to reach equilibrium was determined as 8 hours for 20 wt% Fe-80 wt% Si alloy and slag of CaO-SiO_2-Al_2O_3 at 1873 K.
- The effect of oxygen potential of slag on partition ratio of B (L_B) was investigated by varying SiO_2/Al_2O_3 ratio. Plotting L_B against SiO_2/Al_2O_3 ratio, a negative parabola with a maximum of 5.31 was obtained.
- $P_{O2,\ critical}$ associated with maximum B removal was calculated as 9.01×10^{-18} atm.
- The effect of oxygen potential of slag on P partition ratio (L_P) was examined through changing SiO_2/Al_2O_3 ratio. Plotting L_P vs. SiO_2/Al_2O_3 ratio, a negative parabola with a maximum of 0.11 was obtained.
- $P_{O2,\ critical}$ for P removal was calculated as 6.29×10^{-18} atm.
- Increasing the basicity of slag (CaO/SiO_2 ratio) in the range of 0.31 to 1.125, results in an exponential increase in L_B values.
- L_P values increase with increasing the basicity of slag (CaO/SiO_2 ratio) in range of 0.31 to 1.125.
- Considering the L_P and L_B values achieved in this study, CaO-SiO_2-Al_2O_3 ternary is significantly more effective for removing B compared with P.
- Borate (phosphate) capacity was the first method employed for isolating the effect of basicity on L_B and L_P. The relationships of borate and phosphate capacities with optical basicity of slag was obtained as Ln ($C_{BO_3^{3-}}$) = 36.51 Λ + 13.19 and Ln ($C_{PO_4^{3-}}$) = 43.50 Λ + 25.23, respectively.
- Normalized distribution of B (P) was the second method employed for isolating the effect of basicity on L_B and L_P. The relationships of normalized distribution of B and P with

optical basicity of slag was obtained as Log (D_B) = 15.86 Λ + 3.00 and Log (D_P) = 18.89 Λ + 7.92, respectively.

6- Future Work

The current study was more focused on removal of B and P from ferrosilicon alloy through slag treatment. According to the results, combining solvent refining and slag refining can lead to higher B partition ratios, compared with the studies that applied slag refining only. However, low L_P values indicate that P cannot reach acceptable levels by this process and its removal requires further refining steps. Adding Ca to the alloy might enhance P removal since P and Ca in molten Si can form the stable phase of Ca_3P_2 which easily segregates to the grain boundaries [55]. In other words, Ca addition can help the removal of P in phosphide form.

A series of experiments with a different temperature profile can be performed in order to separate the Si crystals from the alloy phase. Samples can be cooled down to below the liquidus temperature of the alloy. As a result, Si crystals will form. Subsequently, acid leaching can be applied for separating Si crystals from the alloy phase.

References

[1] G. W. Crabtree and N. S. Lewis, "Solar energy conversion," *Physics today*, vol. 60, pp. 37-42, 2007.

[2] K. Morita and T. Miki, "Thermodynamics of solar-grade-silicon refining," *Intermetallics*, vol. 11, pp. 1111-1117, 2003.

[3] B. Gribov and K. Zinov'ev, "Preparation of high-purity silicon for solar cells," *Inorganic materials*, vol. 39, pp. 653-662, 2003.

[4] J. Gumaste, B. Mohanty, R. Galgali, U. Syamaprasad, B. Nayak, S. Singh, *et al.*, "Solvent refining of metallurgical grade silicon," *Solar Energy Materials*, vol. 16, pp. 289-296, 1987.

[5] H. Liaw and F. S. d'Aragona, "Purification of metallurgical-grade silicon by slagging and impurity redistribution," *Solar Cells*, vol. 10, pp. 109-118, 1983.

[6] M. Li, T. Utigard, and M. Barati, "Removal of boron and phosphorus from silicon using cao-sio2-na2o-al2o3 flux," *Metallurgical and Materials Transactions B*, vol. 45, pp. 221-228, 2014.

[7] X. Ma, T. Yoshikawa, and K. Morita, "Removal of boron from silicon-tin solvent by slag treatment," *Metallurgical and Materials Transactions B*, vol. 44, pp. 528-533, 2013.

[8] B. Bathey and M. Cretella, "Solar-grade silicon," *Journal of Materials Science*, vol. 17, pp. 3077-3096, 1982.

[9] K. Morita and T. Miki, "Thermodynamics of solar-grade-silicon refining," *Intermetallics*, vol. 11, pp. 1111-1117, 2003.

[10] P. Woditsch and W. Koch, "Solar grade silicon feedstock supply for PV industry," *Solar energy materials and solar cells*, vol. 72, pp. 11-26, 2002.

[11] R. Y. Zehavi and J. E. Boyle, "Plasma spraying for semiconductor grade silicon,"US Patents, 2008.

[12] A. Istratov, T. Buonassisi, R. McDonald, A. Smith, R. Schindler, J. Rand, *et al.*, "Metal content of multicrystalline silicon for solar cells and its impact on minority carrier diffusion length," *Journal of Applied Physics*, vol. 94, pp. 6552-6559, 2003.

[13] A. M. Mitrašinović, R. D'Souza, and T. A. Utigard, "Impurity removal and overall rate constant during low pressure treatment of liquid silicon," *Journal of Materials Processing Technology*, vol. 212, pp. 78-82, 2012.

[14] J. Wu, W. Ma, B. Jia, B. Yang, D. Liu, and Y. Dai, "Boron removal from metallurgical grade silicon using a CaO–Li 2 O–SiO 2 molten slag refining technique," *Journal of Non-Crystalline Solids*, vol. 358, pp. 3079-3083, 2012.

[15] F. Wang, J. Wu, W. Ma, M. Xu, Y. Lei, and B. Yang, "Removal of impurities from metallurgical grade silicon by addition of ZnO to calcium silicate slag," *Separation and Purification Technology*, vol. 170, pp. 248-255, 2016.

[16] H. Herrmann, H. Herzer, and E. Sirtl, "Modern silicon technology," in *Festkörperprobleme 15*, Springer, 1975, pp. 279-316.

[17] X. Gu, X. Yu, and D. Yang, "Low-cost solar grade silicon purification process with Al–Si system using a powder metallurgy technique," *Separation and Purification Technology*, vol. 77, pp. 33-39, 2011.

[18] T. Ikeda and M. Maeda, "Purification of metallurgical silicon for solar-grade silicon by electron beam button melting," *ISIJ international*, vol. 32, pp. 635-642, 1992.

[19] J. Safarian, G. Tranell, and M. Tangstad, "Processes for upgrading metallurgical grade silicon to solar grade silicon," *Energy Procedia*, vol. 20, pp. 88-97, 2012.
[20] A. Braga, S. Moreira, P. Zampieri, J. Bacchin, and P. Mei, "New processes for the production of solar-grade polycrystalline silicon: A review," *Solar energy materials and solar cells*, vol. 92, pp. 418-424, 2008.
[21] B. Sørensen, "Life-cycle analysis of present and future Si-based solar cells," in *Proc. 2nd World Conf. Pv Solae Energy Conversion, Vienna*, 1998.
[22] F. Chigondo, "From Metallurgical-Grade to Solar-Grade Silicon: An Overview," *Silicon*, pp. 1-10, 2017.
[23] C. Dickson, R. Gould, and W. Felder, "Development of processes for the production of solar grade silicon from halides and alkali metals, phase 1 and phase 2," 1981.
[24] J. Amick, J. Dismukes, R. Francis, L. Hunt, P. Ravishankar, M. Schneider, *et al.*, "Improved High-Purity Arc-Furnace Silicon for Solar Cells," *Journal of The Electrochemical Society*, vol. 132, pp. 339-345, 1985.
[25] H. Aulich and J. Grabmaier, "Process for manufacturing Si useful for semiconductor components from quartz sand," US Patents, 1981.
[26] C. Khattak, D. Joyce, and F. Schmid, "Production of solar grade (SoG) silicon by refining liquid metallurgical grade (MG) silicon," *National Renewable Energy Laboratory*, pp. 8-12, 2001.
[27] B. Ceccaroli and K. Friestad, "Refining of metallurgical grade silicon," US Patents, 2005.
[28] H. M. Liaw and C. J. Varker, "Sequential purification and crystal growth," US Patents, 1980.
[29] N. Nakamura, M. Abe, K. Hanazawa, H. Baba, N. Yuge, and Y. Kato, "Development of NEDO melt-purification process for solar grade silicon and wafers," in *Proc. 2nd World Conf. on Photovoltaic Solar Energy Conversion*, 1998.
[30] C. Alemany, C. Trassy, B. Pateyron, K.-I. Li, and Y. Delannoy, "Refining of metallurgical-grade silicon by inductive plasma," *Solar energy materials and solar cells*, vol. 72, pp. 41-48, 2002.
[31] F. A. Trumbore, "Solid solubilities of impurity elements in germanium and silicon*," *Bell System Technical Journal*, vol. 39, pp. 205-233, 1960.
[32] N. Nakamura, H. Baba, Y. Sakaguchi, and Y. Kato, "Boron removal in molten silicon by a steam-added plasma melting method," *Materials Transactions*, vol. 45, pp. 858-864, 2004.
[33] J. Pires, J. Otubo, A. Braga, and P. Mei, "The purification of metallurgical grade silicon by electron beam melting," *Journal of Materials Processing Technology*, vol. 169, pp. 16-20, 2005.
[34] X. Peng, W. Dong, Y. Tan, and D. Jiang, "Removal of aluminum from metallurgical grade silicon using electron beam melting," *Vacuum*, vol. 86, pp. 471-475, 2011.
[35] E. Krystad, S. Zhang, and G. Tranell, "The kinetics of boron removal during slag refining in the production of solar-grade silicon," in *EPD Congress*, 2012, pp. 471-480.
[36] K.X. Wei, H.F. Lu, W.H. Ma, Y.L. Li, Z. Ding, J.J. Wu, *et al.*, "Boron removal from metallurgical-grade silicon by CaO–SiO2 slag refining," *Rare Metals*, vol. 34, pp. 522-526, 2015.
[37] K. Morita, K. Kume, and N. Sano, "Activity measurement of silicate slags equilibrated with molten silicon alloys," *Scandinavian journal of metallurgy*, vol. 31, pp. 178-183, 2002.

[38] E. J. Jung, B. M. Moon, and D. J. Min, "Quantitative evaluation for effective removal of phosphorus for SoG-Si," *Solar Energy Materials and Solar Cells,* vol. 95, pp. 1779-1784, 2011.
[39] E. J. Jung, B. M. Moon, S. H. Seok, and D. J. Min, "The mechanism of boron removal in the CaO–SiO2–Al2O3 slag system for SoG-Si," *Energy,* vol. 66, pp. 35-40, 2014.
[40] L. Huang, H. Lai, C. Lu, M. Fang, W. Ma, P. Xing, *et al.*, "Evaporation Behavior of Phosphorus from Metallurgical Grade Silicon via Calcium-Based Slag Treatment and Hydrochloric Acid Leaching," *Journal of Electronic Materials,* vol. 45, pp. 541-552, 2016.
[41] H. Kawamura, Y. Yanaba, T. Yoshikawa, and K. Morita, "Reductive removal of phosphorus in silicon using CaO-CaF2 slag," in *Materials Science Forum*, 2013, pp. 284-287.
[42] D. R. Gaskell and D. E. Laughlin, *Introduction to the Thermodynamics of Materials*: CRC Press, 2017.
[43] M. D. Johnston, L. T. Khajavi, M. Li, S. Sokhanvaran, and M. Barati, "High-temperature refining of metallurgical-grade silicon: a review," *JOm,* vol. 64, pp. 935-945, 2012.
[44] C. Jing, J.T. Li, W.H. Chen, C. Chao, and X.T. Luo, "Boron removal from metallurgical silicon using CaO-SiO2-CaF2 slags," *Transactions of Nonferrous Metals Society of China,* vol. 21, pp. 1402-1406, 2011.
[45] A. Istratov, T. Buonassisi, M. Pickett, M. Heuer, and E. Weber, "Control of metal impurities in “dirty” multicrystalline silicon for solar cells," *Materials Science and Engineering: B,* vol. 134, pp. 282-286, 2006.
[46] J. Safarian, G. Tranell, and M. Tangstad, "Boron Removal from Silicon by CaO-Na2O-SiO2 Ternary Slag," *Metallurgical and Materials Transactions E,* vol. 2, pp. 109-118, 2015.
[47] M. Johnston and M. Barati, "Effect of slag basicity and oxygen potential on the distribution of boron and phosphorus between slag and silicon," *Journal of non-crystalline solids,* vol. 357, pp. 970-975, 2011.
[48] L. A. V. Teixeira, Y. Tokuda, T. Yoko, and K. Morita, "Behavior and state of boron in CaO–SiO2 slags during refining of solar grade silicon," *ISIJ international,* vol. 49, pp. 777-782, 2009.
[49] L. K. Jakobsson and M. Tangstad, "Distribution of Boron Between Silicon and CaO-MgO-Al2O3-SiO2 Slags," *Metallurgical and Materials Transactions B,* vol. 45, pp. 1644-1655, 2014.
[50] H. Lai, L. Huang, C. Lu, M. Fang, W. Ma, P. Xing, *et al.*, "Reaction Mechanism and Kinetics of Boron Removal from Metallurgical-Grade Silicon Based on Li2O-SiO2 Slags," *JOM,* vol. 68, pp. 2371-2380, 2016.
[51] L. A. V. Teixeira and K. Morita, "Removal of boron from molten silicon using CaO–SiO2 based slags," *ISIJ international,* vol. 49, pp. 783-787, 2009.
[52] Y. Wang, X. Ma, and K. Morita, "Evaporation removal of boron from metallurgical-grade silicon using CaO-CaCl2-SiO2 slag," *Metallurgical and Materials Transactions B,* vol. 45, pp. 334-337, 2014.
[53] H. Nishimoto and K. Morita, "The rate of boron elimination from molten silicon by slag and Cl2 gas treatment," *Supplemental Proceedings: Materials Processing and Energy Materials, Volume 1,* pp. 701-708, 2011.

[54] M. Johnston and M. Barati, "Distribution of impurity elements in slag–silicon equilibria for oxidative refining of metallurgical silicon for solar cell applications," *Solar energy materials and solar cells,* vol. 94, pp. 2085-2090, 2010.
[55] H. Fujiwara, J. Y. Liang, K. Takeuchi, and E. Ichise, "Reducing removal of phosphorous from calcium containing silicon alloys," *Materials Transactions, JIM,* vol. 37, pp. 923-926, 1996.
[56] T. Yoshikawa and K. Morita, "Refining of silicon during its solidification from a Si–Al melt," *Journal of Crystal Growth,* vol. 311, pp. 776-779, 2009.
[57] K. Morita and T. Yoshikawa, "Thermodynamic evaluation of new metallurgical refining processes for SOG-silicon production," *Transactions of Nonferrous Metals Society of China,* vol. 21, pp. 685-690, 2011.
[58] A. Ciftja, "Refining and Recycling of Silicon: A Review," NTNU, 2008.
[59] T. Yoshikawa and K. Morita, "Solidification refining of Si with Si-Al melt using electromagnetic force [J]," *ISIJ international,* vol. 45, pp. 967-971, 2005.
[60] V. S. Zolotorevsky, N. A. Belov, and M. V. Glazoff, *Casting aluminum alloys* vol. 12: Elsevier Amsterdam, 2007.
[61] J. Juneja and T. Mukherjee, "A study of the purification of metallurgical grade silicon," *Hydrometallurgy,* vol. 16, pp. 69-75, 1986.
[62] A. M. Mitrašinović and T. A. Utigard, "Refining silicon for solar cell application by copper alloying," *Silicon,* vol. 1, pp. 239-248, 2009.
[63] A. M. Mitrašinović and T. A. Utigard, "Copper removal from hypereutectic Cu-Si alloys by heavy liquid media separation," *Metallurgical and Materials Transactions B,* vol. 43, pp. 379-387, 2012.
[64] P. Franke and D. Neuschutz, "Thermodynamic properties of inorganic materials compiled by SGTE," *Landolt-Bornstein Numerical Data and Functional Relationships in Science and Technology: Group IV: Physical Chemistry,* vol. 19, 2002.
[65] X. Ma, T. Yoshikawa, and K. Morita, "Si growth by directional solidification of Si–Sn alloys to produce solar-grade Si," *Journal of Crystal Growth,* vol. 377, pp. 192-196, 2013.
[66] S. Esfahani and M. Barati, "Purification of metallurgical silicon using iron as impurity getter, part II: extent of silicon purification," *Metals and Materials International,* vol. 17, pp. 1009-1015, 2011.
[67] X. Ma, T. Yoshikawa, and K. Morita, "Purification of metallurgical grade Si combining Si–Sn solvent refining with slag treatment," *Separation and Purification Technology,* vol. 125, pp. 264-268, 2014.
[68] J. H. Shin and J. H. Park, "Thermodynamics of Reducing Refining of Phosphorus from Si-Mn Alloy Using CaO-CaF2 Slag," *Metallurgical and Materials Transactions B,* vol. 43, pp. 1243-1246, 2012.
[69] L. Huang, H. Lai, C. Gan, H. Xiong, P. Xing, and X. Luo, "Separation of boron and phosphorus from Cu-alloyed metallurgical grade silicon by CaO–SiO2–CaCl2 slag treatment," *Separation and Purification Technology,* vol. 170, pp. 408-416, 2016.
[70] O. Kubaschewski, *Iron—Binary phase diagrams*: Springer Science & Business Media, 2013.
[71] K. Mills, "The estimation of slag properties," *Short course presented as part of Southern African Pyrometallurgy,* vol. 7, 2011.

[72] B. Keene, K. Mills, and M. Susa, "Slag atlas," *Dusseldorf, Germany: Verlag Stahleisen,* 1995.
[73] M. Susa and K. Mills, "Slag atlas," ed: Optical Properties of Slags: Data for Refractive Indices and Absorption Coefficients, 1995.
[74] M. X. Li, "Boron and Phosphorus Removal from Si-Cu Alloy Using CaO-SiO2-Na2O-Al2O3 Slag," 2014.
[75] J. Chipman, J. Fulton, N. Gokcen, and G. Caskey, "Activity of silicon in liquid Fe-Si and Fe-C-Si alloys," *Acta metallurgica,* vol. 2, pp. 439-450, 1954.
[76] K. Kume, K. Morita, T. Miki, and N. Sano, "Activity measurement of CaO–SiO2–AlO1.5–MgO slags equilibrated with molten silicon alloys," *ISIJ international,* vol. 40, pp. 561-566, 2000.
[77] J. Miettinen, "Reassessed thermodynamic solution phase data for ternary Fe-Si-C system," *Calphad,* vol. 22, pp. 231-256, 1998.
[78] T. Yoshikawa and K. Morita, "Thermodynamic property of B in molten Si and phase relations in the Si–Al–B system," *Materials transactions,* vol. 46, pp. 1335-1340, 2005.
[79] A. Zaitsev, N. y. Zaitseva, and A. Kodentsov, "Thermodynamic properties and phase equilibria in the iron–boron system. Transition of the Fe–B melt into the amorphous state," *Journal of Materials Chemistry,* vol. 13, pp. 943-950, 2003.
[80] A. I. Zaitsev, A. D. Litvina, and N. y. E. e. Shelkova, "Thermodynamic Properties of Si–P Melts," *High Temperature,* vol. 39, pp. 227-232, 2001.
[81] A. Zaitsev, Z. V. Dobrokhotova, A. Litvina, and B. Mogutnov, "Thermodynamic properties and phase equilibria in the Fe–P system," *Journal of the Chemical Society, Faraday Transactions,* vol. 91, pp. 703-712, 1995.
[82] R. Noguchi, K. Suzuki, F. Tsukihashi, and N. Sano, "Thermodynamics of boron in a silicon melt," *Metallurgical and materials transactions B,* vol. 25, pp. 903-907, 1994.
[83] J. Binks and J. Duffy, "A molecular orbital treatment of the basicity of oxyanion units," *Journal of Non-Crystalline Solids,* vol. 37, pp. 387-400, 1980.
[84] J. A. Duffy, "A common optical basicity scale for oxide and fluoride glasses," *Journal of non-crystalline solids,* vol. 109, pp. 35-39, 1989.
[85] V. D. Eisenhüttenleute and M. Allibert, *Slag atlas*: Verlag Stahleisen, 1995.